

**OPTIMIZATION OF STRUCTURAL ELEMENTS
FOR STABILITY AND VIBRATION**

A THESIS

Presented to

The Faculty of the Graduate Division

by

Manohar P. Kamat

In Partial Fulfillment

of the Requirements for the Degree

Doctor of Philosophy

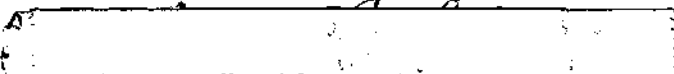
in the School of Engineering Science and Mechanics

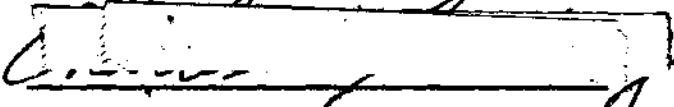
Georgia Institute of Technology

May 1972

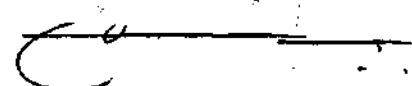
OPTIMIZATION OF STRUCTURAL ELEMENTS
FOR STABILITY AND VIBRATION

Approved:


Chairman



Date approved by Chairman: May 23, 1972

In presenting the dissertation as a partial fulfillment of the requirements for an advanced degree from the Georgia Institute of Technology, I agree that the Library of the Institute shall make it available for inspection and circulation in accordance with its regulations governing materials of this type. I agree that permission to copy from, or to publish from, this dissertation may be granted by the professor under whose direction it was written, or, in his absence, by the Dean of the Graduate Division when such copying or publication is solely for scholarly purposes and does not involve potential financial gain. It is understood that any copying from, or publication of, this dissertation which involves potential financial gain will not be allowed without written permission.



7/25/68

This
DISSERTATION
is
DEDICATED
to my wife,
EVELYNE

TABLE OF CONTENTS

	Page
ACKNOWLEDGEMENTS	v
LIST OF TABLES	vi
LIST OF ILLUSTRATIONS.	ix
SUMMARY.xiii
 CHAPTER	
I. INTRODUCTION.	1
II. STRONGEST COLUMN.	7
Assumptions and Objectives	
Derivation of the Rayleigh Quotient from Energy Principle	
Formulation of the Optimization Problem	
Method of Solution and the Optimization Procedure	
Numerical Results and Conclusions	
III. OPTIMAL VIBRATING BEAM.	50
Assumptions and Objectives	
Formulation of the Problem	
Method of Solution of the Problem	
Numerical Results and Conclusions	
IV. INVESTIGATION INTO THE OPTIMIZATION OF THIN RECTANGULAR PLATES FOR VIBRATION AND STABILITY.	86
Transversely Vibrating Thin Rectangular Plates	
Rectangular Plates Under Destabilizing Loads	
APPENDIX A	149
APPENDIX B	162
APPENDIX C	166
BIBLIOGRAPHY	183
VITA	186

ACKNOWLEDGEMENTS

The author wishes to express his most sincere appreciation to Professor G. J. Simitses, his advisor, for the guidance and advice throughout his graduate studies and for introducing him to this challenging area of research. Sincere appreciation is also extended to Professor C. V. Smith, Jr., for his advice and many hours of helpful discussions during the investigation of this work. The helpful comments of Professors L. W. Rehfield, C. E. S. Ueng, W. W. King and D. V. Ho are kindly appreciated. The author wishes to thank Professor M. E. Raville, Director of the School of Engineering Science and Mechanics, for his encouragement and for offering financial assistance. Thanks are also extended to Mrs. V. Connell for typing the final manuscript of this dissertation. Last, but not least, the author sincerely appreciates the loving encouragement, patience and understanding of his wife, Evelyne, and the sacrifice that both she and their son, Subhash, made during the years of his graduate studies.

Special permission was received from the Graduate Division to number the figures and tables by chapters in order to better fit the needs of this dissertation.

LIST OF TABLES

Table	Page
2.1 Numerical Results for the 16 Element Column shown in Fig. 2.4, case (ii)	45
2.2 Numerical Results for the 16 Element Column shown in Fig. 2.5, case (i)	46
2.3 Numerical Results for the 16 Element Column shown in Fig. 2.6, case (i)	47
2.4 Numerical Results for the 10 Element Column shown in Fig. 2.7	48
2.5 Numerical Results for the 16 Element Column shown in Fig. 2.8, case (i)	49
3.1 Numerical Results for the 10 Element Vibrating Beam shown in Fig. 3.2, case (i)	81
3.2 Numerical Results for the 10 Element Vibrating Beam shown in Fig. 3.3, case (ii)	82
3.3 Numerical Results for the 20 Element Vibrating Beam shown in Fig. 3.5, case (ii)	83
3.4 Numerical Results for the 10 Element Vibrating Beam shown in Fig. 3.7	84
3.5 Numerical Results for the 16 Element Vibrating Beam shown in Fig. 3.9	85
4.1 Numerical Results for the 2×5 Element Half Plate Model shown in Fig. 4.2	107
4.2 Numerical Results for the 3×3 Element Quarter Plate Model shown in Fig. 4.3.	108
4.3 Numerical Results for the 3×3 Element Quarter Plate Model shown in Fig. 4.4.	109
4.4 Numerical Results for the 2×2 Element Quarter Plate Model shown in Fig. 4.5.	110

Table	Page
4.5 Numerical Results for the 3 x 3 Element Quarter Plate Model shown in Fig. 4.5.	111
4.6 Numerical Results for the 4 x 4 Element Quarter Plate Model shown in Fig. 4.5.	112
4.7 Numerical Results for the 2 x 2 Element Quarter Plate Model shown in Fig. 4.6.	113
4.8 Numerical Results for the 3 x 3 Element Quarter Plate Model shown in Fig. 4.6.	114
4.9 Numerical Results for the 4 x 4 Element Quarter Plate Model shown in Fig. 4.6.	115
4.10 Numerical Results for the 2 x 2 Element Quarter Plate Model shown in Fig. 4.7.	116
4.11 Numerical Results for the 3 x 3 Element Quarter Plate Model shown in Fig. 4.7.	117
4.12 Numerical Results for the 3 x 3 Element Quarter Plate Model shown in Fig. 4.8.	118
4.13 Numerical Results for the 2 x 5 Element Half Plate Model shown in Fig. 4.10.	138
4.14 Numerical Results for the 3 x 3 Element Half Plate Model shown in Fig. 4.11.	139
4.15 Numerical Results for the 3 x 3 Element Half Plate Model shown in Fig. 4.12.	140
4.16 Numerical Results for the 2 x 2 Element Quarter Plate Model shown in Fig. 4.13	141
4.17 Numerical Results for the 3 x 3 Element Quarter Plate Model shown in Fig. 4.13	142
4.18 Numerical Results for the 2 x 2 Element Quarter Plate Model shown in Fig. 4.14	143
4.19 Numerical Results for the 3 x 3 Element Quarter Plate Model shown in Fig. 4.14	144
4.20 Numerical Results for the 4 x 4 Element Plate Model shown in Fig. 4.14	145

Table	Page
4.21 Numerical Results for the 3×3 Element Quarter Plate Model shown in Fig. 4.15 (i)146
4.22 Numerical Results for the 3×3 Element Quarter Plate Model shown in Fig. 4.15 (ii).147
4.23 Numerical Results for the 4×4 Element Full Plate Model shown in Fig. 4.16.148

TABLE OF ILLUSTRATIONS

Figure	Page
2.1 A Typical Column on a Continuous Elastic Foundation, Restrained Elastically at the Ends and Subjected to a Varying Axial Load	8
2.2 Optimum Moment of Inertia Distribution for a Column with $k_T^0 = \infty$, $k_R^0 = \infty$, $k_T^L = 0$, $k_R^L = 0$; $m=20$; $n=2$	38
2.3 Optimum Moment of Inertia Distribution for a Column with $k_T^0 = \infty$, $k_R^0 = \infty$, $k_T^L = \infty$, $k_R^L = 0$; $m=20$; $n=2$	39
2.4 Optimum Moment of Inertia Distribution for a Column with $k_T^0 = \infty$, $k_R^0 = \infty$, $k_R^L = 0$; $k_T^L = \text{varying}$; $m=16$; $n=1$	40
2.5 Optimum Moment of Inertia Distribution for a Column with $k_T^0 = \infty$, $k_R^0 = 0$, $k_T^L = \infty$, $k_R^L = 25 E\rho V^3/L^4$; $m=16$; $n=3$	41
2.6 Optimum Moment of Inertia Distribution for a Column with $k_T^0 = \infty$, $k_R^0 = \infty$, $k_T^L = \infty$, $k_R^L = \text{varying}$; $m=16$; $n=3$	42
2.7 Optimum Moment of Inertia Distribution for a Column with $k_T^0 = \infty$, $k_R^0 = \infty$, $k_T^L = 0$, $k_R^L = 0$; $S_0(x) = E\rho V^2(L-x)/L^5$; $m=10$; $n=2$	43
2.8 Optimum Moment of Inertia Distribution for a Column with $k_T^0 = \infty$, $k_R^0 = 0$, $k_T^L = \infty$, $k_R^L = 0$; $m=\text{varying}$; $n=2$; $\beta=\text{varying}$	49
3.1 A Typical Beam on a Continuous Elastic Foundation with Elastically Restrained Ends Under Arbitrarily Varying Axial Load and Dead Mass Distribution	52
3.2 Optimum Area Distribution for a Beam with $k_T^0 = \infty$, $k_R^0 = 0$, $k_T^L = \infty$, $k_R^L = 0$; $\eta=0.0$; $m=20$; $n=\text{varying}$	72
3.3 Optimum Area Distribution for a Beam with $k_T^0 = \infty$, $k_R^0 = 0$, $k_T^L = \infty$, $k_R^L = 0$; $\beta = 10 E\rho V^2/L^6$; $\eta=0.0$; $n=2$; $m=\text{varying}$	73

Figure	Page
3.4 Optimum Area Distribution for a Beam with $k_T^0 = \infty, k_R^0 = 0, k_T^L = \infty, k_R^L = 0; P_0 = P_L = -5 E\rho V^2/L^4;$ $\eta=0.0; m=20; n=2$	74
3.5 Optimum Area Distribution for a Beam with $k_T^0 = \infty, k_R^0 = \infty, k_T^L = 0, k_R^L = 0, \eta=0.5, x_c=L;$ $n=2; m=\text{varying}$	75
3.6 Optimum Area Distribution for a Beam with $k_T^0 = \infty, k_R^0 = \infty, k_T^L = 0, k_R^L = 0; A \geq 0.2725 V/L;$ $\eta=0.0; n=2; m=\text{varying}$	76
3.7 Optimum Area Distribution for a Beam with $k_T^0 = \infty, k_R^0 = \infty, k_T^L = 0, k_R^L = 0; P_0 = P_L = E\rho V^2/L^4;$ $\eta=0.25; m=10; n=2$	77
3.8 Optimum Area Distribution for a Beam with $k_T^0 = \infty, k_R^0 = \infty, k_T^L = \infty, k_R^L = \infty; P_0 = P_L = 10 E\rho V^2/L^4;$ $\eta=0.0; n=2; m=\text{varying}$	78
3.9 Optimum Area Distribution for a Beam with $k_T^0 = \infty, k_R^0 = 0, k_T^L = \infty, k_R^L = 25 E\rho V^3/L^4;$ $m_d(x) = M_0/2L; m=16; n=3$	79
3.10 Optimum Area Distribution for a Beam with $k_T^0 = \infty, k_R^0 = \infty, k_T^L = \infty, k_R^L = 25 E\rho V^2/L^3;$ $m_d(x) = M_0/L; m=16; n=2$	80
4.1 A Typical Transversely Vibrating Thin Rectangular Plate. . . .	101
4.2 Normalized Thickness Distribution for an Optimum Vibrating Rectangular Plate Simply-Supported on Two Opposite Sides with Imposed Cylindrical Bending.	101
4.3 Normalized Thickness Distribution for an Optimum Vibrating Rectangular Plate Simply-Supported on the Sides $x=0, a$ and Free on the Other Two Sides; $h \geq 0.10 h_U$	102
4.4 Normalized Thickness Distribution for an Optimum Vibrating Rectangular Plate Simply-Supported on All Sides; $h \geq 0.10 h_U$	102

Figure	Page
4.5 Normalized Thickness Distribution for an 'Optimum' Vibrating Square Plate Simply-Supported on All Sides.	103
4.6 Normalized Thickness Distribution for an Optimum Vibrating Square Plate Simply-Supported on All Sides with a Concentrated Dead Mass at the Center; $h \geq 0.10 h_U$	104
4.7 Normalized Thickness Distribution for an Optimum Vibrating Square Plate Simply-Supported on All Sides with a Uniformly Distributed Dead Mass; $h \geq 0.001 h_U$	105
4.8 Normalized Thickness Distribution for an Optimum Vibrating Square Plate Simply-Supported on All Sides with a Series of Concentrated Dead Masses; $h \geq 0.10 h_U$	106
4.9 A Typical Rectangular Plate Under In-plane Loading	131
4.10 Normalized Thickness Distribution for an Optimum Rectangular Plate Simply-Supported on Sides $x=0, a$ with Imposed Cylindrical Bending Under Uniaxial Compression.	131
4.11 Normalized Thickness Distribution for an Optimum Rectangular Plate Simply-Supported on Sides $x=0, a$ and Free on Sides $y=0, b$; Under Uniaxial Compression.	132
4.12 Normalized Thickness Distribution for an Optimum Rectangular Plate Simply-Supported on All Sides Under Uniaxial Compression	132
4.13 Normalized Thickness Distribution for an Optimum Square Plate Simply-Supported on All Sides Under Uniaxial Compression; $h \geq 0.10 h_U$	133
4.14 Normalized Thickness Distribution for an Optimum Square Plate Simply-Supported on All Sides Under Equal Biaxial Compression.	134
4.15 Normalized Thickness Distribution for a Square Plate Simply-Supported on All Sides Under Equal Biaxial Compression; $h \geq 0.10 h_U$	135
4.16 Normalized Thickness Distribution for an Optimum Square Plate Simply-Supported on All Sides Under Uniform Shear; $h \geq 0.10 h_U$	136

Figure	Page
4.17 A Typical Stiffened Square Plate	137
A-1 Finite Element Representation of a Column.	149
A-2 Two Typical Adjacent Beam Elements	150
A-3 A Two-Beam Element Model of a Column	151
C-1 A Typical Rectangular Plate Bending Element.	167

SUMMARY

In this dissertation a finite element displacement formulation is proposed for the optimization of structural elements for stability and vibration. For columns, with a given volume and various boundary conditions and axial load distributions, with cross-sections for which the moment of inertia and area are related by $I = \rho A^n$ (ρ and n are positive constants), the optimality condition is reduced to one of constant strain energy density. The problem reduces to the solution of one linear, and one nonlinear ordinary differential equation together with the integral constraint equation of constant volume. The column is discretized using compatible finite elements, and an iterative procedure is used to converge to the optimum material distribution and the maximum critical load subject to an additional constraint of minimum allowable cross-sectional area.

In the case of transversely vibrating beams with $I = \rho A^n$ and a given volume, no solutions of practical interest seem to exist for most boundary conditions without a given dead (non-structural) mass distribution and/or the inequality constraint of minimum allowable cross-sectional area and/or a compressive axial load distribution.

The optimality condition still reduces to a relation between the strain and kinetic energy densities and again, an iterative procedure similar to that of columns is used to converge to the optimum material distribution and the maximum first mode frequency of free vibration.

In addition to the optimization of columns and transversely vibrating beams, an investigation is made into the optimization of thin rectangular plates for vibration and stability. The problem of the optimal design of a thin rectangular freely vibrating plate (transverse vibration) is very similar to the optimal design of the vibrating beam when cast in matrix form for the discretized finite element models, and a similar iterative procedure can again be used. The investigation is limited to some typical boundary conditions and aspect ratios.

In the case of the optimization of thin rectangular plates for stability, the problem is simplified by making the assumption of inextensionality for the derivation of the optimality condition, which then is one of constant strain energy density. Again the investigation is limited to some typical boundary conditions, in-plane loading and aspect ratios. Some of the approximate solutions so obtained are then compared with stiffened plates of the same volume. This comparison weighs heavily in favour of stiffened plates and definitely warrants future research into the optimum stiffener orientation and spacing, the shape of the stiffener cross-section, etc.

CHAPTER I

INTRODUCTION

One of the objectives of the optimum design of structures in general is to obtain a desired structure which meets certain design criteria. These criteria might be minimum deflection, least weight, etc. In addition, in many cases the design is subject to certain constraints such as fixed weight or minimum stiffness. Thus the problem of optimization is basically a problem in the calculus of variations --extremizing certain functionals subject to some given subsidiary constraints.

Complicated structural systems such as buildings, bridges, and water, air or space vehicles are composed of basic structural elements --straight and curved beams, columns, cables, arches, flat and curved plates. The constant demand for light weight efficient systems has led many investigators to the field of structural optimization.

To optimize a complicated system, the variables involved become prohibitively large in number, and the implementation of optimization is almost impossible. Because of this it is hoped that, by first dealing with basic structural elements, one eventually might be able to optimize a system of elements through an existing finite element mechanized program properly modified.

In any structural optimization program one must clearly specify

(i) the design objective and (ii) the geometric and behavioral constraints. In a given problem the design objective could be the minimization of the cost of manufacture or, for some systems where cost is not of prime importance, minimization of total weight to carry the worst possible loads that the system will encounter. This latter design objective in many cases can be accomplished by stating the opposite (duality), which is to carry the most load for a given weight. The geometric constraints are usually associated with space requirements such as lengths or areas. The behavioral constraints are associated with the response of the structure to the loads. Limitations on maximum stress or minimum stiffness are examples of behavioral constraints. The totality of constraints can be classified as equality or inequality constraints. In the treatment of columns and beams, it is assumed that the cross-sectional moment of inertia and area are related by $I(x) = \rho A^n(x)$. This assumption is a restriction but with a suitable choice of ρ and n it covers a large class of structural configurations.

The interest in minimum weight design of columns dates back to around 1770 when Lagrange first treated the strongest column problem but arrived at the wrong result due to computational errors. The correct solution was given by Clausen in 1851 for simply-supported columns with similar cross-sections (i.e. $n=2$) and prescribed shape--not necessarily convex. He found that the best tapering increased the buckling load by one third over that of uniform column of the same volume. Later this

problem was generalized and completely solved by Keller³ who determined that, of all simply-supported columns with convex and similar cross-sections "the strongest column has an equilateral triangle as its cross-section and is tapered along its length, being thickest in the middle and thinnest at its ends. Its buckling load is 61.2% larger than that of a circular cylinder." This was further generalized by Tadjbakhsh and Keller⁴ to four different types of boundary conditions namely simply-supported, clamped-free, clamped-pinned and clamped-clamped. Subsequently Keller and Niordson⁵ treated the problem of finding the height of the tallest column under its own weight. Taylor⁶ and Salinas⁷ showed that the Euler-Lagrange equations obtained as a result of extremizing the total potential energy with a superposed volume constraint, are identical with those obtained by direct minimum volume formulation with superposed stability equations as a constraint. Prager and Taylor⁸ also provided exact solution for a simply-supported column of sandwich construction (i.e. $n=1$). Exact solutions for the case when $I(x) = \rho A^3(x)$ have been obtained by Simites et al.⁹ for two typical types of boundary conditions. These will be omitted from this dissertation for sake of brevity.

An exhaustive search of the existing literature, Refs. 1 and 2, shows that the problem of column optimization with mixed boundary conditions (elastic restraints) has not received any attention. In addition the generalization of moment of inertia to cross-sectional area relations ($n=1,2,3$) yields important results. Finally, since Tadjbakhsh and Keller solutions show that the optimum column, depending upon the

boundary conditions, must have zero stiffness at some stations, the introduction of the inequality constraint (minimum stiffness $[EI_0]$) is important from a practical manufacturing point of view.

As regards the optimal design of vibrating beams, although Beesack¹³, Schwarz^{14,15,16} investigated the effect of density variation on the extreme values of the natural frequencies of strings, beams and plates, the most significant contributions to the present problem would be those of Niordson¹⁷, Turner¹⁸, Taylor^{19,20} and Brach²¹. Niordson treated the problem of a simply-supported vibrating beam through variational formulation. Turner obtained exact and finite element solutions of minimum mass design, for a specified frequency, of bars and beams fastened at one end with a mass attached at the other end. Taylor also obtained solutions, through the variational formulation for the axial vibrations of bars with and without the inequality constraint and also for the transverse vibrations of a cantilever sandwich beam with a distributed mass loading. Finally, Brach considered the transverse vibrations of beams for all classical boundary conditions and for a relation between the moment of inertia and area of the form $I(x) = c_0 + \rho A(x)$. As with columns, optimization of vibrating beams with elastic restraints does not appear to have been attempted by previous investigators.

The only open literature on plates seems to be that on the optimal design of vibrating circular plates²⁴ for three different boundary conditions while an unpublished report of Harvard University³¹ seems to be, to the author's best knowledge, the only work on the optimal design of a simply-supported plate for stability. In both cases of vibration and stability of the circular plate, due to rotational

symmetry, the resulting governing equations are ordinary nonlinear differential equations which have been solved by some numerical techniques. No work on the optimal design of rectangular plates for vibration and stability seems to have been reported in the open literature.

The problems of optimizing columns and vibrating beams lead to nonlinear ordinary differential equations which are fairly difficult to solve even for the simplest boundary conditions. The difficulty increases when the column or the beam is resting on a continuous elastic foundation with elastically restrained ends. As regards the problem of optimal design of thin plates for vibration and stability, they lead to nonlinear partial differential equations which are again still more difficult to solve. Because of this, one must resort to numerical techniques such as finite elements, finite differences, Galerkin, perturbation or some gradient methods. It is decided to use the finite element displacement method for the following reasons:

- (i) The form of the governing matrix equations for the discretized system is not affected by the type of the corresponding governing differential equations (ordinary or partial) for the continuous system.
- (ii) Generalization to all types of boundary conditions and loadings does not require any special treatment.
- (iii) A wealth of literature on some of the most sophisticated finite elements with explicit derivations of the necessary element matrices is readily available. However, even if such explicitly derived finite element matrices are not

readily available, they can be generated by an automated numerical integration scheme and further, with proper non-dimensionalization, they need be generated just once in the entire lifetime of the finite element method computer program.

- (iv) Finally, the method lends itself very easily to automated programming.

This method is used in the solution of the following two problems:

- (i) Strongest columns with a given volume and relation between the cross-sectional moment of inertia and area of the form $I(x) = \rho A^n(x)$, for various boundary conditions and axial loading with or without an inequality constraint of minimum allowable cross-sectional area. Numerical solutions are obtained for various cases and are discussed in Chapter II.
- (ii) Optimal vibrating beams with a given volume and relation between the cross-sectional moment of inertia and area of the form $I(x) = \rho A^n(x)$, for various boundary conditions, and with a given dead (non-structural) mass distribution and/or an inequality constraint of minimum allowable cross-sectional area and/or a given compressive axial load. Numerical solutions obtained for various cases are discussed in Chapter III.

Furthermore, it is proposed to use the same method to investigate the problems of the optimal design of thin rectangular plates for vibration and stability for some boundary conditions and aspect ratios. Numerical solutions obtained are discussed in Chapter IV.

CHAPTER II

STRONGEST COLUMN

Assumptions and Objective

In the development to follow, consideration is restricted to those columns for which the assumptions stated below are valid.

- (i) The material of the column is isotropic and linearly elastic.
- (ii) Cross-sectional planes before deformation remain plane and normal to the deformed axis of the beam after deformation.
- (iii) The column is sufficiently long with a cross-section possessing a plane of symmetry. The loading and deformation are restricted in this plane of symmetry.
- (iv) The minimum cross-sectional moment of inertia, I , can be expressed in terms of the cross-sectional area, A , by the relation

$$I(x) = \rho A^n(x)$$

where ρ and n are positive constants.

Although n can take on all positive values numerical results will be presented only for three specific values of n namely $n = 1, 2$ and 3 .

Consider such a column of specified length and volume (weight) under various boundary conditions (mixed or not -- with or without springs) and subjected to any given arbitrarily varying axial load

distribution as shown in Figure 2.1.

Next, define the critical load parameter as the smallest factor by which the given axial load distribution has to be scaled in order to produce instability in the column.

The problem, then, is to determine the distribution of material along the length of the column such that the critical load parameter is a maximum (design objective) subject to the constraint that the minimum stiffness anywhere along the length of the column is no smaller than a prescribed value (inequality constraint).

It can be shown that this design objective is equivalent to seeking a minimum weight design for a given critical load.

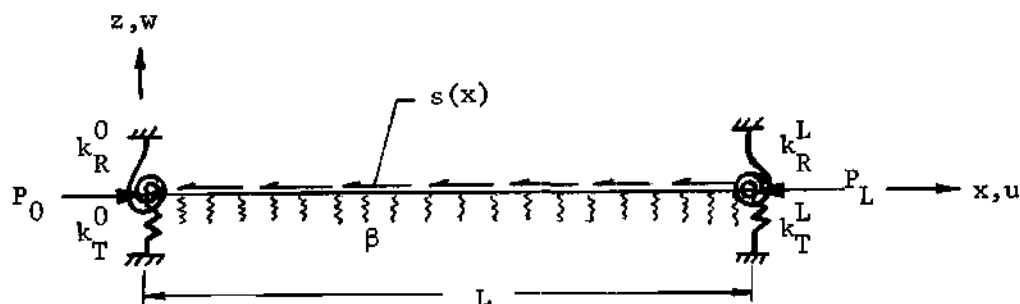


Figure 2.1. A Typical Column on a Continuous Elastic Foundation, Restrained Elastically at the Ends and Subjected to a Varying Axial Load.

Derivation of the Rayleigh Quotient from Energy Principle

From the assumption of plane sections remaining plane and normal to the deformed axis, one has

$$e_{xx} = e_o + z\kappa \quad (2.1.1)$$

where

$$e_o = \frac{du_o}{dx} + \frac{1}{2} \left(\frac{dw}{dx} \right)^2, \quad (2.1.2)$$

$$\kappa = - \frac{d^2 w}{dx^2}, \quad (2.1.3)$$

u_o is the axial displacement of the reference or centroidal axis of the material points of the column and w the lateral displacement of the same points.

The strain energy, U^o , of the column is then given by

$$U^o = \frac{1}{2} \int_0^L \int_A E (e_{xx})^2 dA dx.$$

Substitution for e_{xx} from Eq. (2.1.1) yields

$$U^o = \frac{1}{2} \int_0^L \int_A E \left[\frac{du_o}{dx} + \frac{1}{2} \left(\frac{dw}{dx} \right)^2 - z \left(\frac{d^2 w}{dx^2} \right) \right]^2 dA dx.$$

Upon integrating and utilizing the fact that

$$\int_A z dA = 0$$

(since $z = 0$ is the centroidal axis) the above finally becomes

$$U^o = \frac{1}{2} \int_0^L \left[EA \left\{ \frac{du_o}{dx} + \frac{1}{2} \left(\frac{dw}{dx} \right)^2 \right\}^2 + EI \left(\frac{d^2 w}{dx^2} \right)^2 \right] dx$$

where

$$\int_A z^2 dA = I(x) .$$

Next, the energy stored into the spring supports, U_s^0 , is given by

$$\begin{aligned} U_s^0 = & \frac{1}{2} k_T^0 w^2|_0 + \frac{1}{2} k_T^L w^2|_L + \frac{1}{2} k_R^0 \left(\frac{dw}{dx} \right)^2|_0 + \frac{1}{2} k_R^L \left(\frac{dw}{dx} \right)^2|_L \\ & + \frac{\beta}{2} \int_0^L w^2 dx \end{aligned}$$

and the potential of the external loads (see Fig. 2.1.), T^0 , is given by

$$T^0 = P_L u_o|_L - P_0 u_o|_0 + \int_0^L s(x) u_o dx .$$

Hence, if π denotes the total potential, then

$$\pi = U^0 + U_s^0 + T^0 .$$

By the principle of the stationary value of the total potential, equilibrium is characterized by the vanishing of the first variation of π with respect to the displacements u_o and w .

Hence,

$$\begin{aligned} \delta\pi = & \int_0^L \left\{ EA(u'_0 + \frac{w'^2}{2}) (\delta u'_0 + w' \delta w') + EI w'' \delta w'' + \beta w \delta w \right\} dx + k_T^0 w \delta w|_0 \\ & + k_T^L w \delta w|_L + k_R^0 w' \delta w'|_0 + k_R^L w' \delta w'|_L + P_L \delta u_0|_L \\ & - P_0 \delta u_0|_L + \int_0^L s(x) \delta u_0 dx = 0 \end{aligned} \quad (2.2)$$

where the primes denote differentiation with respect to x . Integrating by parts Eq. (2.2) yields

$$\begin{aligned} - \int_0^L & \left\{ \left[EA(u'_0 + \frac{1}{2} w'^2) \right]' - s(x) \right\} \delta u_0 dx + \int_0^L \left\{ (EI w'')'' - \left[EA(u'_0 \right. \right. \\ & \left. \left. + \frac{1}{2} w'^2) w' \right]' + \beta w \right\} \delta w dx + \left\{ EA(u'_0 + \frac{1}{2} w'^2) \right. \\ & \left. + P_L \right\} \delta u_0|_L - \left\{ EA(u'_0 + \frac{1}{2} w'^2) + P_0 \right\} \delta u_0|_0 + \left\{ EA(u'_0 \right. \\ & \left. + \frac{1}{2} w'^2) w' - (EI w'')' + k_T^L w \right\} \delta w|_L - \left\{ EA(u'_0 \right. \\ & \left. + \frac{1}{2} w'^2) w' - (EI w'')' - k_T^0 w \right\} \delta w|_0 + (EI w'' \\ & \left. + k_R^L w') \delta w'|_L - (EI w'' - k_R^0 w') \delta w'|_0 = 0. \end{aligned}$$

The above gives all equilibrium equations and the associated boundary conditions. Let u_0^0 , w^0 denote the equilibrium configuration. It can

be easily verified that $w^0 \equiv 0$ satisfies the governing differential equation and the boundary conditions on w^0 . Hence, the prebuckled configuration is given by

$$(EAu_o^{0'})' - s(x) = 0 \quad \text{and} \quad w^0 \equiv 0$$

i.e.

$$EAu_o^{0'} = \int_0^x s(\xi) d\xi + c_1$$

or

$$u_o^0 = \int_0^x \frac{1}{EA(\eta)} \left(\int_0^\eta s(\xi) d\xi \right) d\eta + \int_0^x \frac{c_1}{EA(\xi)} d\xi + c_2$$

Assume $u_o^0|_0 = 0$; then it follows that $c_2 = 0$. Also, $EAu_o^{0'}|_0 = -P_0$ implies that $c_1 = -P_0$ and $EAu_o^{0'}|_L = -P_L$ implies that

$$\int_0^L s(x) dx = P_0 - P_L.$$

Hence, finally one has

$$EAu_o^{0'} = -P_0 + \int_0^x s(\xi) d\xi = -S_o(x). \quad (2.3)$$

It is necessary to scale the given applied axial loading by a certain factor λ in order to produce instability in the column. Assume that at

the instant of instability the prebuckled configuration is given by $u_0 = \lambda u_0^0$, $w = w^0 \equiv 0$. Then, it follows that $EAu_0' = -\lambda S_0(x)$.

Next, it is necessary to consider the second variation of the total potential in order to investigate the stability of the prebuckled equilibrium configuration. If $\delta^2\pi|_{u^0, w}$ is greater than zero, then the equilibrium configuration is stable; while if $\delta^2\pi|_{u^0, w}$ is less than zero, the equilibrium configuration is unstable. The critical point is then characterized by $\delta^2\pi|_{u^0, w} = 0$ for some virtual displacements and > 0 for all other virtual displacements. This implies that $\delta^2\pi|_{u^0, w}$ is stationary at the critical point with respect to the virtual displacements. Thus, the factor λ is obtained by requiring that $\delta^2\pi|_{u^0, w} = 0$. That is to say

$$\begin{aligned} \delta^2\pi|_{u^0, w} = & \int_0^L \left\{ EA(\delta u_0')^2 - \lambda S_0(x)(\delta w')^2 + EI(\delta w'')^2 + \beta(\delta w)^2 \right\} dx \\ & + k_T^0(\delta w)^2|_0 + k_T^L(\delta w)^2|_L + k_R^0(\delta w')^2|_0 + k_R^L(\delta w')^2|_L = 0. \end{aligned} \quad (2.4)$$

With the notation $\delta u_0 = u^*$ and $\delta w = w^*$, Eq. (2.4) becomes

$$\begin{aligned} \delta^2\pi|_{u^0, w} = & \int_0^L \left\{ EA(u^{*'})^2 - \lambda S_0(x)(w^{*'})^2 + EI(w^{*''})^2 + \beta(w^*)^2 \right\} dx \\ & + k_T^0(w^*)^2|_0 + k_T^L(w^*)^2|_L + k_R^0(w^{*'})^2|_0 \\ & + k_R^L(w^{*'})^2|_L = 0 \end{aligned}$$

where u^* and w^* denote incremental quantities from the prebuckled configuration at the instant of instability. It then follows from the above that

$$\lambda = \frac{\int_0^L [EI(w^{*''})^2 + EA(u^{*'})^2] dx + U_s^*}{\int_0^L S_o(x)(w^{*'})^2 dx} \quad (2.5)$$

where

$$U_s^* = k_T^0(w^*)^2|_0 + k_T^L(w^*)^2|_L + k_R^0(w^{*'})^2|_0 + k_R^L(w^{*'})^2|_L + \int_0^L \beta^{*2} dx \text{ and}$$

denotes twice the incremental energy stored into the spring supports.

Since, as stated earlier $\delta^2 \pi|_{u^0, w^0}$ is stationary with respect to u^* , setting the variation of $\delta^2 \pi|_{u^0, w^0}$ with respect to this variable independently equal to zero leads to

$$(EAu^{*'})' = 0 \quad (2.6.1)$$

together with the boundary conditions

$$\text{either } EAu^{*'} = 0 \quad \text{or} \quad u^* = 0 \quad \text{at } x = 0, L. \quad (2.6.2)$$

Equations (2.6.1) and (2.6.2) imply that

$$EA(u^{*'}) = 0. \quad (2.7)$$

Since EA is not zero everywhere in the range $0 \leq x \leq L$ it follows that $u^{*'} = 0$ for $0 \leq x \leq L$. The expression for λ can therefore be written as

$$\lambda = \frac{\int_0^L EI (w'')^2 dx + U_s}{\int_0^L S_o(x) (w')^2 dx} \quad (2.8)$$

where for the sake of convenience, it has been decided to drop the stars on w with the understanding that it represents the incremental deformation from the prebuckled configuration and that λ is stationary with respect to w at the critical point.

Formulation of the Optimization Problem

It is required to maximize λ_{cr} (the lowest λ) with respect to variations in the cross-sectional area $A(x)$ subject to the constant volume constraint

$$\int_0^L A dx = V. \quad (2.9)$$

Since $I(x) = \rho A^n(x)$ the new functional that must be extremized is

$$\lambda^* = \frac{\int_0^L E \rho A^n w''^2 dx + U_s}{\int_0^L S_o(x) w'^2 dx} - \lambda_1 \left[\int_0^L A dx - V \right] \quad (2.10)$$

where λ_1 is an undetermined Lagrange multiplier. Since λ^* is stationary with respect to both w and A setting the variations of λ^* with respect

to w and A independently equal to zero leads to the stability equation with the associated boundary conditions and the optimality condition respectively.

$$\begin{aligned} \delta_{w''} \lambda^* = & \frac{2}{\left[\int_0^L S_0(x) w'^2 dx \right]} \left[\int_0^L (E\rho A^n w'')'' \delta w dx + \int_0^L \beta w \delta w dx \right. \\ & + E\rho A^n w'' \delta w' \Big|_0^L - (E\rho A^n w'')' \delta w \Big|_0^L + k_T^0 w \delta w \Big|_0 + k_T^L w \delta w \Big|_L \\ & + k_R^0 w' \delta w' \Big|_0 + k_R^L w' \delta w' \Big|_L - \lambda \left(S_0(x) w' \right) \delta w \Big|_0^L \\ & \left. + \lambda \int_0^L \left(S_0(x) w' \right)' \delta w dx \right] = 0 . \end{aligned}$$

The above implies that

$$[E\rho A^n w'']'' + \lambda [S_0(x) w']' + \beta w = 0 \quad (2.11)$$

with

$$\left. \begin{aligned} E\rho A^n w'' - k_R^0 w' &= 0 \\ (E\rho A^n w'')' + \lambda S_0(x) w' + k_T^0 w &= 0 \end{aligned} \right\} \text{at } x = 0 , \quad (2.12.1)$$

$$\left. \begin{aligned} E\rho A^n w'' + k_R^L w' &= 0 \\ (E\rho A^n w'')' + \lambda S_0(w) w' - k_T^L w &= 0 \end{aligned} \right\} \text{at } x = L . \quad (2.12.2)$$

$$\delta_{A''}^{\lambda*} = \frac{1}{\left[\int_0^L S_0(x) w'^2 dx \right]} \left[\int_0^L \left\{ E \rho n A^{n-1} w''^2 - \lambda_1 \left(\int_0^L S_0(x) w'^2 dx \right) \right\} \delta A dx \right] = 0.$$

If δA is arbitrary, i.e. the cross-sectional area is not prescribed, then it follows that

$$A^{n-1} w''^2 = c^2. \quad (2.13)$$

Equation (2.13) is valid only in those regions where $A(x)$ is not prescribed. If A as determined by the use of Eq. (2.13) happens to be less than A_0 , (A_0 being the prescribed minimum value of area) then the constraint $A = A_0$ must be satisfied.

The optimality condition as given by Eq. (2.13) can also be expressed in terms of the linear strain energy density and the average strain energy density as follows:

the linear strain energy density, W , is given by

$$W = \frac{1}{2} E I w''^2 = \frac{1}{2} E \rho A^n w''^2 = \frac{E \rho A}{2} [A^{n-1} w''^2]$$

and

$$\frac{W}{A} = \frac{E \rho c^2}{2} = \text{constant}. \quad (2.14)$$

Also, the total strain energy of the entire column, U , is

$$U = \int_0^L W \, dx = \int_0^L \frac{W}{A} A \, dx = \frac{E_0 c^2}{2} V.$$

Thus finally

$$\frac{U}{V} = \frac{W}{A} = \frac{E_0 c^2}{2} = \text{constant}. \quad (2.15)$$

In Eq. (2.15) the optimality condition is independent of n . It is seen that for an optimum column the linear strain energy density per unit area is equal to the average strain energy density in the column (a constant).

Method of Solution and the Optimization Procedure

Method of Solution

Mathematically stated the problem of unconstrained optimization (i.e. without any inequality constraint) of columns reduces to the determination of functions $w(x)$ and $I(x)$ or $A(x)$ which satisfy the following three equations together with certain given boundary conditions.

$$[E_0 A^n w'']'' + \lambda [S_0(x) w']' + \beta w = 0 \quad (2.16)$$

$$A^{n-1} w''^2 = c^2 \quad (2.17)$$

and

$$\int_0^L A \, dx = V . \quad (2.18)$$

It is understood that λ is the lowest eigenvalue of Eq. (2.16). By elimination of one variable Eqs. (2.16) and (2.17) could be reduced to one single non-linear integro-differential equation. In the case of a constant axial load with $\beta = 0$ the same would be an ordinary non-linear differential equation. Exact solutions of the latter have been obtained as mentioned in the Introduction, by Tadjbakhsh and Keller⁴ for all classical boundary conditions and $n = 2$. However, for columns with elastically restrained ends and $\beta \neq 0$, an exact solution seems to be out of the question, and one is forced to resort to numerical techniques such as the finite elements, finite differences, Galerkin or perturbation methods. The finite element displacement method being a direct derivative of the principle of stationary value of total potential seems to be a very good candidate for the solution of the present problem.

The details of the finite element displacement method as applied to buckling of columns are developed in full in the Appendix A.

In terms of the finite elements Eq. (2.16) becomes

$$[[K] - \lambda [K_G]] \{q\} = \{0\} \quad (2.19)$$

where $[K]$ is the assembled nonsingular stiffness matrix for the entire column including the effect of the elastic foundation and the elastic restraints if any, λ is the lowest eigenvalue, $[K_G]$ the assembled

nonsingular stability matrix for the entire column and $\{q\}$ the vector of the unrestrained degrees of freedom of the column.

Equation (2.14) when multiplied throughout by A and integrated over the extent of, say, the i^{th} element takes the form

$$\frac{U_i}{v_i} = \frac{U}{V} = \frac{Epc^2}{2} = \text{constant} \quad (2.20)$$

where

$$\left. \begin{array}{l} U_i = \text{strain energy of the } i^{\text{th}} \text{ element} \\ v_i = \text{volume of the } i^{\text{th}} \text{ element} \end{array} \right\} i = 1, \dots, m$$

$$U = \sum_{i=1}^m U_i$$

$$V = \sum_{i=1}^m v_i .$$

Finally, Eq. (2.18) becomes for the discretized system

$$\sum_{i=1}^m A_i \ell_i = \sum_{i=1}^m \left(\frac{I_i}{\rho} \right)^{1/n} \ell_i = V . \quad (2.21)$$

Next, it remains to determine I_i , $i=1\dots m$; $\{q\}$ and the corresponding λ_{cr} which satisfy Eqs. (2.19), (2.20) and (2.21). This can be accomplished through the use of an iterative scheme to be described in the following section.

Unconstrained Optimization Procedure

It is attempted to meet the optimality condition by successive iterations starting from a column of uniform cross-section (i.e. all the m elements having the same cross-sectional moment of inertia complying with the given volume V). Each iteration involves the solution of the eigenvalue problem as expressed by Eq. (2.19), for an assumed moment of inertia distribution, to obtain the lowest eigenvalue and the corresponding eigenvector. Having obtained λ_{cr} and $\{q\}_{cr}$ from Eq. (2.19) the average linear strain energy density in each element can be calculated as follows:

$$\frac{U_i}{v_i} = \frac{1}{2} \frac{\{q_i\}^T [k_i] \{q_i\}}{\left(\frac{I_i}{\rho}\right)^{1/n} \ell_i} . \quad (2.22)$$

This distribution of the linear strain energy density is utilized for deciding the inertias of the elements for the next iteration. The recurrence relation for doing so being motivated by the following reasoning.

Assume that the r^{th} iteration begins with the i^{th} finite element having the moment of inertia I_i^r ($i=1\dots m$). After determining the associated eigenvalue and the eigenvector, the average strain energy density in each element and the average strain energy density for the entire column are computed; these quantities are denoted by U_i^r/v_i^r ($i=1,\dots,m$) and U^r/V , where $U^r = \sum_{i=1}^m U_i^r$ and $V = \sum_{i=1}^m v_i^r$ (specified volume). Suppose that the optimality condition is not satisfied; that is

$U_i^r/v_i^r \neq U^r/V$ for all values of i . Therefore, it is now necessary to select new values for each I_i , denoted by I_i^{r+1} , such that at the end of the $(r+1)$ st iteration, U_i^{r+1}/v_i^{r+1} is closer to U^{r+1}/V for all finite elements.

The $(r+1)$ st iteration begins with the requirement that

$$\frac{U_i^{r+1}}{v_i^{r+1}} = c^{r+1} \frac{U^r}{V}, \quad i=1,2,\dots,m$$

which is equivalent to a statement that

$$\frac{U^{r+1}}{V} = c^{r+1} \frac{U^r}{V}.$$

This equation can be rewritten as

$$c^{r+1} \frac{U^r}{V} = \frac{U_i^{r+1}}{U_i^r} \frac{U_i^r}{v_i^r} \frac{v_i^r}{v_i^{r+1}}, \quad i=1,2,\dots,m. \quad (2.23)$$

The quantity v_i^r/v_i^{r+1} can easily be expressed in terms of the moment of inertia values as follows:

$$\frac{v_i^r}{v_i^{r+1}} = \frac{\ell_i \left(\frac{I_i^r}{\rho} \right)^{1/n}}{\ell_i \left(\frac{I_i^{r+1}}{\rho} \right)^{1/n}} = \left(\frac{I_i^r}{I_i^{r+1}} \right)^{1/n} \quad (2.24)$$

the ratio U_i^{r+1}/U_i^r is taken in the form

$$\frac{U_i^{r+1}}{U_i^r} = \left(\frac{I_i^r}{I_i^{r+1}} \right)^\alpha \quad \alpha > 0, \quad i=1,2,\dots,m. \quad (2.25)$$

This relation is based on the following reasoning. Since the total volume is constant, it follows that there will be some finite elements with an increase in moment of inertia and some with a decrease. After this redistribution of moment of inertia, it is assumed that those elements with increased (decreased) inertia will have a decrease (increase) in buckling curvature; and since the strain energy involves the curvature squared, the net result is a decrease (increase) in energy. From this argument follows the inverse relationship given by Eq. (2.25)

After substitution of Eqs. (2.24) and (2.25) into Eq. (2.23), the recurrence relation finally assumes the form

$$I_i^{r+1} = b^{r+1} \left[\frac{U_i^r / v_i^r}{U^r / V} \right]^p I_i^r \quad (2.26)$$

where $p = n/(n\alpha + 1)$ and $b^{r+1} = (1/C^{r+1})^p$. The constant b^{r+1} is determined by the requirement

$$\sum_{i=1}^m \left(\frac{I_i^{r+1}}{\rho} \right)^{1/n} \ell_i = V \quad (2.27)$$

and the value of the exponent p is selected such that

$$\lambda_{cr}^{r+1} \geq \lambda_{cr}^r.$$

It will now be shown that one can always select a positive value of the exponent p in Eq. (2.26) which will insure that

$$\lambda_{cr}^{r+1} \geq \lambda_{cr}^r .$$

The proof will be presented for a continuous system with only minor modifications necessary for a discrete system.

From Rayleigh's quotient one has for the continuous system

$$\lambda_{cr}^{r+1} = \frac{\int_0^L EI^{r+1} (w^{r+1'})^2 dx + U_s^{r+1}}{D_n^{r+1}} \quad (2.28.1)$$

where w^{r+1} is the eigenvector corresponding to the lowest eigenvalue λ_{cr}^{r+1} and

$$D_n^{r+1} = \int_0^L S_0(x) (w^{r+1'})^2 dx . \quad (2.28.2)$$

The recurrence relation for the continuous system can be written as

$$I^{r+1} = b^{r+1} I^r R^p \quad (2.29.1)$$

where

$$R = \frac{W^r V}{A^r U^r} , \quad (2.29.2)$$

W^r being the linear strain energy density, A^r the area of cross-section and U^r the total strain energy in the r^{th} iteration. The exponent p is

assumed to be positive and the constant b^{r+1} has to be evaluated from the volume constraint

$$\int_0^L \left(\frac{I^{r+1}}{\rho} \right)^{1/n} dx = V$$

i.e.

$$(b^{r+1})^{1/n} \int_0^L \left(\frac{I^{r+1}}{\rho} \right)^{1/n} (R)^{p/n} dx = V$$

or

$$b^{r+1} = \frac{V^n}{\left[\int_0^L \left(\frac{I^r}{\rho} \right)^{1/n} (R)^{p/n} dx \right]^n} . \quad (2.30)$$

Note that $(I^r/\rho)^{1/n}$ is not only a continuous function of x but greater than or equal to zero for $0 \leq x \leq L$ and further $(R)^{p/n}$ is also continuous for $0 \leq x \leq L$, since R is bounded. Hence, by the mean value theorem of integral calculus¹¹ the denominator, D , of Eq. (2.30) can be written as

$$D = \left\{ \left[\int_0^L \left(\frac{I^{r+1}}{\rho} \right)^{1/n} dx \right] (R)^{p/n} \Big|_{x=\xi_1} \right\}^n ; 0 < \xi_1 < L$$

and since

$$\left[\int_0^L \left(\frac{I^{r+1}}{\rho} \right)^{1/n} dx \right]^n = V^n$$

it follows that

$$b^{r+1} = \frac{1}{R^p|_{x=\xi_1}}$$

or

$$I^{r+1} = I^r \frac{R^p}{(R^p)|_{x=\xi_1}} \quad . \quad (2.31)$$

Substituting for I^{r+1} from Eq. (2.31) into Eq. (2.28.1) gives

$$\lambda_{cr}^{r+1} = \frac{\int_0^L EI^r (w^{r+1})^2 \left[\frac{R^p}{R^p|_{x=\xi_1}} \right] dx + U_s^{r+1}}{D_n^{r+1}} \quad .$$

By another application of the mean-value theorem, the above can be written as

$$\lambda_{cr}^{r+1} = \frac{\left[\int_0^L EI^r (w^{r+1})^2 dx \right] \left[\frac{R^p|_{x=\xi_2}}{R^p|_{x=\xi_1}} \right] + U_s^{r+1}}{D_n^{r+1}} \quad , \quad 0 < \xi_2 < L \quad .$$

Let $R(\xi_1) = R_1$ and $R(\xi_2) = R_2$. Note that R_1 and R_2 are positive by virtue of the positive definiteness of the strain energy density. Then the expression for λ_{cr}^{r+1} can be written as

$$\lambda_{cr}^{r+1} = \frac{\left[\int_0^L EI^r (w^{r+1})^2 dx \right] \left[\frac{R_2}{R_1} \right]^p + U_s^{r+1}}{D_n^{r+1}} \quad . \quad (2.32)$$

Since w^{r+1} is a kinematically admissible displacement field for the moment of inertia distribution I^r , it follows that

$$\frac{\int_0^L EI^r (w^{r+1})^2 dx + U_s^{r+1}}{D_n^{r+1}} \geq \lambda_{cr}^r. \quad (2.33.1)$$

Assume that the left hand side of Eq. (2.33.1) is equal to $\lambda_{cr}^r (1 + \epsilon)$ where $\epsilon > 0$. Then

$$\lambda_{cr}^r (1 + \epsilon) D_n^{r+1} - U_s^{r+1} = \int_0^L EI^r (w^{r+1})^2 dx > 0. \quad (2.33.2)$$

Next, from Eqs. (2.32) and (2.33.1) it is clear that if $R_2/R_1 \geq 1$ it is guaranteed that $\lambda_{cr}^{r+1} \geq \lambda_{cr}^r$ for any $p > 0$. However if $(R_2/R_1) < 1$ the question arises "Does a value of $p > 0$ exist such that $\lambda_{cr}^{r+1} \geq \lambda_{cr}^r$?" Assume that $p > 0$ does exist. This means that

$$\begin{aligned} \frac{\left[\int_0^L EI^r (w^{r+1})^2 dx \right] \left[\frac{R_2}{R_1} \right]^p + U_s^{r+1}}{D_n^{r+1}} &= \lambda_{cr}^{r+1} \\ &= (1 + \delta) \lambda_{cr}^r, \quad \delta > 0. \quad (2.34) \end{aligned}$$

Hence,

$$(1 + \delta) \lambda_{cr}^{r+1} D_n^{r+1} - U_s^{r+1} = \left[\int_0^L EI^r (w^{r+1})^2 dx \right] \left[\frac{R_2}{R_1} \right]^p.$$

From Eq. (2.33.2), it therefore follows that

$$\left[\frac{R_2}{R_1} \right]^p \geq \frac{\lambda_{cr}^r (1 + \delta) D_n^{r+1} - U_s^{r+1}}{\lambda_{cr}^r (1 + \epsilon) D_n^{r+1} - U_s^{r+1}}$$

or

$$p \leq \log \left\{ \frac{\lambda_{cr}^r (1 + \delta) D_n^{r+1} - U_s^{r+1}}{\lambda_{cr}^r (1 + \epsilon) D_n^{r+1} - U_s^{r+1}} \right\} / \log \left[\frac{R_2}{R_1} \right]. \quad (2.35)$$

It can be seen that the right hand side of Eq. (2.35) exists by virtue of Eq. (2.34) and is positive. Hence this value of p given by Eq. (2.35) is sufficient to guarantee that

$$\lambda_{cr}^{r+1} \geq \lambda_{cr}^r.$$

It should be noted at this point, that at any stage during the iterative scheme when $R(x)$ does not vanish anywhere along the length of the column, in other words if R_{\max}/R_{\min} is finite, it can be shown by proceeding similarly as before that a negative value of p does also exist which guarantees that $\lambda_{cr}^{r+1} \geq \lambda_{cr}^r$. Since it has been proposed to start with a uniform cross-section column, it is well known that regardless of the boundary conditions there will always be a point or points in the range $0 \leq x \leq L$ at which $R(x)$ vanishes and hence, at least for the continuous system, it is imperative to start the iterative scheme with $p > 0$ and continue the iterative scheme with $p > 0$ until it is guaranteed

that $R(x) \neq 0$ for $0 \leq x \leq L$. Although for the discretized system the corresponding quantity $(U_i^r V)/(v_i^r U^r)$ is a finite quantity, the ratio

$$\left[\frac{U_i^r V}{v_i^r U^r} \right]_{\max} / \left[\frac{U_j^r V}{v_j^r U^r} \right]_{\min}$$

is still an extremely large number especially if m is a fairly large number and again it is imperative to start the iterative scheme with $p > 0$ in order to achieve a fairly rapid convergence.

If one begins with the assumption that $\alpha = 1$ in Eq. (2.26) the initial value of p can be assumed to be $(n/n+1)$. The iterative scheme can be continued with this value of p for as long as $\lambda_{cr}^{r+1} > \lambda_{cr}^r$. If $\lambda_{cr}^{r+1} < \lambda_{cr}^r$ then the value of p is reduced (see Eq. (2.35)) by a factor of $\frac{1}{2}$ or $\frac{1}{4}$ and the iteration is repeated. This process is carried on until no substantial change either in the value of λ_{cr} or the moment of inertia of each element is possible and the linear strain energy density distribution is essentially uniform. It must be stated at this point that starting the iterative scheme with a value of p equal to $0.75(n/n+1)$ or $0.5(n/n+1)$ or less for columns with rotational springs of moderate stiffness (see Fig. 2.6) is found to be more suitable from the point of view of the number of effective iterations necessary for convergence.

To summarize, as long as $R(x)$ is different from unity Eq. (2.29) with a suitable value of p guarantees that $\lambda_{cr}^{r+1} \geq \lambda_{cr}^r$. Thus assuming that there is a unique solution the iterative procedure guarantees a monotonic convergence to the maximum load though not always via a

monotonic convergence of the linear strain energy density distribution.

Constrained Optimization Procedure

In the case of the inequality constraint, assume the value of the prescribed minimum inertia to be I_0 .

The constrained optimization proceeds exactly in the same manner as the unconstrained optimization until such time at which the inertias of some elements violate the inequality constraint. This can be determined by checking the final value of the inertia of each element corresponding to Eq. (2.26) in each iteration against the prescribed minimum value I_0 . The inertias of those elements which violate the inequality constraint are arbitrarily set equal to the prescribed minimum value, I_0 , while the inertias of the remaining elements are adjusted to satisfy the volume constraint

$$\sum_{i=1}^j \left(\frac{I_i^{r+1}}{\rho} \right)^{1/n} \ell_i = V_1$$

where V_1 = total volume minus the volume of the effective elements with prescribed inertias. It should be noted that in the case of the inequality constraint the strain energy density will be equal to a constant only in those region where the inequality constraint is not effective. The regions within which the inequality constraint is effective the strain energy density will have different values.

Numerical Results and Conclusions

The method commonly used for the solution of the eigenvalue

problem as specified by Eq. (2.19), namely

$$[K] - \lambda[K_G] \{q\} = \{0\}$$

is the matrix iteration technique which converges to the highest eigenvalue. Premultiplying both sides of Eq. (2.19) by $[K]^{-1}$ yields

$$[K]^{-1} [K_G] - \frac{1}{\lambda} [I] \{q\} = \{0\}$$

i.e.

$$[F] - \omega[I] \{q\} = \{0\} \quad (2.36)$$

where

$$[F] = [K]^{-1} [K_G] \text{ and } \omega = \frac{1}{\lambda}.$$

Matrix iteration with an arbitrary vector converges to ω_{\max} and the corresponding eigenvector. The critical load parameter is then given by $\lambda_{cr} = (1/\omega_{\max})$.

Due to ill-conditioning of the stiffness matrix, rapid convergence to an accurate eigenvector is almost impossible with a finite number of iterations. This can be overcome by the following perturbation technique. Assume λ_{cr} and $\{q\}_{cr}$ obtained by the matrix iteration

technique to be approximations to the exact solutions. Using this λ_{cr} and $\{q\}_{cr}$ the residual vector can be computed as:

$$\{r\} = \left[[K] - \lambda_{cr} [K_G] \right] \{q\}_{cr} . \quad (2.37)$$

Assume that $\lambda_{exact} = \lambda_{cr} + \Delta\lambda$ and $\{q\}_{exact} = \{q\}_{cr} + \{\Delta q\}$. Then, it follows that

$$\left[[K] - (\lambda_{cr} + \Delta\lambda) [K_G] \right] \{q_{cr} + \Delta q\} = \{0\} .$$

Expanding the above and using Eq. (2.37) one has:

$$\{r\} + [K] \{\Delta q\} - \Delta\lambda [K_G] \{q\}_{cr} - \Delta\lambda [K_G] \{\Delta q\} - \lambda_{cr} [K_G] \{\Delta q\} = \{0\} . \quad (2.38)$$

Discarding the second order terms Eq. (2.38) becomes

$$\{r\} + \left[[K] - \lambda_{cr} [K_G] \right] \{\Delta q\} - \Delta\lambda [K_G] \{q\}_{cr} = \{0\} . \quad (2.39)$$

Since $\{\Delta q\}$ is a correction to the eigenvector $\{q\}_{cr}$ any one of the components of $\{\Delta q\}$ can be arbitrarily set equal to zero. Then Eq. (2.39) constitutes a system of n equations in n unknowns which are the $n-1$ components of $\{\Delta q\}$ and $\Delta\lambda$. Solution of this system of equations yields the desired corrections. With new approximations λ_N and $\{q\}_N$ the new residual vector can be computed and the norm of this residual vector can be determined. If this norm is found to be greater than a preset

quantity the process can be repeated. The convergence of the process is extremely rapid and for further details the reader is referred to Ref. 12.

In the case of columns, since the first two eigenvectors and eigenvalues are well separated, the eigenvector and eigenvalue of the zeroth iteration (i.e. corresponding to the uniform cross-section column) are the starting quantities of the first iteration of the optimization procedure. This necessitates that changes in moment of inertias of the elements in the first and subsequent iterations be small. Accomplishment of the above requires that the assumed value of p be small. This is another reason for starting the iterative scheme with a value of p less than $n/n+1$ in the case of columns with moderately stiff rotational springs (see Fig. 2.6). Using these known approximations and applying the perturbation technique outlined previously the corresponding exact quantities can be determined without having to invert an ill-conditioned stiffness matrix followed by an invariably large number of matrix iterations. The same procedure is adopted for successive iterations of the optimization procedure resulting in a substantial saving of computer time and a high accuracy of the computed eigenvectors and eigenvalues, which is extremely essential for the success of the optimization procedure.

Conclusions

The criterion for convergence on the optimality condition is

$$\left[(U_i/v_i)_{\max} / (U_j/v_j)_{\min} - 1.0 \right] \times 100 \leq 0.50 .$$

It is mandatory to define convergence based on the average linear strain energy density and not on the critical load parameter, because the average linear strain energy density may be highly non-uniform and yet the critical load parameter may be extremely close to its final value with the subsequent increase being hardly a fraction of one per cent.

The number of iterations required is small for all the classical boundary conditions and some of the elastically restrained cases. The agreement of the results of the finite element solution with the exact solution (Ref. 4) is excellent. Since the optimum moment of inertia distributions and critical load parameters for the simply-supported and clamped-clamped boundary conditions can be obtained from the corresponding quantities of a clamped-free column, results are presented for the latter. The critical load parameter is in error by about one per cent with the exact value, while the curve obtained by joining the mid-points of the steps of the finite element solution seems to be a very good approximation for the exact moment of inertia distribution (see Fig. 2.2).

Convergence is found to be rather slow for the case of a column clamped at one end and supported at the other with an infinitely stiff translational spring and a moderately stiff rotational spring, especially for $n=2,3$. However even in this case, the critical load parameter achieved 99% of its maximum load after only five or six iterations.

The number of iterations required is not only a function of the degree of nonlinearity (i.e. higher values of n) but also a function of the element and nodal disposition. However, the number of iterations does not bear a direct relation to the number of elements. The optimum

moment of inertia distribution and the critical load parameter are also affected to some extent by the nodal disposition with regard to points of inflection (see Fig. 2.3).

The iterative scheme used demands an extremely accurate calculation of the critical load parameter and the corresponding mode shape. All the calculations are therefore performed in double precision. As the number of iterations increases the critical load parameter does not change significantly, while the moment of inertia distribution does change until the optimality condition is met. Hence, if the critical load parameter is not determined accurately to several decimal places it may not be possible to find values of p that will lead to higher and higher values of the load parameter.

Figures 2.4 through 2.6 show the optimum moment of inertia distributions for three typical classes of elastically restrained cases. Figure 2.4 is the case of a column clamped at one end and supported at the other on a translational spring. If the point of inflection is defined to be the point at which the moment vanishes for $0 < x < L$, then it can be easily seen with the use of the stress-strain law and the optimality condition that the point of inflection corresponds to the point of least moment of inertia i.e. the element which contains this point. Thus Fig. 2.4 shows the shift of the point of inflection with increased spring stiffness, approaching the clamped-pinned condition. In fact, a parametric study of this case shows the gradual change of the boundary conditions and the corresponding optimum moment of inertia distributions from a pure cantilever case to an intermediate simply-supported case and finally to a clamped-pinned case.

Figure 2.5 is the case of a column pinned at one end and supported at the other with an infinitely stiff translational spring and a moderately stiff rotational spring. The limiting cases are the simply-supported and clamped-pinned conditions. This figure also shows the effect of imposing the inequality constraint which is effective for elements 1, 12 and 13 resulting in a change of the overall moment of inertia distribution and a slight reduction of the critical load.

Figure 2.6 is the case of a column clamped at one end and supported at the other with an infinitely stiff translational spring and a moderately stiff rotational spring. The limiting cases are the clamped-pinned and the fully clamped-clamped conditions. This figure also shows the comparison between the fully clamped-clamped case and the elastically restrained case. The convergence for the elastically restrained case is extremely slow in comparison with the fully clamped-clamped case, which converged within a matter of three to four iterations.

Figure 2.7 is the case of a cantilever column under a linearly varying axial load distribution. It is seen that the maximum critical load parameter is nearly twice that of the corresponding value for a uniform column of the same volume.

Finally Fig. 2.8 shows the optimum moment of inertia distributions for a simply-supported column under constant axial load for two different values of the foundation modulus β . It can be seen that for a relatively flexible foundation the material distribution is similar to that of a simply-supported column, but with a relatively stiff foundation, the material distribution is similar to two, three or higher

simply-supported columns over the same length.

In general, through the use of the finite element displacement method, optimization of columns under all possible boundary conditions and destabilizing loads can be successfully accomplished.

It can be seen that although ρ has been assumed to be a constant throughout this development the cases for which ρ is a function of x or for which n takes on different values over different portions of the column or for which $I(x) = c_0 + \rho A(x)$ can be treated very similarly. This will be briefly touched upon in the following chapter in connection with the optimal vibrating beam.

Numerical results for some typical cases are tabulated in Tables 2.1 through 2.5. In these tables, the symbol $(I_e)_i$ is used to denote the quantity $I_i / (\rho(V/L)^n)$, the symbol c_i^2 to denote the quantity $(U_i V / v_i U)$ and the symbols λ_{OPT} and λ_U to denote the critical loads of the finite element models with the optimum and uniform moment of inertia distributions respectively.

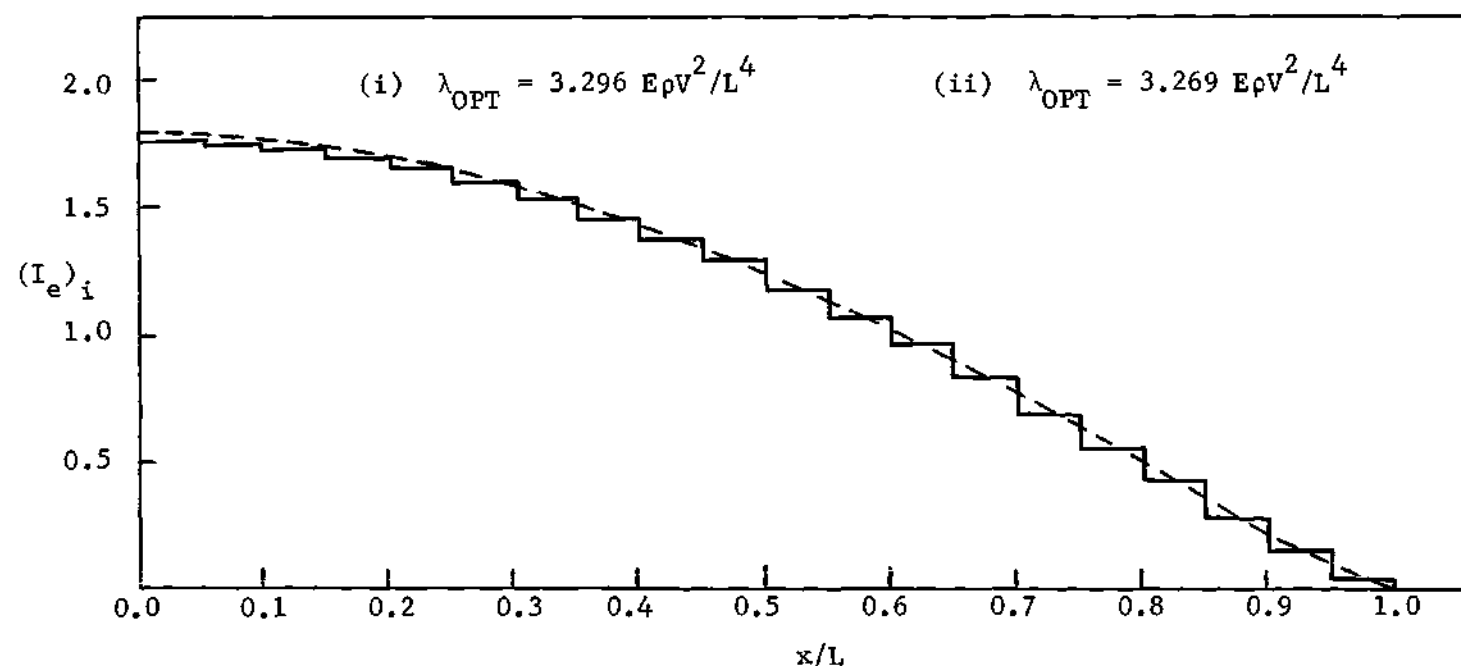


Figure 2.2. Optimum Moment of Inertia Distribution for a Column with
 $k_T^0 = \infty$, $k_R^0 = \infty$, $k_T^L = 0$, $k_R^L = 0$; $m = 20$; $n = 2$;

- (i) ----- Exact Solution (Reference 4)
(ii) ——— Finite Element Solution

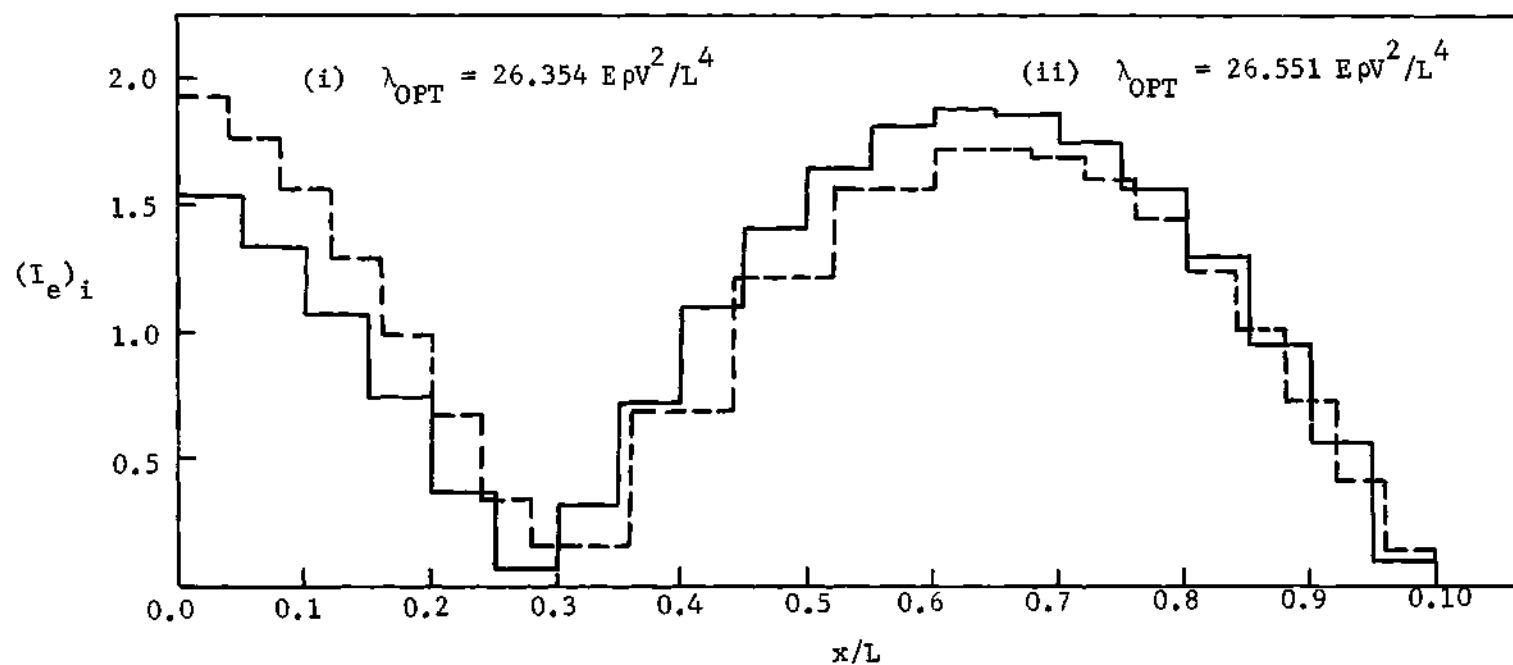


Figure 2.3. Optimum Moment of Inertia Distribution for a Column with
 $k_T^0 = \infty$, $k_R^0 = \infty$, $k_T^L = \infty$, $k_R^L = 0$; $m = 20$; $n = 2$;

- (i) ----- Unequal Subdivisions
(ii) ————— Equal Subdivisions

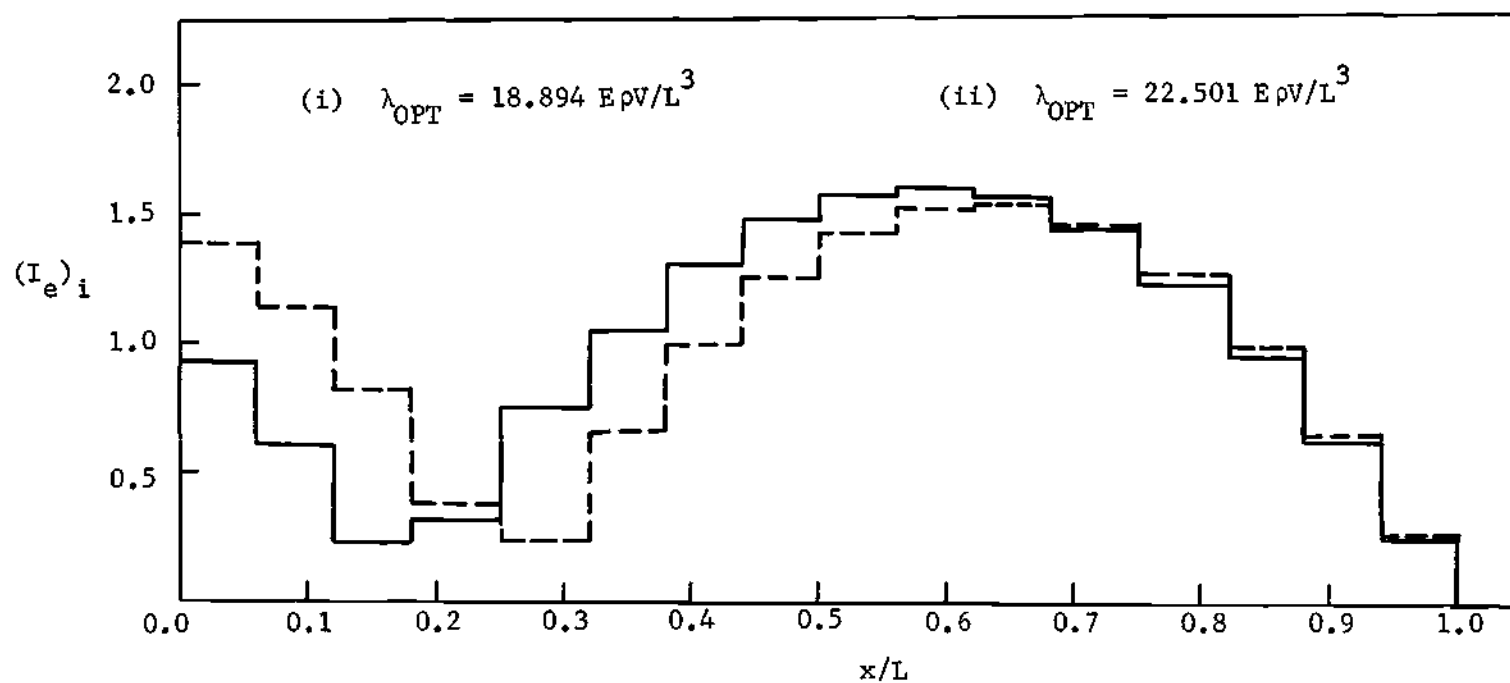


Figure 2.4. Optimum Moment of Inertia Distribution for a Column with
 $k_T^0 = \infty$, $k_R^0 = \infty$, $k_R^L = 0$; $m = 16$; $n = 1$;

- (i) — $k_T^L = 25 E \rho V / L^4$;
(ii) - - - $k_T^L = 50 E \rho V / L^4$.

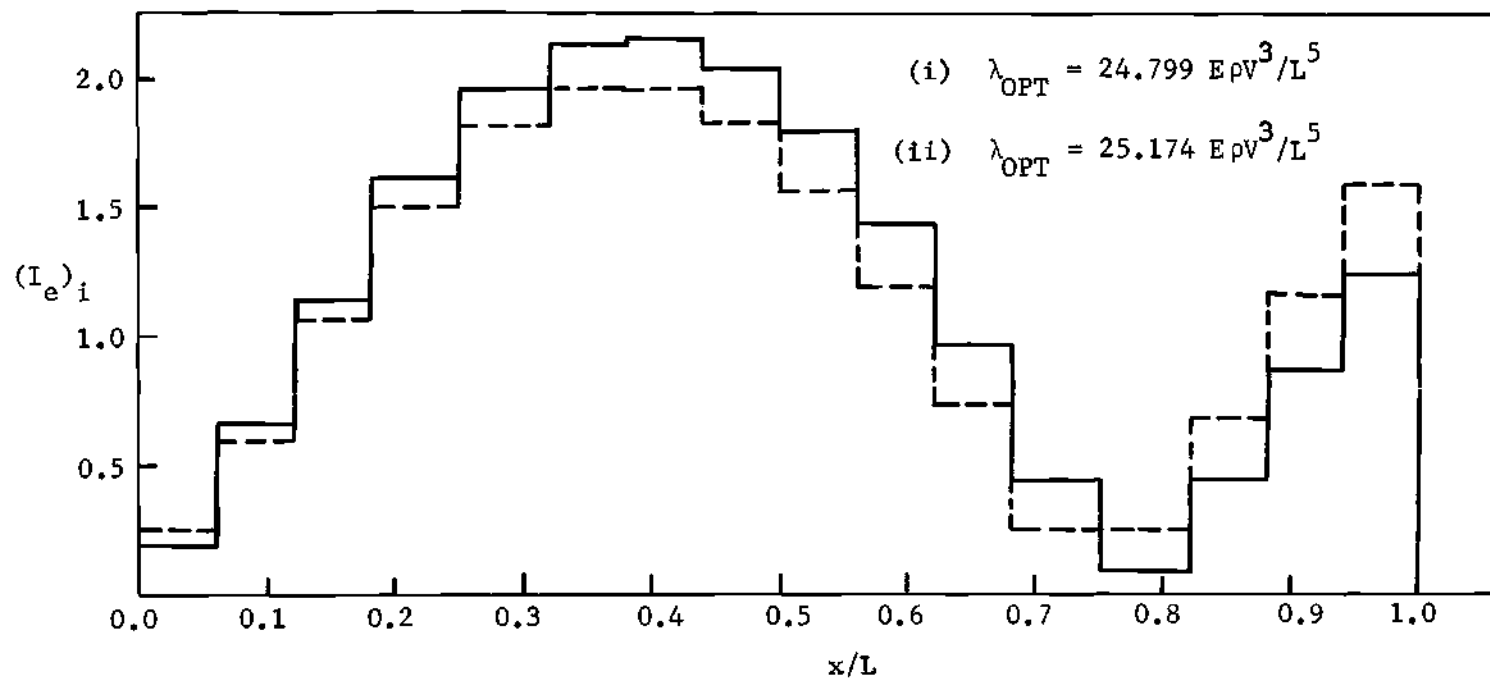


Figure 2.5. Optimum Moment of Inertia Distribution for a Column with
 $k_T^0 = \infty$, $k_R^0 = 0$, $k_T^L = \infty$, $k_R^L = 25 E \rho V^3 / L^4$; $m = 16$; $n = 3$;

- (i) ----- Constrained $I \geq 0.25 \rho V^3 / L^3$
(ii) ——— Unconstrained

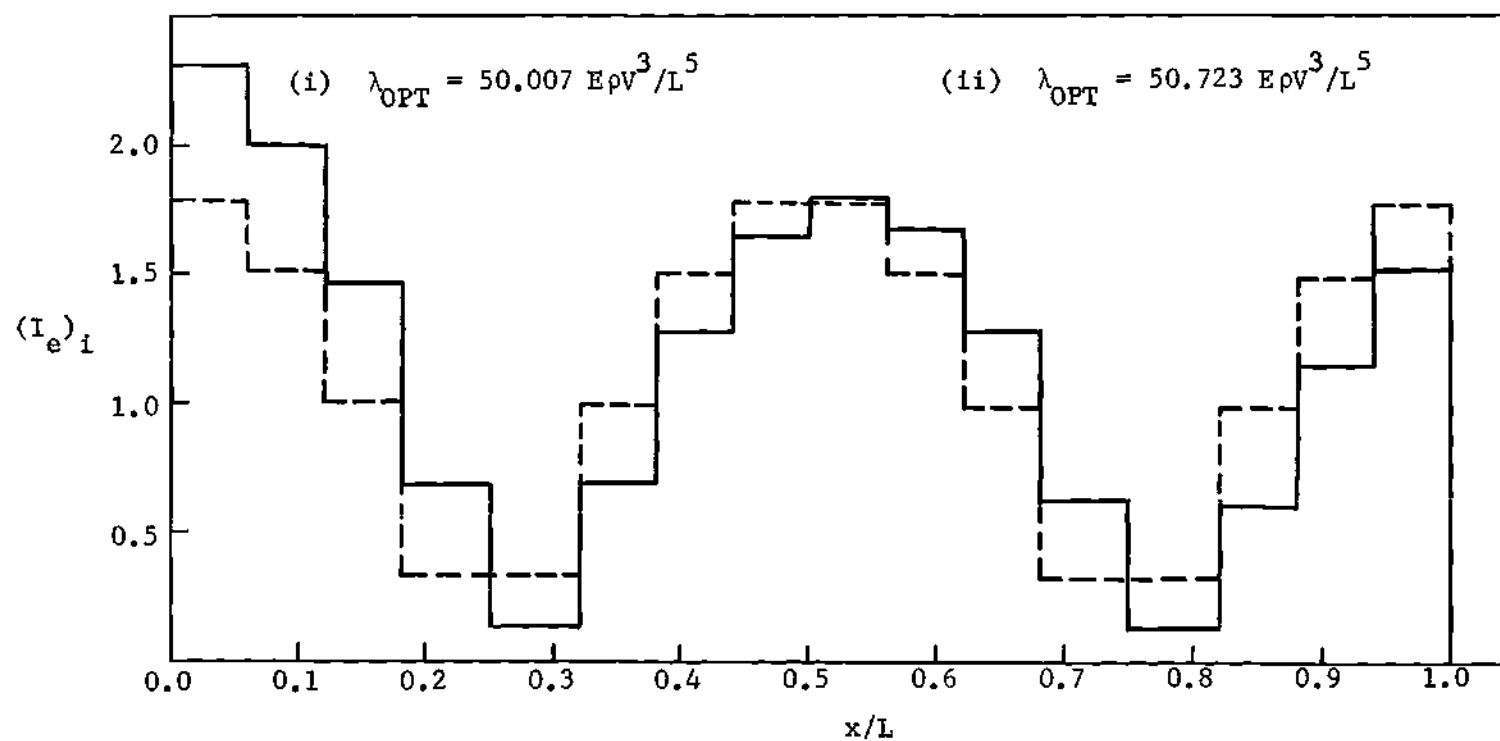


Figure 2.6. Optimum Moment of Inertia Distribution for a Column with

$$k_T^0 = \infty, k_R^0 = \infty, k_T^L = \infty, m = 16; n = 3;$$

(i) $\text{----- } k_R^L = 50 E \rho V^3 / L_4;$

(ii) $\text{——— } k_R^L = \infty.$

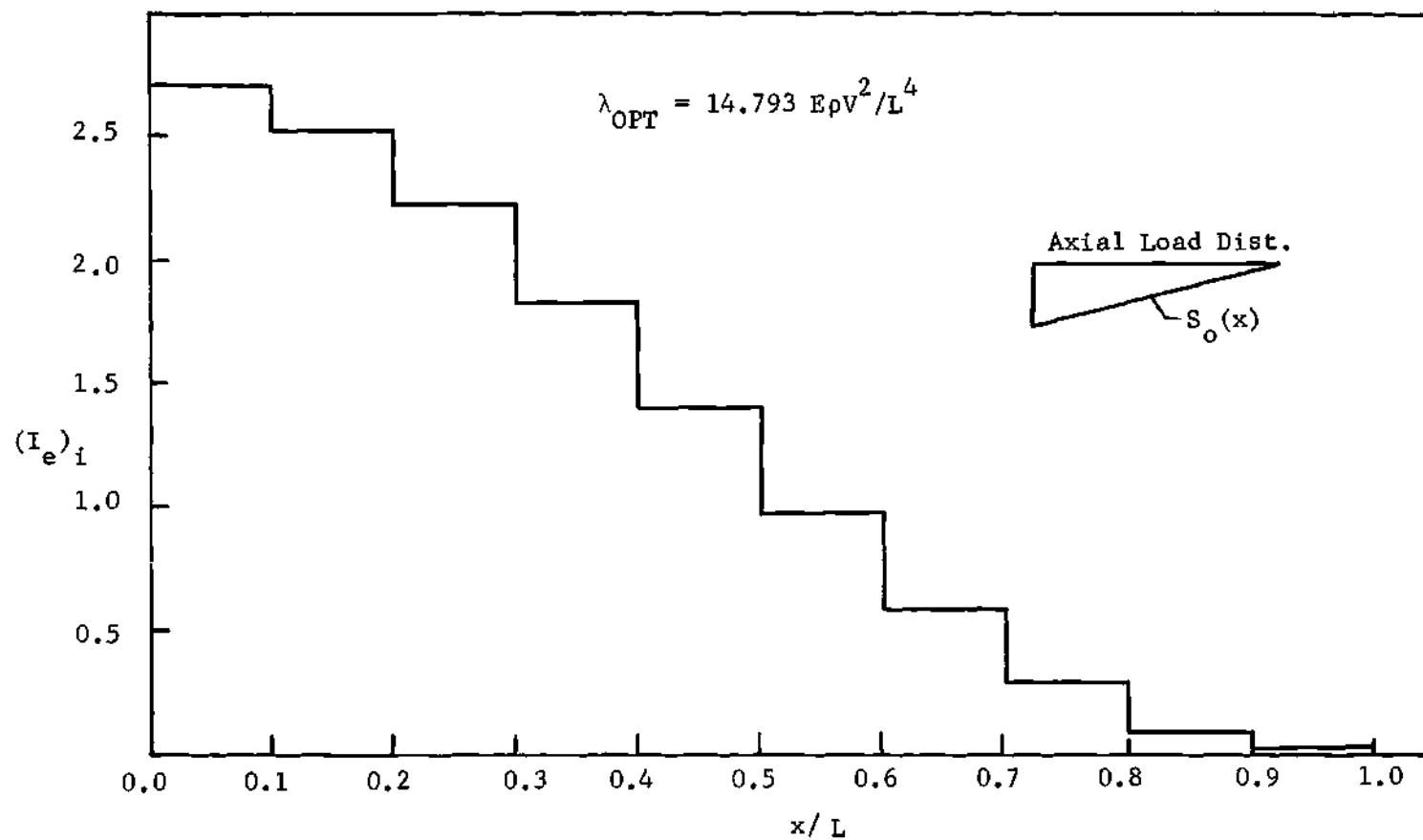


Figure 2.7. Optimum Moment of Inertia Distribution for a Column with $k_T^0 = \infty$, $k_R^0 = \infty$, $k_T^L = 0$, $k_R^L = 0$; $S_o(x) = E \rho V^2 (L-x)/L^5$; $m = 10$; $n = 2$

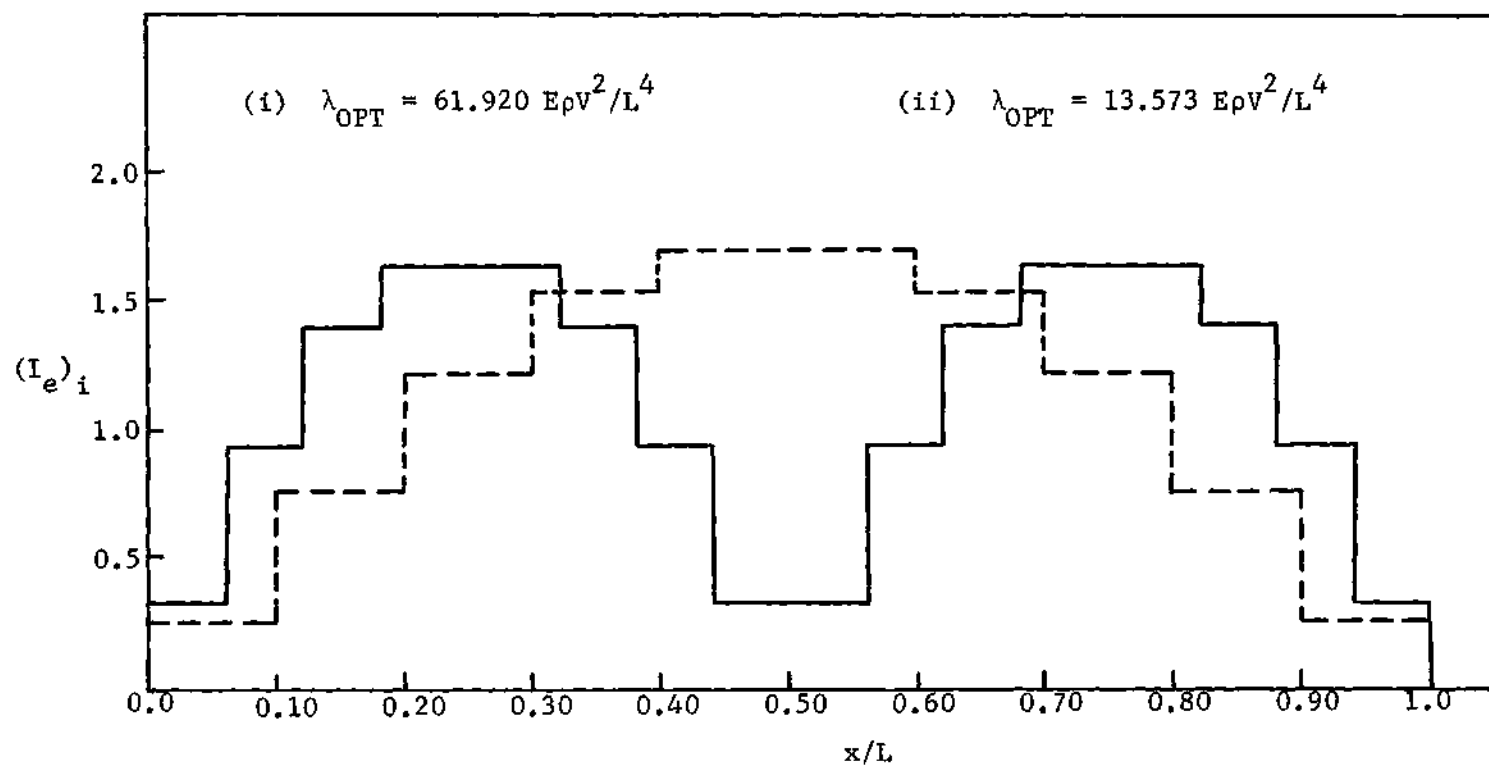


Figure 2.8. Optimum Moment of Inertia Distribution for a Column with

$k_T^0 = \infty$, $k_R^0 = 0$, $k_T^L = \infty$, $k_R^L = 0$; $n = 2$; and with

(i) — $\beta = 500 E_{\rho} V^2 / L^6$, $m = 16$;

(ii) - - - $\beta = 10 E_{\rho} V^2 / L^6$, $m = 10$

Table 2.1. Numerical Results for the 16 Element Column shown in Fig. 2.4, Case (ii)

$$\lambda_{\text{OPT}} = 22.501 \text{ E}\rho\text{V/L}^3 = 1.185 \lambda_u$$

Element No.	$(I_e)_i$	c_i^2
1	1.3847	0.9991
2	1.1429	0.9990
3	0.8217	0.9987
4	0.3982	0.9977
5	0.2486	1.0026
6	0.6649	1.0011
7	0.9999	1.0006
8	1.2563	1.0004
9	1.4322	1.0003
10	1.5272	1.0023
11	1.5412	1.0018
12	1.4638	1.0002
13	1.2756	1.0001
14	1.0031	1.0001
15	0.6692	1.0001
16	0.2729	1.0001

Table 2.2. Numerical Results for the 16 Element Column shown in Fig. 2.5, Case (i)

$$\lambda_{\text{OPT}} = 24.799 \text{ E} \rho V^3 / L^5 = 1.324 \lambda_U$$

Element No.	$(I_e)_i$	c_i^2
1	0.2500	_____
2	0.5992	1.0364
3	1.0672	1.0364
4	1.4951	1.0364
5	1.8170	1.0364
6	1.9652	1.0364
7	1.9617	1.0364
8	1.8254	1.0364
9	1.5630	1.0364
10	1.1899	1.0364
11	0.7355	1.0364
12	0.2500	_____
13	0.2500	_____
14	0.6761	1.0364
15	1.1637	1.0364
16	1.5823	1.0364

Table 2.3. Numerical Results for the 16 Element Column shown in Fig. 2.6, Case (i)

$$\lambda_{\text{OPT}} = 50.007 \text{ E}\rho V^3/L^5 = 1.318 \lambda_U$$

Element No.	$(I_e)_i$	c_i^2
1	2.3248	1.0004
2	2.0114	1.0005
3	1.4622	1.0009
4	0.6878	1.0027
5	0.1406	0.9979
6	0.6892	0.9979
7	1.2762	0.9992
8	1.6686	0.9979
9	1.8080	0.9998
10	1.6786	0.9999
11	1.2949	1.0000
12	0.6582	1.0000
13	0.1278	1.0000
14	0.6134	0.9999
15	1.1693	1.0000
16	1.5281	0.9999

Table 2.5. Numerical Results for the 16 Element Column shown in Fig. 2.8, Case (i)

$$\lambda_{\text{OPT}} = 61.92 \text{ E} \rho V^2 / L^4 = 1.187 \lambda_U$$

Element No.	$(I_e)_i$	c_i^2
1	0.3251	0.9978
2	0.9392	1.0008
3	1.3987	1.0004
4	1.6335	1.0001
5	1.6335	1.0001
6	1.3987	1.0004
7	0.9392	1.0008
8	0.3251	0.9978
9	0.3251	0.9978
10	0.9392	1.0008
11	1.3987	1.0004
12	1.6335	1.0001
13	1.6335	1.0001
14	1.3987	1.0004
15	0.9392	1.0008
16	0.3251	0.9978

CHAPTER III

OPTIMAL VIBRATING BEAM

Assumptions and Objective

It is assumed that the beams under consideration in this chapter satisfy the following assumptions.

- (i) The material of the beam is isotropic and linearly elastic.
- (ii) Cross-sectional planes before deformation remain plane and normal to the deformed axis of the beam after deformation.
- (iii) The transverse displacement w of the reference axis does not lead to any stretching of this axis (inextensional deformation).
- (iv) The only kinetic energy considered is due to transverse motion. All other kinetic energies are considered negligibly small.
- (v) The cross-section possesses a plane of symmetry. The loading and deformation are restricted in this plane of symmetry.
- (vi) The cross-sectional moment of inertia, I , about the axis normal to the plane of vibration, can be expressed in terms of the cross-sectional area, A , by the relation

$$I(x) = \rho A^n(x) \quad (3.1)$$

where ρ and n have the same significance as in Chapter II.

Consider such a beam of specified length and volume (mass) resting on a continuous elastic foundation with various boundary conditions (mixed or not -- with or without springs) and subjected to any given arbitrarily varying axial load and/or dead (non-structural) mass distribution. The problem, then, is to determine the distribution of structural material along the length of the beam so as to maximize the fundamental (first mode) frequency of free transverse vibrations (design objective) subject to the constraint that the minimum area of the beam is not smaller than a specified value A_0 (inequality constraint).

Although the practicality of increasing the fundamental (first mode) frequency is not as important as increasing the buckling load of a column, nevertheless such a design is required in a number of cases. The above can be used to avoid resonance or in other cases to ensure response in the first mode.

In addition to the type of relation given by Eq. (3.1), extensions to other type of relations (Ref. 21) will be briefly demonstrated. This problem, along with the method of solution, is in many ways similar to the one treated in Chapter II. Hence, only those features of the present solution which are substantially different from the problem of Chapter II will be elaborated upon.

Formulation of the Problem

The principle of the conservation of energy when applied to a freely vibrating beam yields

$$\omega^2 = \frac{V_{\max}}{\mu} \quad (3.2)$$

where V_{\max} is the maximum total potential energy of the system at some instant of time, μ is a constant depending upon the distribution of mass and the mode shape such that $\mu\omega^2$ is the maximum total kinetic energy of the system in the same mode at some other instant of time. It is assumed that time is measured from the straight equilibrium configuration.

Further, Rayleigh's principle states that in a natural mode of vibration of a conservative system the frequency of vibration, ω , is stationary.

The motion of the beam which is assumed to be periodic can be expressed in the form

$$v(x,t) = w(x) e^{-i\omega t} . \quad (3.3)$$

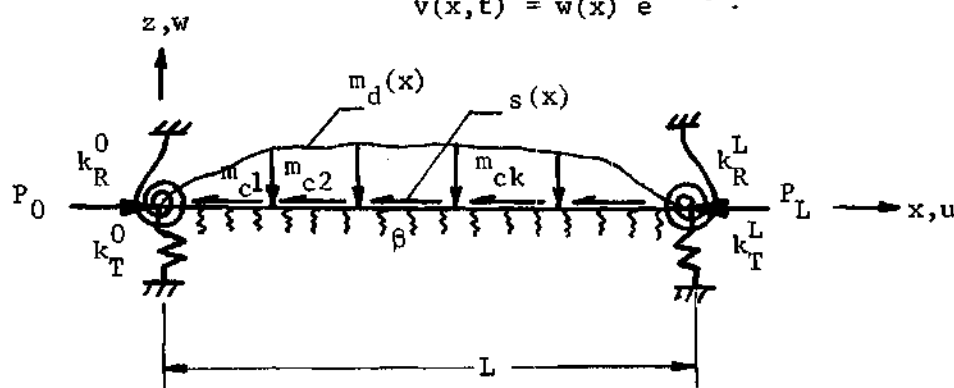


Figure 3.1. A Typical Beam on a Continuous Elastic Foundation with Elastically Restrained Ends Under Arbitrarily Varying Axial Load and Dead Mass Distribution.

The total potential energy of the beam with the afore mentioned assumptions (see Fig. 3.1) and with the same notation as in Chapter II is then

given by

$$V_{\max} = \frac{1}{2} \int_0^L E \rho A^n w''^2 dx + \frac{U_s}{2} - \frac{1}{2} \int_0^L S_o(x) w'^2 dx \quad (3.4)$$

since $I = \rho A^n$.

The total kinetic energy of the beam is likewise given by

$$\frac{1}{2} \omega^2 = \frac{1}{2} \omega^2 \int_0^L \frac{\gamma}{g} A w^2 dx + \frac{1}{2} \omega^2 \left[\int_0^L m_d w^2 dx + \sum_{i=1}^k m_{ci} w_i^2 \right] \quad (3.5)$$

where

γ = specific weight of the material of the beam

g = acceleration due to gravity

m_d = non-structural (dead) mass distribution

m_{ci} = concentrated non-structural mass at the i^{th} point,

$i=1 \dots k; k \leq (m+1).$

Substitution of Eqs. (3.4) and (3.5) into Eq. (3.2) finally

yields

$$\omega^2 = \frac{\int_0^L E \rho A^n w''^2 dx + U_s - \int_0^L S_o(x) w'^2 dx}{\int_0^L \frac{\gamma}{g} A w^2 dx + \int_0^L m_d w^2 dx + \sum_{i=1}^k m_{ci} w_i^2} \quad (3.6)$$

Since ω^2 is stationary with respect to displacement w this implies that $\delta_{w''}(\omega^2) = 0$. This yields the equation of motion along with the

associated boundary conditions. These are:

$$[E\rho A^n w'']'' - \omega^2 \left(\frac{\gamma}{g} A + m_d \right) w + \beta w + [S_o(x) w']' = 0, \quad (3.7)$$

$$\left. \begin{aligned} E\rho A^n w'' - k_R^0 w' &= 0 \\ [E\rho A^n w'']' + k_T^0 w + S_o(x) w' &= 0 \end{aligned} \right\} \text{ at } x = 0, \quad (3.8.1)$$

$$\left. \begin{aligned} E\rho A^n w'' + k_R^L w' &= 0 \\ [E\rho A^n w'']' - k_T^L w + S_o(x) w' &= 0 \end{aligned} \right\} \text{ at } x = L, \quad (3.8.2)$$

and

$$\left\{ [E\rho A^n w'']' + S_o(x) w' \right\}_{x=c_i^-} - \left\{ [E\rho A^n w'']' + S_o(x) w' \right\}_{x=c_i^+} = \omega^2 m_{ci} \quad (3.8.3)$$

$$[E\rho A^n w'']_{x=c_i^-} = [E\rho A^n w'']_{x=c_i^+}$$

$$w|_{x=c_i^-} = w|_{x=c_i^+} \quad \text{and} \quad w'|_{x=c_i^-} = w'|_{x=c_i^+}, \quad (3.8.4)$$

$x=c_i$ being the point of application of i^{th} concentrated mass m_{ci} ,
 $i=1, \dots, k$.

For any given area distribution, the square of the fundamental frequency, ω_1^2 , can be obtained by solving Eqs. (3.7) through (3.8.4) for

the lowest eigenvalue.

Next, it is required to maximize the fundamental frequency ω_1 with respect to variations in the cross-sectional area $A(x)$ subject to the constant volume constraint

$$\int_0^L A \, dx = V. \quad (3.9)$$

Hence, the new functional that must be extremized is

$$(\omega_1^2)^* = \frac{\int_0^L E \rho A^n w''^2 \, dx + U_s - \int_0^L S_o(x) w'^2 \, dx}{\int_0^L \frac{\gamma}{g} A w^2 \, dx + \int_0^L m_d w^2 \, dx + \sum_{i=1}^k m_{ci} w_i^2} - \lambda_1 \left[\int_0^L A \, dx - V \right]$$

where λ_1 is an undetermined Lagrange multiplier. The necessary condition for $(\omega_1^2)^*$ to be stationary with respect to $A(x)$ is

$$\int_0^L \left\{ E \rho n A^{n-1} w''^2 - \lambda_1 \left[\int_0^L \frac{\gamma}{g} A w^2 \, dx + \int_0^L m_d w^2 \, dx + \sum_{i=1}^k m_{ci} w_i^2 \right] - \omega_1^2 \frac{\gamma}{g} w^2 \right\} \delta A \, dx = 0.$$

Hence, if δA is arbitrary, i.e. the area is not prescribed, then the above implies that

$$E \rho n A^{n-1} w''^2 - \omega_1^2 \frac{\gamma}{g} w^2 = c = \text{constant}. \quad (3.10)$$

Equation (3.10) is valid only in those regions where the area is not prescribed. In other regions, in the event that the area as determined by the use of Eq. (3.10) happens to be less than A_0 the constraint $A = A_0$ has to be satisfied.

Thus the problem of unconstrained optimization reduces to the solution of Eqs. (3.7) through (3.10), it being understood that ω_1^2 is the square of the fundamental frequency.

Multiplication of Eq. (3.10) throughout by A followed by integration from $x = 0$ to $x = L$ yields

$$n \int_0^L E \rho A^n w'^2 dx - \omega_1^2 \int_0^L \frac{\gamma}{g} A w^2 dx = c \int_0^L A dx$$

or

$$c = \frac{2(nU_B - U_T)}{V} ; \quad 2U_T = \omega_1^2 \int_0^L \frac{\gamma}{g} A w^2 dx .$$

Equation (3.10) is therefore written as

$$E \rho n A^{n-1} w'^2 - \omega_1^2 \frac{\gamma}{g} w^2 = \frac{2}{V} (nU_B - U_T) . \quad (3.11)$$

Notice that for a beam with classical boundary conditions for $n=1$, the constant c is zero while for the same beam with elastic restraints the constant c is negative.

It can also be seen that Eqs. (3.7) through (3.10) remain unchanged in the event that ρ is a function of x . For relations of the

form

$$I(x) = c_0 + \rho A(x)$$

although Eqs. (3.7) through (3.8) have to be modified, as it will be seen later, the corresponding matrix equations in terms of finite elements remain the same, in form, while the optimality condition for this case is similar to the case of $n=1$ with a new constant c_2 .

$$E\rho w''^2 - \omega_1^2 \frac{\gamma}{g} w^2 = \text{constant} = c_2$$

where $c_2 = \frac{2}{V} (U_B - U_0 - U_T) = -\frac{2}{V} U_0$ (since $U_B = U_T$) and U_0 is given by

$$U_0 = \int_0^L E c_0 w''^2 dx .$$

Method of Solution of the Problem

The finite element displacement method is used, which reduces to the Rayleigh-Ritz method when the assumed displacement function satisfies compatibility exactly. Further, as will be seen in the course of this development, the optimality condition, Eq. (3.9), when transformed in terms of finite elements, is much simpler to handle.

Some comments regarding the finite element displacement method as applied to vibrating beams are given in the Appendix B. For more details of the same, the reader is referred to Refs. 22 and 23.

In terms of finite elements the equation of motion together with

the boundary conditions becomes

$$[K_V] - \omega^2[M] \{q\} = \{0\} \quad (3.12)$$

where $[K_V]$ is the assembled nonsingular stiffness matrix including the effect of the elastic foundation, the elastic restraints, if any, and any given arbitrarily varying axial load distribution; ω^2 is the eigenvalue, $[M]$ is the assembled mass matrix for the entire beam including the dead mass; and $\{q\}$ is the vector of the unrestrained degrees of freedom of the beam. Having determined the fundamental frequency (the lowest eigenvalue) and the corresponding eigenvector $\{q\}_1$ by the solution of the eigenvalue problem as specified by Eq. (3.12), the strain energy and the kinetic energy densities in each element can be determined. These are given by

$$\left. \begin{aligned} \frac{U_{bi}}{V_i} &= \frac{1}{2} \frac{\{q_i\}^T [k_i] \{q_i\}}{A_i \ell_i} \end{aligned} \right\} i=1,2,\dots,m \quad (3.13.1)$$

and

$$\left. \begin{aligned} \frac{U_{ti}}{V_i} &= \frac{1}{2} \frac{\{q_i\}^T [M_i] \{q_i\}}{A_i \ell_i} \end{aligned} \right\} \quad (3.13.2)$$

where $[k_i]$ is the stiffness matrix of the i^{th} element without the effect of the elastic foundation and the axial load, while $[M_i]$ is the mass matrix of the i^{th} element without the effect of the dead (non-structural) mass.

Next, the optimality condition is transformed in terms of the finite elements. Multiplying Eq. (3.10) throughout by A and integrating over the extent of the i^{th} element, one obtains

$$\int_{x_i}^{x_{i+1}} E \rho n A^{n-1} w'^2 dx - \omega_1^2 \int_{x_i}^{x_{i+1}} \frac{\gamma}{g} A w^2 dx = c \int_{x_i}^{x_{i+1}} A dx ,$$

i.e.

$$2nU_{bi} - 2U_{ti} = cv_i \quad (3.14)$$

or

$$n \left(\frac{U_{bi}}{v_i} \right) - \left(\frac{U_{ti}}{v_i} \right) = \frac{c}{2} = c_1 .$$

Equation (3.14) can be written as

$$\frac{n \left(\frac{U_{bi}}{v_i} \right)}{c_1 + \left(\frac{U_{ti}}{v_i} \right)} = 1.0 \quad \text{if } c_1 > 0$$

and

$$\frac{n \left(\frac{U_{bi}}{v_i} \right) - c_1}{\left(\frac{U_{ti}}{v_i} \right)} = 1.0 \quad \text{if } c_1 < 0 .$$

Equation (3.14) expresses the optimality condition in terms of finite elements.

Unconstrained Optimization Procedure

The objective of this optimization procedure is to make the ratio $[n(U_{bi}/v_i)]/(c_1 + (U_{ti}/v_i))$ if $c_1 > 0$ or the ratio $[n(U_{bi}/v_i) - c_1]/(U_{ti}/v_i)$ if $c_1 < 0$ equal to unity. This is similar to the objective in Chapter II where it was required to make the ratio $(U_i V/v_i U)$ equal to unity. Hence, a similar procedure is employed.

One begins with a uniform beam, i.e. a beam having a uniform cross-section, and a given volume V . Then using Eqs. (3.13.1) and (3.13.2) the strain energy and kinetic energy densities in each of the elements can be determined. These distributions of strain and kinetic energy densities are used for deciding the inertias of the elements for the next iterations. Let these quantities be denoted by U_{bi}^r/v_i^r and U_{ti}^r/v_i^r for the r^{th} iteration. Let the corresponding average quantities for the entire beam be denoted by U_B^r/V and U_T^r/V where

$$U_B^r = \sum_{i=1}^m U_{bi}^r \quad ; \quad U_T^r = \sum_{i=1}^m U_{ti}^r$$

and

$$V = \sum_{i=1}^m v_i^r = \text{specified volume} \quad .$$

The inertias of the elements for the next iteration are assumed to be given by the following recurrence relations

$$I_i^{r+1} = c^{r+1} I_i^r \left[\frac{n(U_{bi}^r/v_i^r)}{c_1 + (U_{ti}^r/v_i^r)} \right]^p \quad \text{if } c_1 > 0$$

and

$$I_i^{r+1} = c^{r+1} I_i^r \left[\frac{n(U_{bi}^r/v_i^r) - c_1}{(U_{ti}^r/v_i^r)} \right]^p \quad \text{if } c_1 < 0$$

where c^{r+1} is a constant to be determined from the constant volume constraint and the exponent p is assumed to be positive. Next, it will be shown that as long as the ratio inside the brackets in the above recurrence relations is different from unity a value of $p > 0$ exists which will guarantee that $(\omega_1^2)^{r+1} \geq (\omega_1^2)^r$. As before, the proof is presented for a continuous system.

From Rayleigh's quotient one has for the continuous system

$$(\omega^2)^{r+1} = \frac{\int_0^L EI^{r+1} (w^{r+1})^2 dx + U_{sa}^{r+1}}{\int_0^L \frac{\gamma}{g} \left(\frac{1}{\rho} \right)^{1/n} (w^{r+1})^2 dx + m_e^{r+1}} \quad (3.15)$$

where w^{r+1} is the eigenvector corresponding to the lowest eigenvalue $(\omega_1^2)^{r+1}$ and

$$U_{sa}^{r+1} = k_T^0 (w^{r+1})^2|_0 + k_T^L (w^{r+1})^2|_L + k_R^0 (w^{r+1})^2|_0$$

$$+ k_R^L (w^{r+1})^2|_L + \int_0^L \beta (w^{r+1})^2 dx - \int_0^L S_o(x) (w^{r+1})^2 dx$$

and

$$m_e^{r+1} = \int_0^L m_d (w^{r+1})^2 dx + \sum_{i=1}^k m_{ci} (w_i^{r+1})^2.$$

The corresponding recurrence relations for the continuous system can be written as

$$I^{r+1} = c^{r+1} I^r R^p \quad (3.16)$$

where

$$R = \frac{nEI^r (w^{r''})^2}{c_1 + \frac{\gamma}{g} \frac{(I^r)^{1/n}}{\rho} (w^r)^2} \quad \text{if } c_1 > 0$$

and

$$R = \frac{nEI^r (w^{r''})^2 - c_1}{\frac{\gamma}{g} \frac{(I^r)^{1/n}}{\rho} (w^r)^2} \quad \text{if } c_1 < 0.$$

Notice that $R \geq 0$ for $0 \leq x \leq L$. Furthermore, R is also continuous for $0 \leq x \leq L$, which implies that for $p > 0$, $R^{p/n}$ is positive and continuous for $0 \leq x \leq L$.

The constant c^{r+1} in Eq. (3.16) must be evaluated from the volume constraint

$$\int_0^L \left(\frac{I^{r+1}}{\rho} \right)^{1/n} dx = V ,$$

i.e.

$$(c^{r+1})^{1/n} \int_0^L I^{r/n} R^{p/n} dx = V .$$

By the mean-value theorem of integral calculus the above can be written as

$$(c^{r+1})^{1/n} \left[\int_0^L \left(\frac{I^r}{\rho} \right)^{1/n} dx \right] (R^{p/n})|_{x=\xi_1} , \quad 0 < \xi_1 < L .$$

Since,

$$\int_0^L \left(\frac{I^r}{\rho} \right)^{1/n} dx = V ,$$

it follows that

$$c^{r+1} = \frac{1}{R^p|_{x=\xi_1}} .$$

Hence, Eq. (3.16) becomes

$$I^{r+1} = I^r \frac{R^p}{R^p|_{x=\xi_1}} . \quad (3.17)$$

Substitution of I^{r+1} in Eq. (3.17) yields

$$(\omega_1^2)^{r+1} = \frac{\left\{ \int_0^L EI^r \left[\frac{R^p}{R^p|_{x=\xi_1}} \right] (w^{r+1})^2 dx \right\} + U_{sa}^{r+1}}{\int_0^L \frac{\gamma}{g} \left(\frac{I^r}{\rho} \right)^{1/n} \left[\frac{R^p}{R^p|_{x=\xi_1}} \right]^{1/n} (w^{r+1})^2 dx + m_e^{r+1}}.$$

By another application of the mean-value theorem the expression for

$(\omega_1^2)^{r+1}$ can be written as

$$(\omega_1^2)^{r+1} = \frac{\left[\int_0^L EI^r (w^{r+1})^2 dx \right] \left(\frac{R^p|_{x=\xi_2}}{R^p|_{x=\xi_1}} \right) + U_{sa}^{r+1}}{\left[\int_0^L \frac{\gamma}{g} \left(\frac{I^r}{\rho} \right)^{1/n} (w^{r+1})^2 dx \right] \left(\frac{R^p|_{x=\xi_3}}{R^p|_{x=\xi_1}} \right) + m_e^{r+1}};$$

$$0 < \xi_2 < L ; \quad 0 < \xi_3 < L .$$

Let $R_1 = R(\xi_2)/R(\xi_1)$ and $R_2 = [R(\xi_3)/R(\xi_1)]^{1/n}$. Next, by virtue of the positive definiteness of the strain and the kinetic energy densities R_1 and R_2 are both positive. Since the relative magnitudes of R_1 and R_2 as compared to one are not known, all four possibilities, listed below, are considered.

$$(i) \quad R_1 \geq 1 \text{ and } R_2 \leq 1 ;$$

$$(ii) \quad R_1 \geq 1 \text{ and } R_2 \geq 1 ;$$

$$(iii) \quad R_1 \leq 1 \text{ and } R_2 \leq 1 ;$$

$$(iv) \quad R_1 \leq 1 \text{ and } R_2 \geq 1 .$$

For the first possibility it can be very easily seen that

$$(\omega_1^2)^{r+1} \geq \frac{\int_0^L EI^r (w^{r+1})^2 dx + U_{sa}^{r+1}}{\int_0^L \frac{\gamma}{g} \left(\frac{I^r}{\rho}\right)^{1/n} (w^{r+1})^2 dx + m_e^{r+1}} . \quad (3.18)$$

Since w^{r+1} is a kinematically admissible displacement field for the moment of inertia distribution I^r , the quantity on the right hand side of Eq. (3.18) is greater than or equal to $(\omega_1^2)^r$ by Rayleigh's principle. Hence, it will be guaranteed that $(\omega_1^2)^{r+1} \geq (\omega_1^2)^r$ for all values of $p > 0$. As regards the remaining three cases, if a suitable value of p , which would guarantee that $(\omega_1^2)^{r+1} \geq (\omega_1^2)^r$, can be shown to exist for case (iv), it would immediately follow that the same value of p would also guarantee that $(\omega_1^2)^{r+1} \geq (\omega_1^2)^r$ for cases (ii) and (iii). Assume that for case (iv) $R_1 < 1$ and $R_2 > 1$; the expression for $(\omega_1^2)^{r+1}$ can then be written as

$$(\omega_1^2)^{r+1} \geq \frac{\left[\int_0^L EI^r (w^{r+1})^2 dx + U_{sa}^{r+1} \right]}{\left[\int_0^L \frac{\gamma}{g} \left(\frac{I^r}{\rho}\right)^{1/n} (w^{r+1})^2 dx + m_e^{r+1} \right]} \times \left(\frac{R_1}{R_2}\right)^p .$$

Next, because of the kinematic admissibility of w^{r+1} for the moment of inertia distribution I^r assume that

$$\frac{\int_0^L EI^r (w^{r+1})^2 dx + U_{sa}^{r+1}}{\int_0^L \frac{\gamma}{g} \left(\frac{I^r}{\rho} \right)^{1/n} (w^{r+1})^2 dx + m_e^{r+1}} = (1+\epsilon) (\omega_1^2)^r$$

where $\epsilon > 0$. Therefore, the range of the values of p which will guarantee that $(\omega_1^2)^{r+1} \geq (\omega_1^2)^r$ is given by

$$p \leq \frac{\log (1/1+\epsilon)}{\log (R_1/R_2)}. \quad (3.19)$$

Thus, it can be seen that as long as R (see Eq. (3.16)) is different from unity for $0 \leq x \leq L$ a value of p can always be determined which will guarantee that $(\omega_1^2)^{r+1} \geq (\omega_1^2)^r$.

The iterative scheme can therefore be started with a value of p equal to 1 or less and the scheme can be continued with this value of p as long as $(\omega_1^2)^{r+1} \geq (\omega_1^2)^r$. If $(\omega_1^2)^{r+1} < (\omega_1^2)^r$, then the value of p is reduced by a factor of $\frac{1}{2}$ or $\frac{1}{4}$ and the iteration is repeated. This process is carried on until no substantial change either in the value of (ω_1^2) or the moment of inertia distribution is possible and the function R is essentially uniform. As in Chapter II this procedure guarantees a monotonic convergence to the maximum first mode frequency though not always via a monotonic convergence of the ratio (R_{\max}/R_{\min}) .

Constrained Optimization Procedure

In the case of the inequality constraint, assume the value of the prescribed minimum inertia to be I_0 .

The constrained optimization proceeds exactly in the same manner

as the unconstrained optimization until such time at which the moments of inertia of some elements violate the inequality constraint. The moments of inertia of these elements are arbitrarily set equal to the prescribed minimum value I_0 , while the moments of inertia of the remaining elements must be recalculated. Assume the number of elements with prescribed moments of inertia to be j and their volume to be V_c . The new value of c_1 can be determined for the remaining $(m-j)$ elements. Let this new value of c_1 be denoted by c_3 . Hence, the new moments of inertia of these $(m-j)$ elements are given by

$$I_i^{r+1} = c^{r+1} \left[\frac{n(U_{bi}^r/v_i^r)}{c_3^r + (U_{ti}^r/v_i^r)} \right]^p I_i^r \quad \text{if } c_3^r > 0$$

or by

$$I_i^{r+1} = c^{r+1} \left[\frac{n(U_{bi}^r/v_i^r) - c_3^r}{(U_{ti}^r/v_i^r)} \right]^p I_i^r \quad \text{if } c_3^r < 0$$

where c^{r+1} is determined from the constraint

$$\sum_{i=1}^{(m-j)} \left(\frac{I_i^{r+1}}{\rho} \right)^{1/n} \ell_i = (V - V_c) \quad .$$

It should be noted that, in the case of the inequality constraint the quantity $[n(U_{bi}/v_i) - (U_{ti}/v_i)]$ will be equal to a constant only over those $(m-j)$ elements which do not violate the inequality constraint. For the j elements with prescribed inertias the afore mentioned quantity

will have different values.

Numerical Results and Conclusions

The criterion for convergence on the optimality condition is

$$\left[\frac{\left((nU_{bi} - U_{ti})/v_i \right)_{\max}}{\left((nU_{bj} - U_{tj})/v_j \right)_{\min}} - 1.0 \right] \times 100 \leq 0.50 .$$

A number of cases of freely vibrating beams with various boundary conditions and area-moment of inertia relations is discussed below.

A uniform cross-section freely vibrating simply-supported beam with $I = \rho A$, ($n=1$), satisfies the optimality condition trivially, i.e. $(U_{bi} - U_{ti})/v_i = (U_B - U_T)/V = 0$, $i=1, \dots, m$ and hence no increase in the fundamental frequency is possible. On the other hand, for a freely vibrating simply-supported beam with $I(x) = \rho A^n(x)$, $n=2$ and 3 , a finite (6% for $n=2$ and 11.15% for $n=3$) increase of the fundamental frequency is obtained (see Fig. 3.2). This six per cent increase for $n=2$ compares very favourably with the 6.6% increase obtained by Niordson, Ref. 17.

Figure 3.3 shows the optimum area distribution for a simply-supported beam on an elastic foundation of moderate stiffness. Two different finite element models are used, one with $m = 10$ and another with $m = 20$.

Figure 3.4 shows the effect of an axial tensile prestress on the optimum distribution of area for a simply-supported beam with $I(x) = \rho A^2(x)$.

Beams with other types of boundary conditions (at least those

shown in Figs. 3.5 through 3.10) do not possess a finite optimum fundamental frequency, (the optimum frequency of the stepped beam increases with increasing number of elements) in the absence of a dead mass distribution and/or a concentrated dead mass and/or a compressive load ($P/P_{cr} < 1$) and/or an inequality constraint. It seems that as soon as one of the ends of the beam is fully clamped, (in the limit) the optimum material distribution is one with all of the structural mass of the beam lumped at the clamped-end. The resulting fundamental frequency approaches infinity.

For beams other than simply-supported beams no finite frequency seems to exist when vibrating under the influence of an axial tensile prestress.

Figure 3.7 shows a vibrating cantilever beam under the combined influence of a compressive axial load and a linearly varying dead mass distribution for $n = 2$.

Figure 3.8 shows a clamped-clamped beam under the influence of a compressive axial load for $n = 2$. Results are presented for $m = 20$ and $m = 40$.

Figures 3.9 and 3.10 show two typical cases of the elastically restrained vibrating beams under the influence of a uniformly distributed dead mass.

As regards the optimization procedure most of the conclusions given in Chapter II hold true here except that higher values of p than those used for columns can perhaps be entertained. In most cases, the convergence is rapid provided that the corresponding continuous system

does possess a finite frequency.

It is worthwhile noting that the effect of shear deformation and rotary inertia can be very easily accounted for without changing the basic form of the optimality condition. For such cases, nU_{bi} would be replaced by $(nU_{bi} + U_{si})$, where U_{si} is the strain energy of the i^{th} element due to the effect of shear deformation and U_{ti} would correspond to the total kinetic energy of the i^{th} element, which is composed of the kinetic energy of translation and n times the kinetic energy of rotation of the beam cross-section. The stiffness and mass matrices would have to be altered to take this effect into account. It appears that the same optimization procedure can be used. Including these effects would then perhaps ensure a finite frequency for the beam regardless of the boundary conditions and the dead mass distribution and/or a compressive axial load and/or an inequality constraint. This would be a subject of further research.

From Appendices A and B it is clear that except for the matrix $[M_v^i]$ no new element matrices are required to be calculated for this problem. The assembled stiffness and mass matrices are readily obtained by a marginal change in the computer program used for optimization of columns. The only additional quantities that are required to be calculated are the kinetic energy densities (U_{ti}/v_i) and U_T/V followed by the ratios $n(U_{bi}/v_i)/(c_1 + (U_{ti}/v_i))$ if $c_1 > 0$ or the ratio $(n(U_{bi}/v_i) - c_1)/(U_{ti}/v_i)$ if $c_1 < 0$.

Numerical results for some typical cases are tabulated in Tables 3.1 through 3.5 where the symbol $(I_e)_i$ denotes $I_i/\rho(V/L)^n$; the symbol

c_i denotes the quantity $(nU_{bi} - U_{ti})/(c_1 v_i)$, the symbol E_m denotes the quantity $(E\rho g/\gamma)$; the symbols $(\omega_1^2)_{OPT}$ and $(\omega_1^2)_U$ denote the squares of the fundamental frequencies of the finite element models with the optimum and the uniform moment of inertia distributions respectively; η denotes the ratio of the total dead mass to the structural mass M_0 of the beam; and finally x_c denotes the x coordinate of the point of application of the concentrated dead mass, if any.

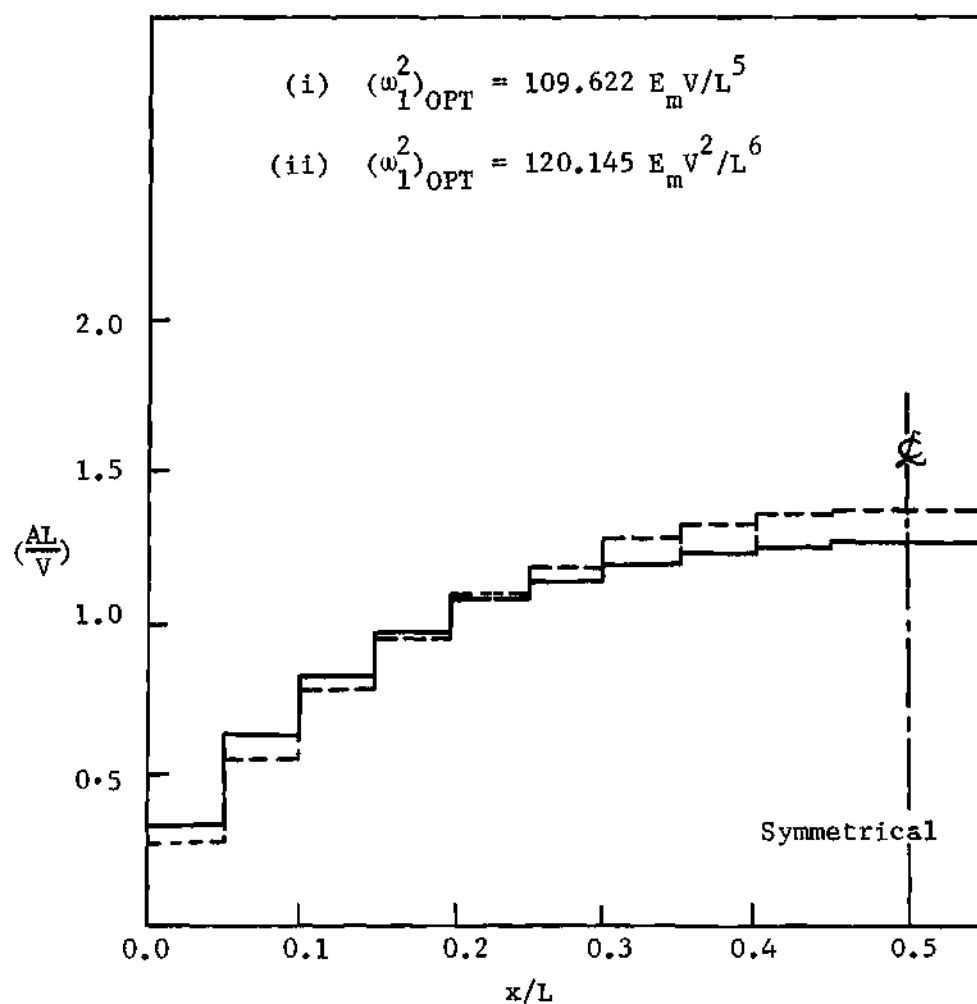


Figure 3.2. Optimum Area Distribution for a Beam with
 $k_T^0 = \infty$, $k_R^0 = 0$, $k_T^L = \infty$, $k_R^L = 0$;

$$\eta = 0.0; m = 20$$

(i) ——— $n = 2$;

(ii) - - - - - $n = 3$.

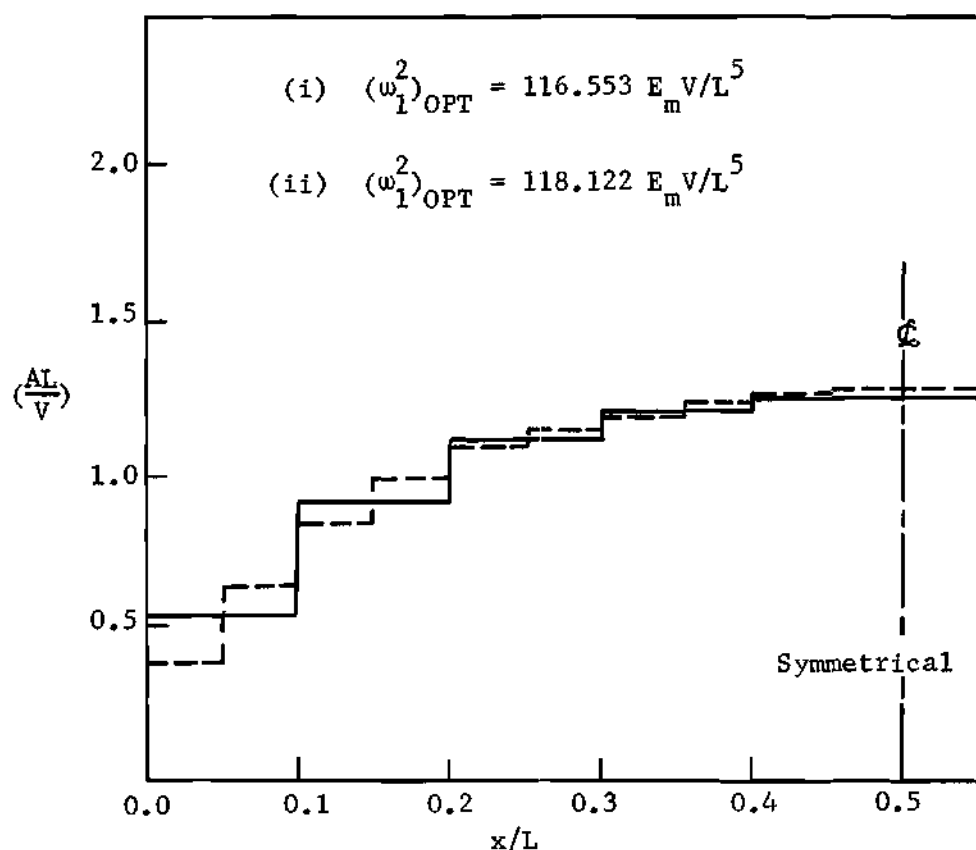


Figure 3.3. Optimum Area Distribution for a Beam with
 $k_T^0 = \infty$, $k_R^0 = 0$, $k_T^L = \infty$, $k_R^L = 0$; $\beta = 10 E_p V^2/L^6$;

$$\eta = 0.0; n = 2$$

(i) ——— $m = 10$;

(ii) - - - - - $m = 20$.

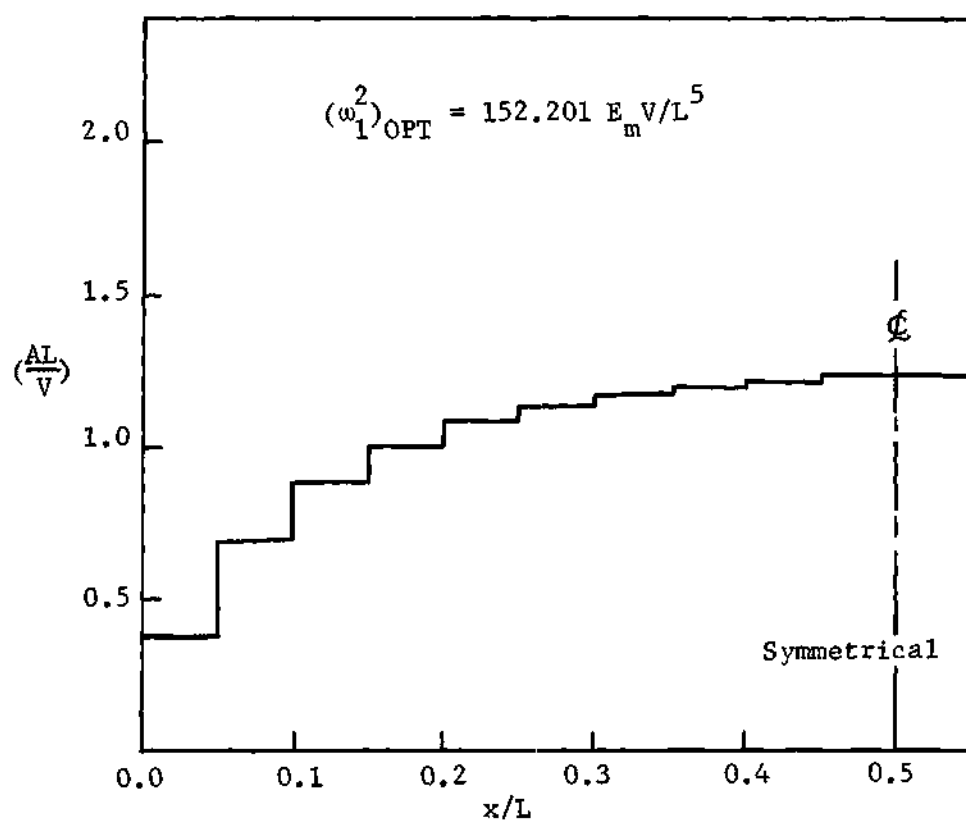


Figure 3.4. Optimum Area Distribution for a Beam with
 $k_T^0 = \infty$, $k_R^0 = 0$, $k_T^L = \infty$, $k_R^L = 0$; $P_0 = P_L = \sim 5 E \rho V^2 / L^4$;
 $\eta = 0.0$; $m = 20$; $n = 2$.

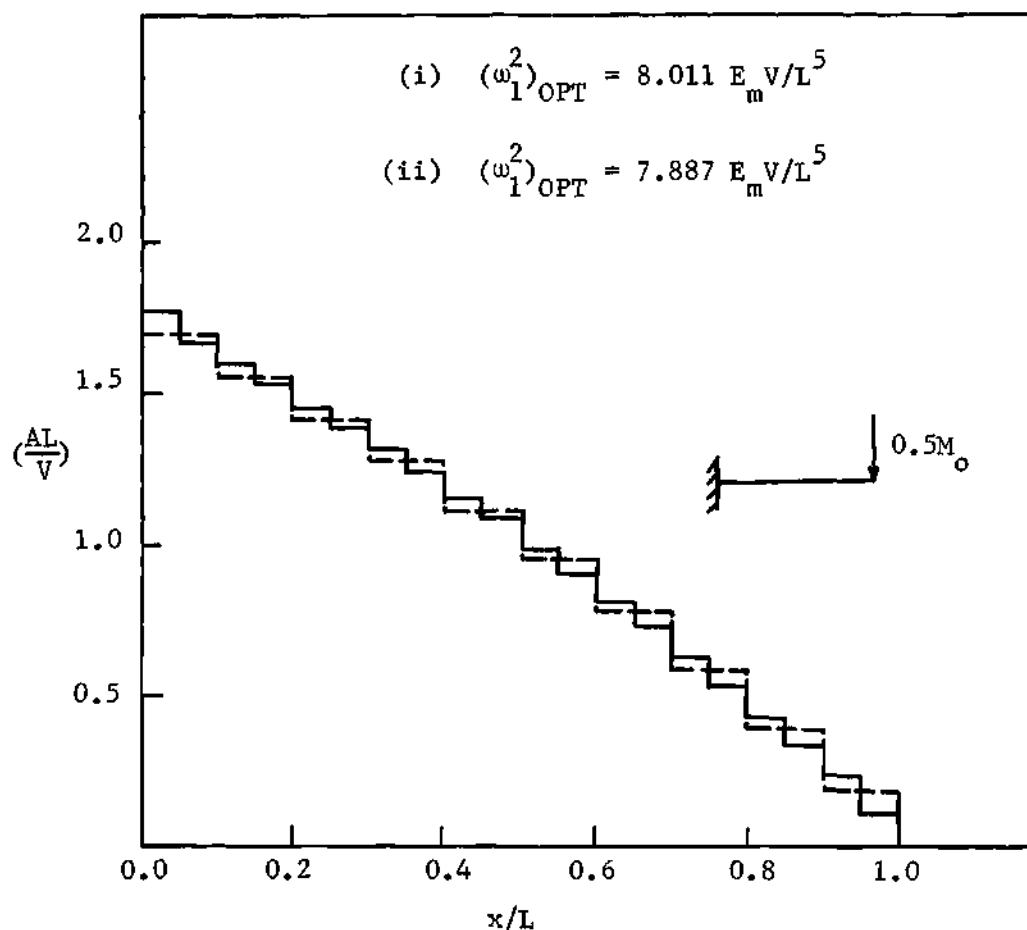


Figure 3.5. Optimum Area Distribution for a Beam with
 $k_T^0 = \infty$, $k_R^0 = \infty$, $k_T^L = 0$, $k_R^L = 0$;

$$\eta = 0.5, x_c = L; n = 2;$$

(i) ----- $m = 10$;

(ii) ————— $m = 20$.

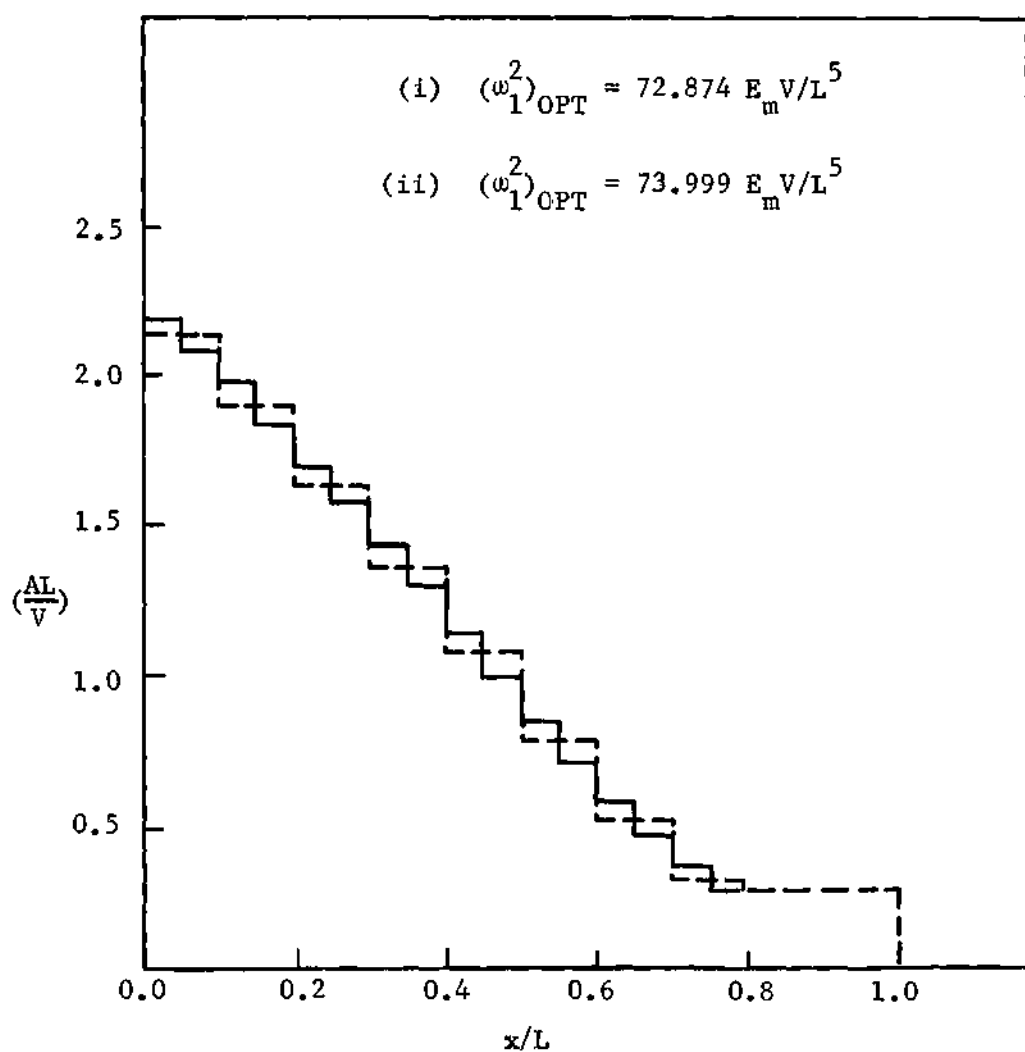


Figure 3.6. Optimum Area Distribution for a Beam with
 $k_T^0 = \infty$, $k_R^0 = \infty$, $k_T^L = 0$, $k_R^L = 0$; $A \geq 0.2725 V/L$;

$$\eta = 0.0; n = 2;$$

$$(i) \text{ ---- } m = 10;$$

$$(ii) \text{ ——— } m = 20.$$

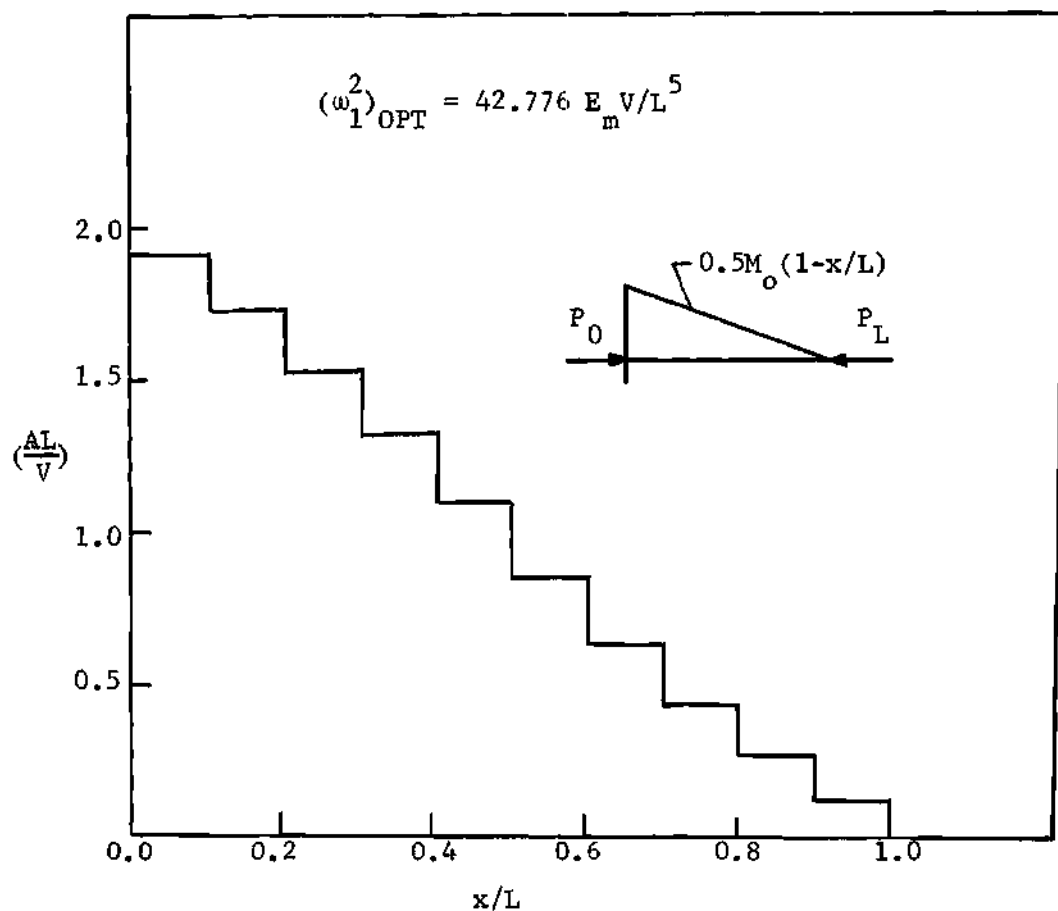


Figure 3.7. Optimum Area Distribution for a Beam with
 $k_T^0 = \infty$, $k_R^0 = \infty$, $k_T^L = 0$, $k_R^L = 0$; $P_o = P_L = E\rho V^2/L^4$;
 $\eta = 0.25$; $m = 10$; $n = 2$.

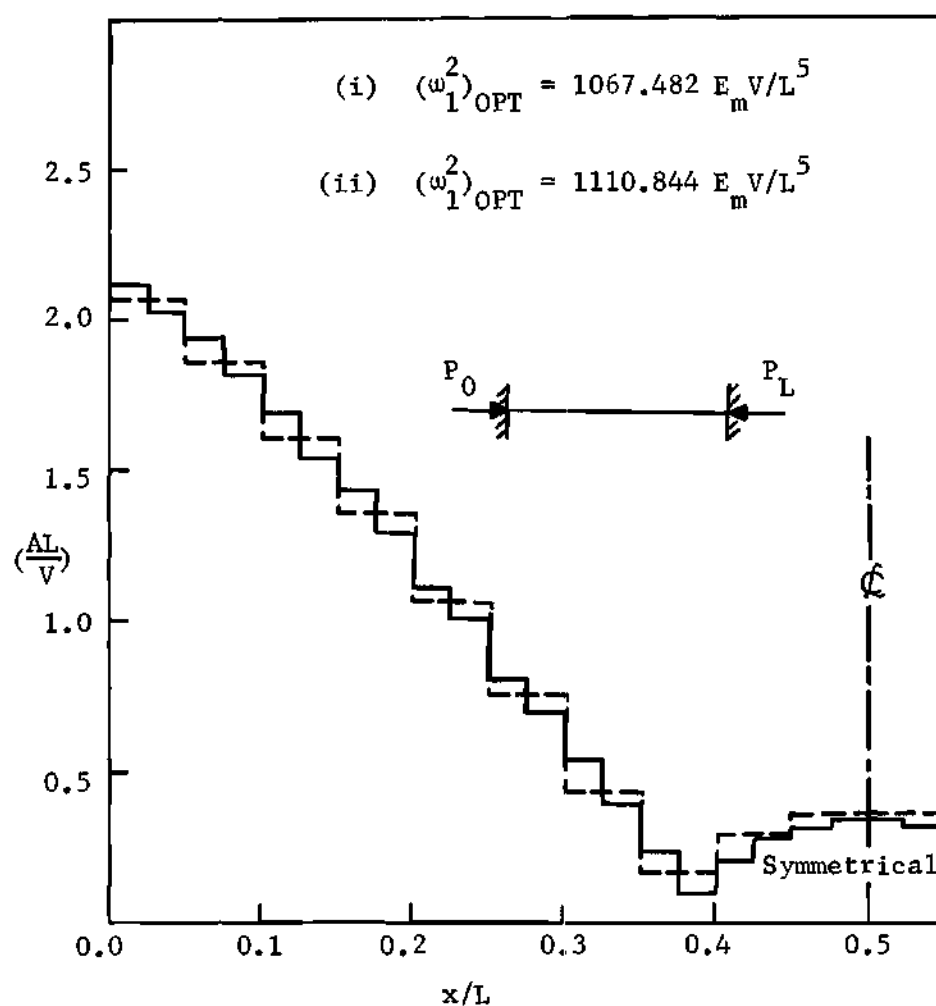


Figure 3.8. Optimum Area Distribution for a Beam with
 $k_T^0 = \infty$, $k_R^0 = \infty$, $k_T^L = \infty$, $k_R^L = \infty$; $P_0 = P_L = 10 E \rho V^2/L^4$

$$\eta = 0.0; n = 2;$$

$$(i) \text{ ---- } m = 20;$$

$$(ii) \text{ ——— } m = 40.$$

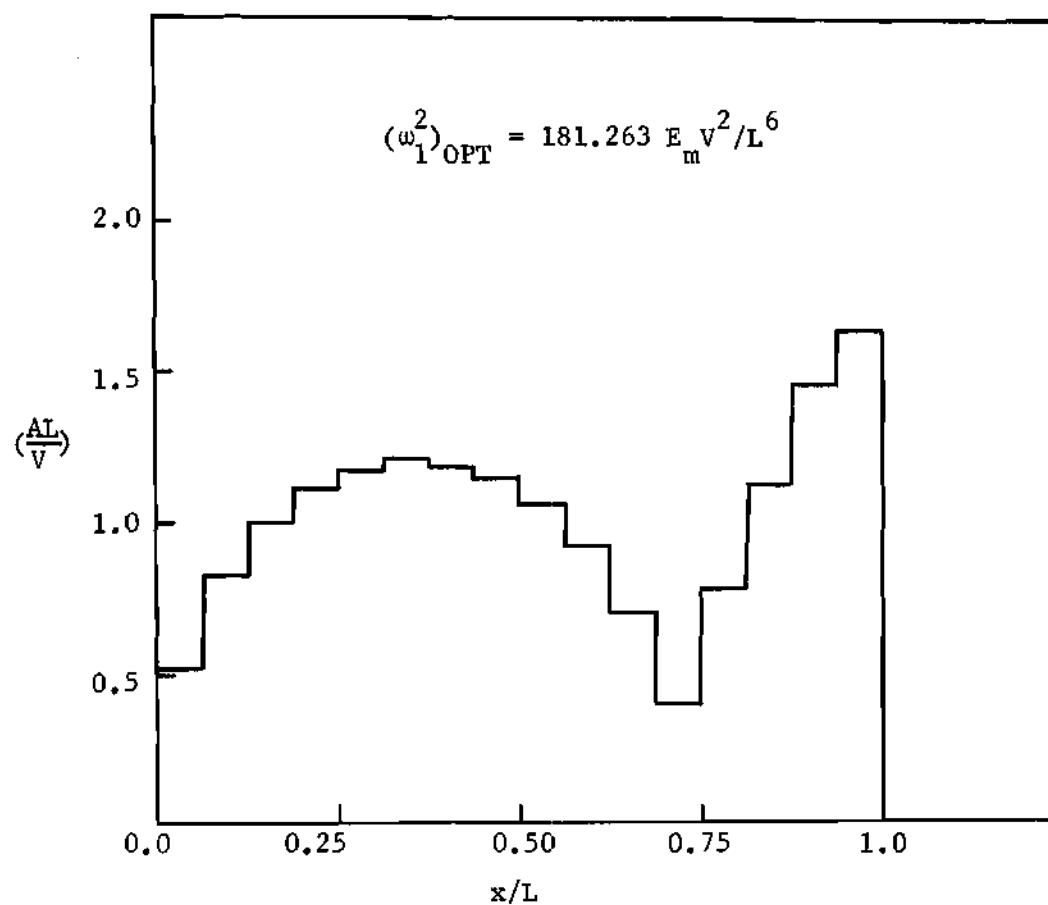


Figure 3.9. Optimum Area Distribution for a Beam with
 $k_T^0 = \infty$, $k_R^0 = 0$, $k_T^L = \infty$, $k_R^L = 25 E \rho V^3 / L^4$;

$$m_d(x) = M_0 / 2L; m = 16; n = 3.$$

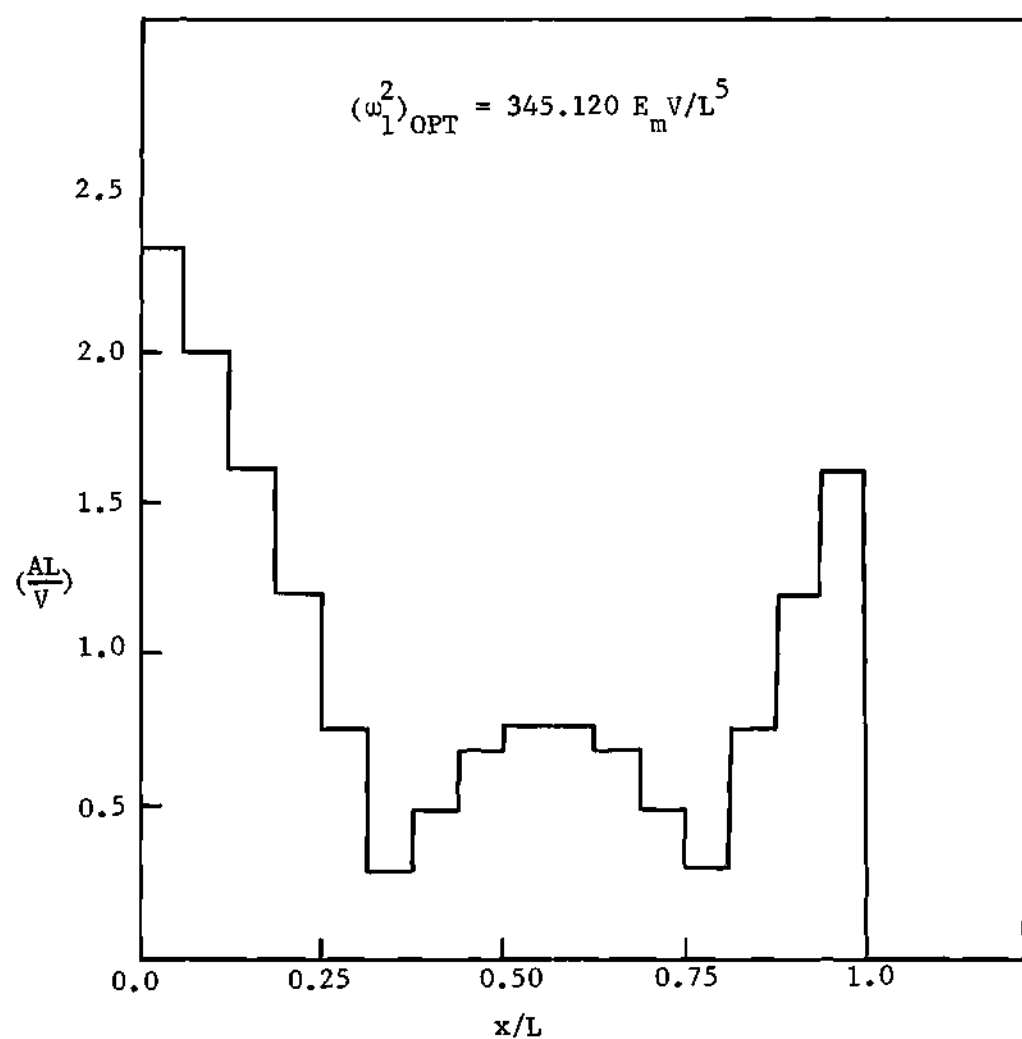


Figure 3.10. Optimum Area Distribution for a Beam with
 $k_T^0 = \infty$, $k_R^0 = \infty$, $k_T^L = \infty$, $k_R^L = 25 E \rho V^2/L^3$;

$$m_d(x) = M_o/L; m = 16; n = 2.$$

Table 3.1. Numerical Results for the 10 Element Vibrating Beam shown in Fig. 3.2, Case (i)

$$(\omega_1)_{\text{OPT}}^2 = 109.622 \frac{E}{m} V/L^5 = 1.125 (\omega_1)_U^2$$

Element No.	$(I_e)_i$	c_i
1	0.1176	0.9980
2	0.4008	0.9982
3	0.6976	0.9981
4	0.9553	0.9983
5	1.1641	0.9982
6	1.3270	0.9995
7	1.4498	1.0003
8	1.5377	1.0012
9	1.5944	1.0018
10	1.6222	1.0022

Table 3.2. Numerical Results for the 10 Element Vibrating Beam shown in Fig. 3.3, Case (ii)

$$(\omega_1)_{\text{OPT}}^2 = 118.122 \text{ EV/L}^5 = 1.10 (\omega_1)_U^2$$

Element No.	$(I_e)_i$	c_i
1	0.1230	0.9993
2	0.4157	0.9992
3	0.7147	0.9992
4	0.9675	0.9992
5	1.1676	0.9994
6	1.3213	0.9997
7	1.4358	1.0001
8	1.5171	1.0005
9	1.5693	1.0009
10	1.5948	1.0010

Table 3.3. Numerical Results for the 20 Element Vibrating Beam shown in Fig. 3.5, Case (ii)

$$(\omega_1)_{\text{OPT}}^2 = 8.011 E_m V/L^5 = 1.975 (\omega_1)_U^2$$

Element No.	$(I_e)_i$	c_i
1	3.0108	1.0004
2	2.7862	1.0004
3	2.5660	1.0004
4	2.3504	1.0003
5	2.1395	1.0003
6	1.9355	1.0002
7	1.7328	1.0002
8	1.5379	1.0002
9	1.3495	1.0001
10	1.1683	1.0000
11	0.9953	0.9999
12	0.8318	0.9998
13	0.6789	0.9996
14	0.5381	0.9994
15	0.4107	0.9992
16	0.2979	0.9991
17	0.2008	0.9989
18	0.1203	0.9989
19	0.0574	0.9989
20	0.0144	0.9990

Table 3.4. Numerical Results for the 10 Element Vibrating Beam shown in Fig. 3.7.

$$(\omega_1)_{\text{OPT}}^2 = 42.776 E_m V/L^5 = 6.18 (\omega_1)_U^2$$

Element No.	$(I_e)_i$	c_i
1	3.7171	1.0004
2	3.0386	1.0004
3	2.3841	1.0004
4	1.7668	1.0002
5	1.2118	1.0002
6	0.7524	1.0000
7	0.4142	0.9998
8	0.1972	0.9993
9	0.0755	0.9982
10	0.0156	0.9966

Table 3.5. Numerical Results for the 16 Element Vibrating Beam shown in Fig. 3.9.

$$(\omega_1)_{\text{OPT}}^2 = 181.263 E_m v^2 / L^6 = 1.31 (\omega_1)_U^2$$

Element No.	$(I_e)_i$	c_i
1	0.1397	1.0000
2	0.5432	1.0000
3	0.9811	1.0000
4	1.3355	1.0000
5	1.5641	0.9999
6	1.6550	0.9998
7	1.6090	0.9998
8	1.4333	0.9997
9	1.1417	0.9995
10	0.7594	0.9993
11	0.3399	0.9988
12	0.0586	1.0000
13	0.4554	1.0011
14	1.3674	1.0006
15	2.6581	1.0005
16	4.2439	1.0004

CHAPTER IV

INVESTIGATION INTO THE OPTIMIZATION OF THIN
RECTANGULAR PLATES FOR VIBRATION AND STABILITYTransversely Vibrating Thin Rectangular PlatesAssumptions and Objective

This development is restricted to plates for which the following assumptions are valid.

- (i) The material of the plate is isotropic and linearly elastic.
- (ii) The deflection w of the plate is small in comparison with the plate thickness h .
- (iii) The normal stresses in the direction transverse to the plate can be neglected.
- (iv) Material points on the normal to the midsurface before deformation remain on the normal after deformation with unchanged distances from the midsurface.
- (v) The only kinetic energy considered is due to transverse motion. All other kinetic energies are considered negligibly small.

As regards the objective, it is required to distribute the material over the extent of the plate with a given aspect ratio (see Fig. 4.1), total volume (mass) and with various boundary conditions so as to maximize its fundamental frequency under the influence of any given arbitrarily varying dead (non-structural) mass distribution (design objective) subject to the constraint that the minimum thickness is no smaller than

a specified value h_0 (inequality constraint). The necessity of increasing the fundamental frequency is again to avoid resonance or to ensure response in the first mode.

Formulation of the Problem

The motion of the plate which is assumed to be periodic can be expressed by the relation

$$v(x,y,t) = w(x,y) e^{-i\omega t} .$$

For such a periodic motion the Raleigh quotient is obtained from the relation

$$V_{\max} = T_{\max} \quad (4.1.1)$$

where V_{\max} is the maximum potential energy of the plate at some instant of time and T_{\max} is the maximum kinetic energy of the plate at some other instant of time. For the free vibration of a plate the total potential energy is equal to the strain energy of pure bending of the plate.

The strain-displacement relations for pure bending of the plate with the afore mentioned assumptions are given by (see Fig. 4.1)

$$\epsilon_{xx} = -zv_{,xx} ,$$

$$\epsilon_{yy} = -zv_{,yy} ,$$

$$\gamma_{xy} = -2zv_{,xy}$$

and

$$\epsilon_{zz} = \gamma_{yz} = \gamma_{xz} = 0 \quad .$$

The bending strain energy of the plate is then given by

$$U_B = \int_0^a \int_0^b \int_{-h/2}^{h/2} W(\epsilon_{xx}, \epsilon_{yy}, \gamma_{xy}) \, dx \, dy \, dz$$

where W is the strain energy density function with the property that

$$\frac{\partial W}{\partial \epsilon_{xx}} = \sigma_{xx} \quad ; \quad \frac{\partial W}{\partial \epsilon_{yy}} = \sigma_{yy} \quad ; \quad \frac{\partial W}{\partial \gamma_{xy}} = \tau_{xy} \quad .$$

Next, for an isotropic material in plane stress ($\sigma_{zz} = 0$) one has

$$\sigma_{xx} = \frac{E}{(1-\nu^2)} (\epsilon_{xx} + \nu \epsilon_{yy}) \quad ,$$

$$\sigma_{yy} = \frac{E}{(1-\nu^2)} (\epsilon_{yy} + \nu \epsilon_{xx}) \quad ,$$

$$\tau_{xy} = \frac{E}{2(1+\nu)} \gamma_{xy} \quad .$$

Hence, it follows that

$$W(\epsilon_{xx}, \epsilon_{yy}, \gamma_{xy}) = \frac{E}{2(1-\nu^2)} \left[\epsilon_{xx}^2 + \epsilon_{yy}^2 + 2\nu \epsilon_{xx} \epsilon_{yy} + \frac{(1-\nu)}{2} \gamma_{xy}^2 \right] \quad .$$

Using the strain-displacement relations the expression for the maximum strain energy density, W_m , finally becomes

$$W_m = \frac{Ez^2}{2(1-\nu^2)} \left[(w_{,xx} + w_{,yy})^2 - 2(1-\nu)(w_{,xx} w_{,yy} - w_{,xy}^2) \right].$$

Hence,

$$V_{\max} = \frac{1}{2} \int_0^a \int_0^b D \left[(w_{,xx} + w_{,yy})^2 - 2(1-\nu)(w_{,xx} w_{,yy} - w_{,xy}^2) \right] dx dy \quad (4.1.2)$$

where

$$D = \frac{Eh^3}{12(1-\nu^2)}.$$

The kinetic energy of the plate is given by

$$T_{\max} = U_{TT} = \frac{\omega^2}{2} \left[\int_0^a \int_0^b m(x,y) w^2 dx dy + \int_0^a \int_0^b m_d(x,y) w^2 dx dy + \sum_{i=1}^k m_{ci} w_i^2 \right]$$

and since $m(x,y) = \frac{\gamma}{g} h(x,y)$, where γ is the specific weight of the material of the plate and g is the acceleration due to gravity, the expression for U_{TT} finally becomes

$$U_{TT} = \frac{\omega^2}{2} \left[\int_0^a \int_0^b \frac{\gamma}{g} h w^2 dx dy + \int_0^a \int_0^b m_d(x,y) w^2 dx dy + \sum_{i=1}^k m_{ci} w_i^2 \right] \quad (4.1.3)$$

In Eq. (4.1.3), $m_d(x,y)$ is the dead (non-structural) mass distribution and m_{ci} is the concentrated mass at the point i of the plate, $i=1\dots k$. Substitution of Eqs. (4.1.2) and (4.1.3) into (4.1.1) yields

$$\omega^2 = \frac{\int_0^a \int_0^b \left[D(w_{,xx} + w_{,yy})^2 - 2(1-\nu)(w_{,xx} w_{,yy} - w_{,xy}^2) \right] dx dy}{\int_0^a \int_0^b \frac{\gamma}{g} h w^2 dx dy + \int_0^a \int_0^b m_d w^2 dx dy + \sum_{i=1}^k m_{ci} w_i^2}$$

or

$$\omega^2 = \frac{\int_0^a \int_0^b \frac{Eh^3}{12(1-\nu^2)} \kappa^2 dx dy}{\int_0^a \int_0^b \frac{\gamma}{g} h w^2 dx dy + T_e} \quad (4.1.4)$$

where

$$\kappa^2 = (w_{,xx} + w_{,yy})^2 - 2(1-\nu)(w_{,xx} w_{,yy} - w_{,xy}^2) \quad (4.1.5)$$

and

$$T_e = \int_0^a \int_0^b m_d w^2 dx dy + \sum_{i=1}^k m_{ci} w_i^2 \quad (4.1.6)$$

Next, by Rayleigh's principle, ω^2 , the square of the fundamental frequency, is stationary with respect to the displacement w . Setting the variation of ω^2 , as defined by Eq. (4.1.4), with respect to w equal to zero, therefore yields the governing equation of motion together with

the associated boundary conditions. These are (see Fig. 4.1)

$$\begin{aligned} & \left[D(w_{,xx} + \nu w_{,yy}) \right]_{,xx} + 2(1-\nu) \left[Dw_{,xy} \right]_{,xy} + \left[D(w_{,yy} + \nu w_{,xx}) \right]_{,yy} \\ & + \omega^2 \left(\frac{\gamma}{g} h + m_d \right) w = 0 \end{aligned} \quad (4.1.7)$$

Either

or

$$\left. \begin{aligned} w &= 0 \quad \left[D(w_{,xx} + \nu w_{,yy}) \right]_{,x} + 2 \left[D(1-\nu)w_{,xy} \right]_{,y} = 0 \\ w_{,x} &= 0 \quad D[w_{,xx} + \nu w_{,yy}] = 0 \end{aligned} \right\} \text{along } x=0, a \quad (4.1.8.1)$$

$$\left. \begin{aligned} w &= 0 \quad \left[D(w_{,yy} + \nu w_{,xx}) \right]_{,y} + 2 \left[D(1-\nu)w_{,xy} \right]_{,x} = 0 \\ w_{,y} &= 0 \quad D[w_{,yy} + \nu w_{,xx}] = 0 \end{aligned} \right\} \text{along } x=0, b \quad (4.1.8.2)$$

In addition to these are the conditions of continuity of deflection w , the slopes $w_{,x}$, $w_{,y}$, moment and known discontinuities of shear at the points of application of the concentrated masses.

For any thickness distribution, h , Eq. (4.1.7) together with the boundary conditions (4.1.8.1) and (4.1.8.2) is solved to obtain the lowest eigenvalue ω_1^2 (the square of the fundamental frequency). Next, it is required to maximize ω_1^2 with respect to variations in h subject to

the constant volume constraint

$$\int_0^a \int_0^b h \, dx dy = V . \quad (4.1.9)$$

Hence, the functional that must be extremized is

$$(\omega_1^2)^* = \frac{\int_0^a \int_0^b \frac{Eh^3}{12(1-\nu^2)} \kappa^2 \, dx dy}{\int_0^a \int_0^b \frac{\gamma}{g} h w^2 \, dx dy + T_e} - \lambda_1 \left[\int_0^a \int_0^b h \, dx dy - V \right]$$

where λ_1 is an undetermined Lagrange multiplier. The necessary condition for $(\omega_1^2)^*$ to be stationary with respect to h is given by

$$\int_0^a \int_0^b \left\{ \frac{3Eh^2}{12(1-\nu^2)} \kappa^2 - \omega_1^2 \frac{\gamma}{g} w^2 - \lambda_1 \left(\int_0^a \int_0^b \frac{\gamma}{g} h w^2 \, dx dy + T_e \right) \right\} \delta h \, dx dy = 0 .$$

Hence, for arbitrary variations δh the above yields

$$\frac{3Eh^2}{12(1-\nu^2)} \kappa^2 - \omega_1^2 \frac{\gamma}{g} w^2 = c = \text{constant} . \quad (4.1.10)$$

Equation (4.1.10) is valid only in those regions where the thickness is not prescribed. In other regions for which the thickness, as determined by the use of Eq. (4.1.10) happens to be less than h_0 , the constraint $h = h_0$ is used.

Multiplication of Eq. (4.1.10) throughout by h followed by integration over the area of the plate yields

$$3 \int_0^a \int_0^b \frac{Eh^3}{12(1-\nu^2)} \kappa^2 dx dy - \omega_1^2 \int_0^a \int_0^b \frac{\gamma}{g} hw^2 dx dy = c \int_0^a \int_0^b h dx dy ,$$

i.e.

$$6U_B - 2U_T = cV$$

or

$$c = \left(\frac{6U_B - 2U_T}{V} \right) ; \quad 2U_T = \omega_1^2 \int_0^a \int_0^b \frac{\gamma}{g} hw^2 dx dy .$$

Equation (4.1.10) can therefore be written as

$$\frac{3Eh^2}{12(1-\nu^2)} \kappa^2 - \omega_1^2 \frac{\gamma}{g} w^2 = \left(\frac{6U_B - 2U_T}{V} \right) . \quad (4.1.11)$$

It is understood that Eqs. (4.1.7), (4.1.8.1), (4.1.8.2), (4.1.11) and (4.1.9) are solved simultaneously in order to obtain the fundamental frequency ω_1 and the corresponding thickness distribution h .

Method of Solution of the Problem

The proposed method is again the finite element displacement method, and although the governing equations in this case are partial differential equations, the corresponding equations in terms of the finite element formulation are exactly the same as those of Chapter III for the case of $n=3$, namely

$$[[K_V]_p - \omega^2 [M]_p] \{q\} = \{0\} \quad (4.1.12)$$

$$\frac{3U_{bi}}{v_i} - \frac{U_{ti}}{v_i} = c_1 = \frac{c}{2} = \left(\frac{3U_B - U_T}{V} \right) \quad (4.1.13)$$

Where $[K_V]_p$ is the assembled nonsingular stiffness matrix for the entire plate in bending and $[M]_p$ is the assembled mass matrix for the entire plate including the effect of the non-structural mass and with the prescribed boundary conditions imposed while other quantities are as defined before in Chapter III. The explicit derivation of the plate bending element stiffness and mass matrices together with other details are given in Appendix C.

Optimization Procedure

The unconstrained optimization procedure is exactly the same as in Chapter III and the steps involved can be briefly summarized as follows:

- (i) Begin with a uniform thickness plate complying with the given volume V .
- (ii) Solve the eigenvalue problem as specified by Eq. (4.1.12) to obtain ω_1^2 and the corresponding eigenvector.
- (iii) Calculate the strain and kinetic energy densities in each element, namely $3U_{bi}/v_i$ and U_{ti}/v_i , $i=1\dots m$ and the constant c_1 for the entire plate.
- (iv) Use the recurrence relation, which is

$$h_i^{r+1} = C^{r+1} \left[\frac{(3U_{bi}^r/v_i^r)}{c_i^r + (U_{ti}^r/v_i^r)} \right]^p h_i^r, \quad p > 0 \quad (4.1.14)$$

to determine the thickness of the elements in the $(r+1)^{st}$ iteration.

In Eq. (4.1.14), C^{r+1} is a constant to be determined from the constant volume constraint

$$\sum_{i=1}^m a_i b_i h_i^{r+1} = V/4 \quad (\text{see Fig. C-1}) ,$$

and the value of the exponent p is selected so as to render

$$(\omega_1^2)^{r+1} \geq (\omega_1^2)^r .$$

The proof for the existence of such a p for the continuous system follows on exactly the same lines as the one in Chapter III and therefore it is not given here. The initial value of p can be assumed to be one or less and the iterative scheme is continued with this value of p for as long as $(\omega_1^2)^{r+1} \geq (\omega_1^2)^r$. If it so happens that at some stage $(\omega_1^2)^{r+1} < (\omega_1^2)^r$, the value of p is reduced by a factor of $\frac{1}{2}$ or $\frac{1}{4}$ and the iteration is repeated. This process is continued until no substantial change in the value of ω_1^2 is present and the criterion for convergence on the optimality condition is met.

The constrained optimization procedure is exactly the same as the one described in Chapter III and therefore it is not repeated here.

Numerical Results and Conclusions

The determination of the lowest eigenvalue and corresponding eigenvector is more difficult in the case of plates than it is for columns and vibrating beams. The reason is that the first two eigenvalues are not very well separated for the non-uniform plate. For each iteration of the optimization procedure an approximate lowest eigenvalue and the corresponding eigenvector is determined by the inversion of the stiffness matrix followed by a high number of matrix iterations. During the process of the matrix iterations a check is simultaneously made on the closeness of the first two eigenvalues. (The details of the method for resolving two close eigenvalues are described at great lengths in Ref. 25, pp. 277-279). If the first two eigenvalues are fairly well separated the method of perturbation correction is used to improve the approximate eigenvalue and eigenvector. The desired norm of the residual vector (see Chapter II) is obtained in one or two perturbation corrections; and no difficulty is experienced for the cases shown in Figs. 4.2 through 4.8. It must be noted at this point, that this perturbation scheme, although a powerful scheme, is successful only when the two successive eigenvalues are fairly well separated; and no more than perhaps one or two perturbation corrections are required to improve the approximate eigenvalue and eigenvector.

In the optimization of a vibrating square plate clamped along all edges and carrying a uniformly distributed dead mass, the exact lowest eigenvalue and the corresponding eigenvector for non-uniform geometry could not be obtained by the present scheme owing to numerical

difficulties. The author feels that the root of the problem lies in the closeness of eigenvalues for the non-uniform geometry. This suggests that a radically different and a much more efficient method is required for the eigenvalue analysis. One such scheme is perhaps to use a perturbation technique to obtain an exact inverse of the stiffness matrix. Once an exact inverse of the stiffness matrix is obtained, the method outlined in Ref. 25 for resolving two close eigenvalues can be successfully employed. Although there is little doubt that the exact lowest eigenvalue and the corresponding eigenvector can be computed by this scheme, the computer time entailed in doing so may be prohibitively excessive. Other schemes which may be equally successful are the gradient techniques of determining the lowest eigenvalue and the corresponding eigenvector. Since the author has not attempted neither of these schemes the discussion of their relative merits is out of the question.

The criterion for convergence on the optimality condition for all the cases shown in Figs. 4.2 through 4.8 is

$$\left[\left(\frac{3U_{bi} - U_{ti}}{c_1 v_i} \right)_{\max} / \left(\frac{3U_{bj} - U_{ti}}{c_1 v_j} \right)_{\min} - 1.0 \right] \times 100 < 5.0 \quad .$$

However, the 8×8 element model shown in Fig. 4.5 is not carried to full convergence since all that is of interest in this case is the order of magnitude of the optimum frequency and not its exact final value in order to arrive at the final conclusion.

The convergence in all the cases shown is very slow, brought

about, to some extent, by the necessity to use smaller values of the exponent p in the recurrence relation to avoid drastic changes in the mode shapes due to insignificant changes in the thickness distribution. In Figs. 4.2 through 4.8 the normalized thickness is defined to be the ratio h_i/h_U where $h_U = V/ab$ and in Figs. 4.6 and 4.8 M_0 denotes the total structural mass of the plate.

Tables 4.1 through 4.12 show the percent increase of the fundamental frequency obtained in each case over the fundamental frequency of a uniform thickness plate of the same volume. In these tables the symbol D_v denotes the quantity $[Eg/12v(1-v^2)](V/ab)^2$; the symbols $(\omega_1^2)_{OPT}$ and $(\omega_1^2)_U$ denote the squares of the fundamental frequencies of the finite element models with the optimum and uniform thickness distributions respectively and finally, the symbol $(c_1)_i$ denotes the quantity $(3U_{bi} - U_{ti})/(c_1 v_i)$.

Figure 4.2 shows the thickness distribution for a rectangular vibrating plate simply-supported on two sides and forced to bend cylindrically. The purpose is to model a vibrating beam using rectangular plate bending elements and to provide a check on the numerical computations involved in the vibrating plate optimization computer program. The optimum frequency obtained agrees extremely well with the optimum frequency for a simply-supported vibrating beam with $I(x) = \rho A^3(x)$ and $m=10$. The numerical results for this case are tabulated in Table 4.1.

Figure 4.3 shows the thickness distribution for a rectangular vibrating plate with aspect ratio $a/b = 1/3$, simply-supported along the edges $x=0$ and $x=a$ and free on the other two edges using a 6×6 element

model. The numerical results for this case with $h \geq h_o = 0.10 h_U$ are tabulated in Table 4.2. Figure 4.4, on the other hand, shows the thickness distribution for a rectangular vibrating plate with aspect ratio $a/b = 1/3$ and simply-supported along all edges. The numerical results for this case with $h \geq h_o = 0.10 h_U$ are tabulated in Table 4.3. Both these cases indicate that except for some portion of the plate in the center, where the plate behaves like a simply-supported vibrating beam, the tendency to concentrate the material towards the corners exists. This implies that such a tendency would be more pronounced as the mode shape departs further from a cylindrical surface. This would be the case as the aspect ratio, a/b , approaches unity and all the edges are simply-supported. This is confirmed by the results of a simply-supported vibrating square plate to be discussed next.

Figure 4.5 shows the thickness distributions for a vibrating square plate simply-supported on all sides using a 4×4 , a 6×6 and an 8×8 element models. The numerical results for these three models, tabulated in Tables 4.4 through 4.6, indicate that no finite frequency and corresponding optimum shape can possibly exist. It can be seen that the material of the plate has a tendency to be concentrated more and more at the four corners of the plate as the number of elements of the model increases.

Figure 4.6 shows the thickness distribution for a vibrating square plate simply-supported on all sides but with a concentrated dead mass at the center of the plate. A 4×4 , a 6×6 and an 8×8 element models are used in this investigation. The results indicate that an

8 x 8 element model would be a good approximation of the continuous system. The changes in thickness distributions and corresponding fundamental frequencies diminish as one proceeds to a higher element model. The numerical results for these three models with $h \geq h_o = 0.10 h_U$ are tabulated in Tables 4.7 through 4.9.

Figure 4.7 shows the thickness distribution for a vibrating square plate simply-supported on all sides and carrying a uniformly distributed dead mass. A 4 x 4 and a 6 x 6 element models are used in this investigation. The numerical results for these models with $h \geq h_o = 0.10 h_U$ are tabulated in Tables 4.10 and 4.11. It is not surprising that the fundamental frequency of the 4 x 4 element model is higher than the fundamental frequency corresponding to the 6 x 6 element model. By Rayleigh's principle, for any given thickness distribution the resulting lowest eigenvalue (fundamental frequency), with the assumed displacement field, has the exact solution as a lower bound. On the other hand, the exact optimum frequency of the discretized system has the optimum frequency of the corresponding continuous system as an upper bound. The final optimum frequency of the discretized system therefore approaches the exact value either from above or below.

Finally, Fig. 4.8 shows the thickness distribution for a vibrating square plate simply-supported on all sides with dead line masses acting along the center lines of the plate using a 6 x 6 element model. These dead line masses are transformed into equivalent concentrated masses as shown in the figure. Numerical results for this case with $h \geq h_o = 0.10 h_U$ are tabulated in Table 4.12.

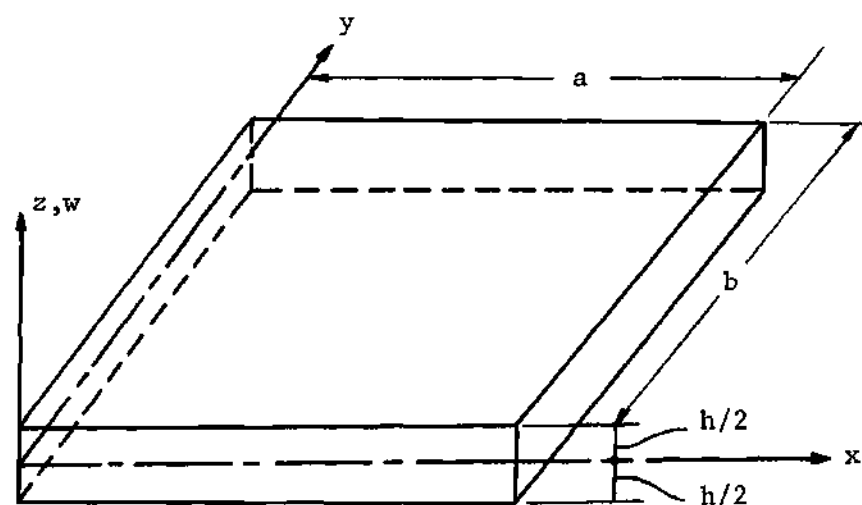


Figure 4.1. A Typical Transversely Vibrating Thin Rectangular Plate

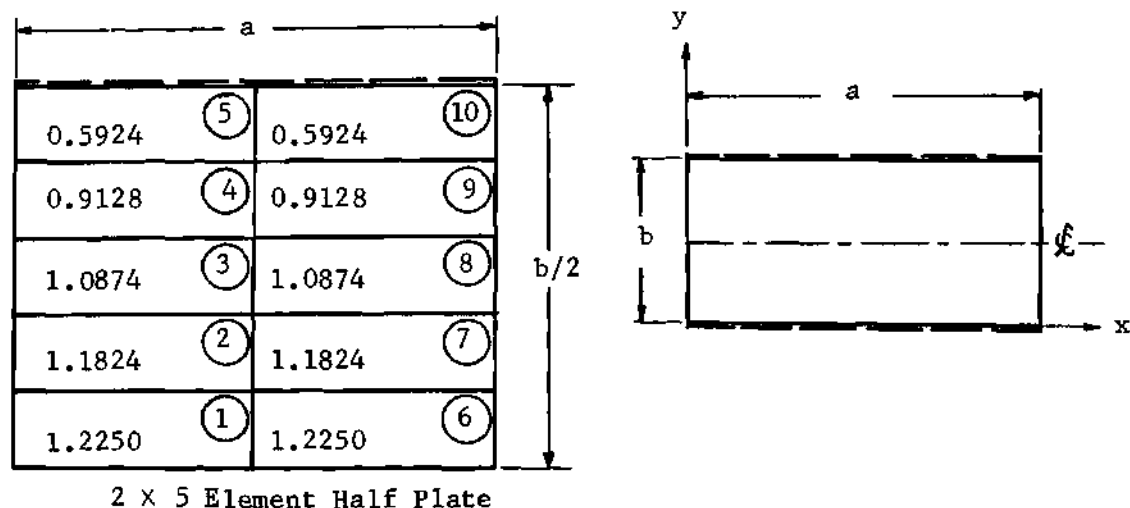
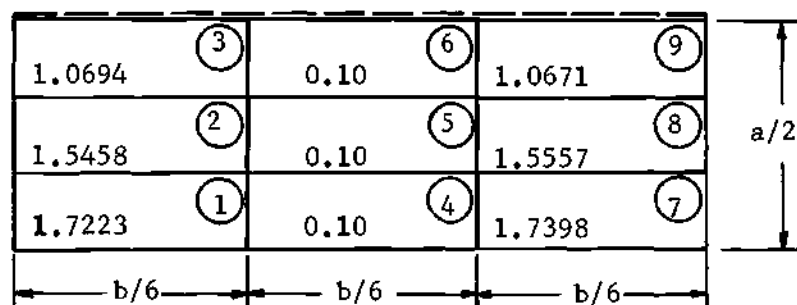


Figure 4.2. Normalized Thickness Distribution for an Optimum Vibrating Rectangular Plate Simply-Supported on Two Opposite Sides with Imposed Cylindrical Bending



3 x 3 Element Quarter Plate (Not to scale)

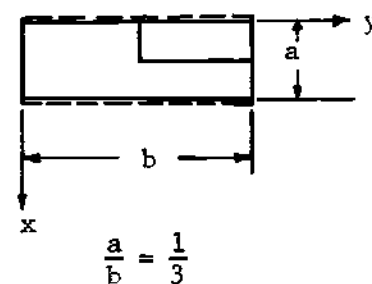
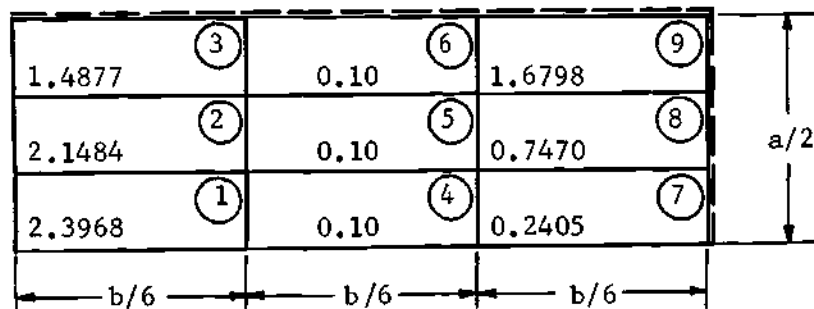


Figure 4.3. Normalized Thickness Distribution for an Optimum Vibrating Rectangular Plate Simply-Supported on the Sides $x = 0, a$ and Free on the Other Two Sides; $h \geq 0.10 h_U$



3 x 3 Element Quarter Plate (Not to scale)

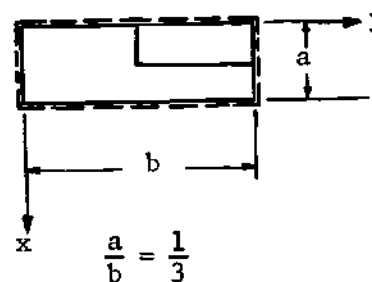
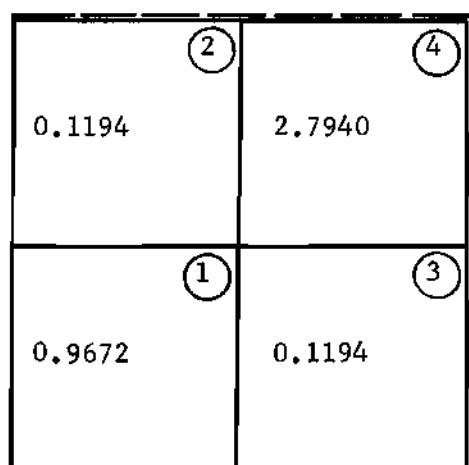
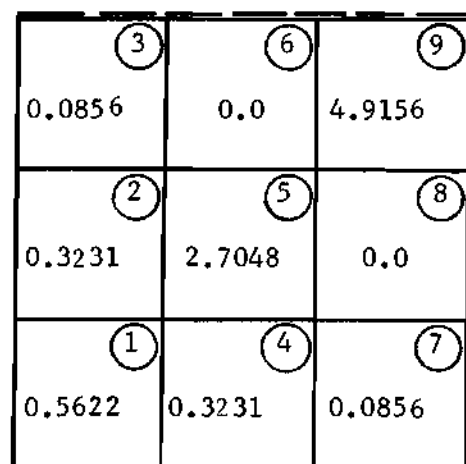


Figure 4.4. Normalized Thickness Distribution for an Optimum Vibrating Rectangular Plate Simply-Supported on All Sides; $h \geq 0.10 h_U$



2 x 2 Element Quarter Plate



3 x 3 Element Quarter Plate

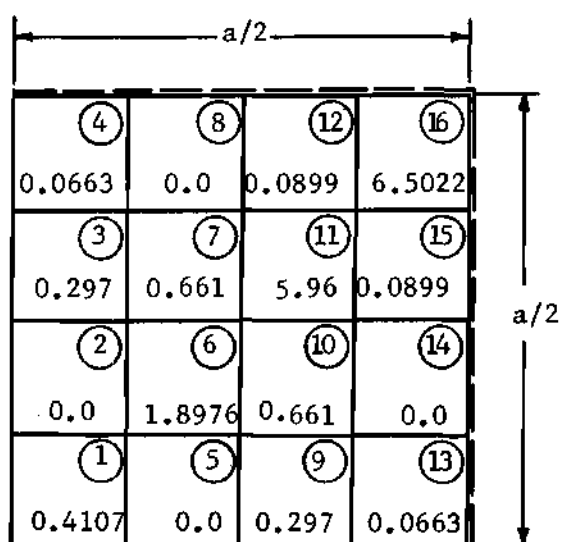
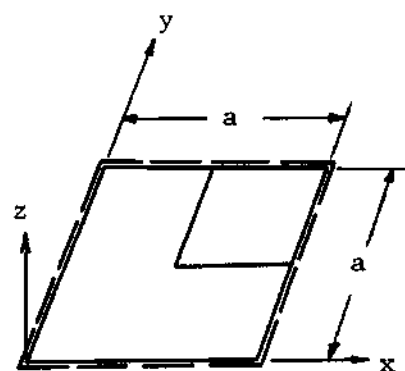
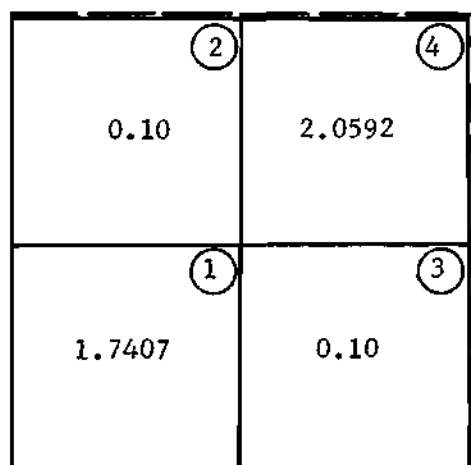
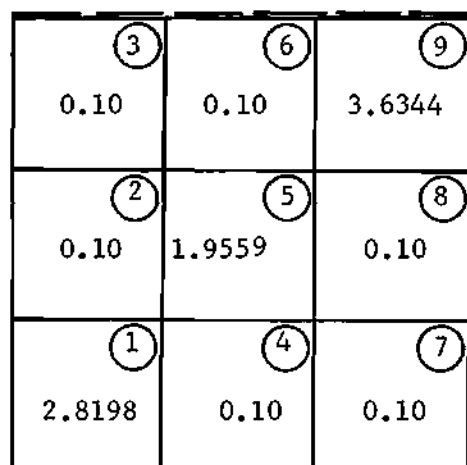
4 x 4 Element Quarter Plate
(Not carried to full convergence)

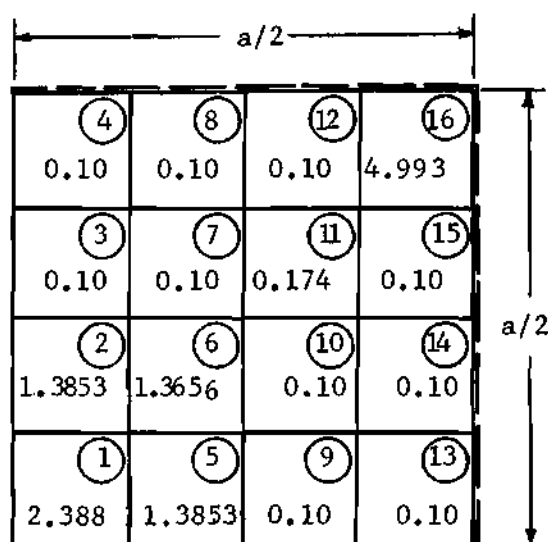
Figure 4.5. Normalized Thickness Distribution for an 'Optimum' Vibrating Square Plate Simply-Supported on All Sides



2 x 2 Element Quarter Plate



3 x 3 Element Quarter Plate



4 x 4 Element Quarter Plate

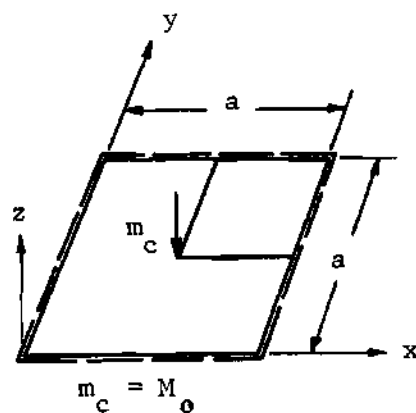
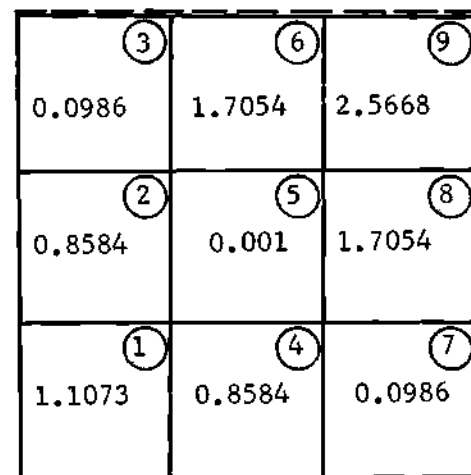
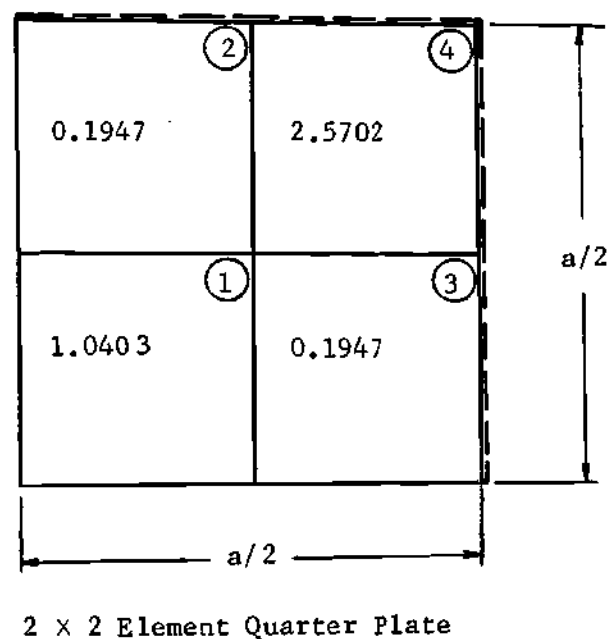


Figure 4.6. Normalized Thickness Distribution for an Optimum Vibrating Square Plate Simply-Supported on All Sides with a Concentrated Dead Mass at the Center; $h \geq 0.10 h_U$.



3 x 3 Element Quarter Plate
 $m_d(x,y) \equiv 0.50 M_0/ab$

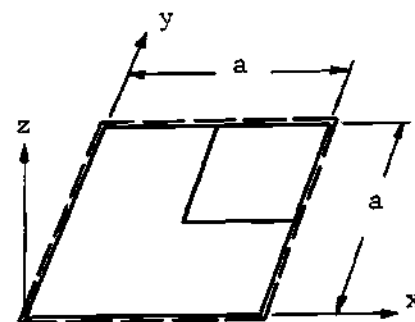
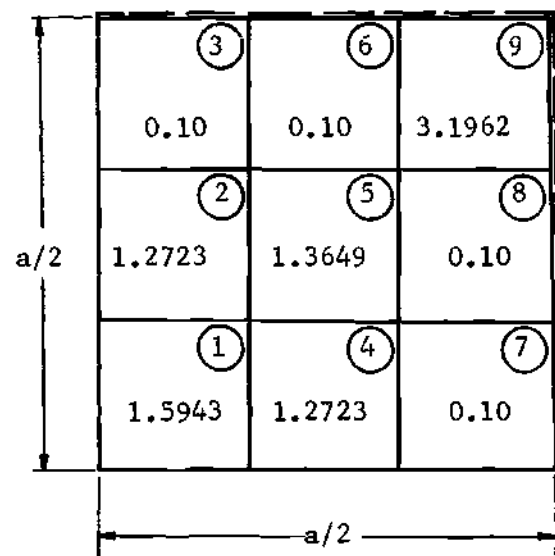
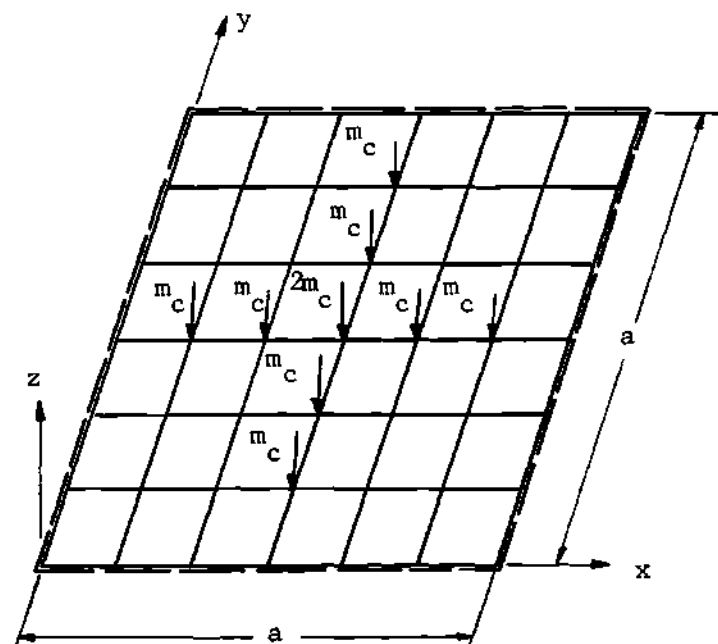


Figure 4.7. Normalized Thickness Distribution for an Optimum Vibrating Square Plate Simply-Supported on All Sides with a Uniformly Distributed Dead Mass;
 $h \geq 0.001 h_U$.



3 × 3 Element Quarter Plate



$$m_c = 0.10 M_0$$

Figure 4.8. Normalized Thickness Distribution for an Optimum Vibrating Square Plate Simply-Supported on All Sides with a Series of Concentrated Dead Masses; $h \geq 0.10 h_U$.

Table 4.1. Numerical Results for the 2×5 Element Half Plate Model shown in Fig. 4.2.

$$(\omega_1)_{\text{OPT}}^2 = 117.25 D_v / b^4 = 1.205 (\omega_1)_U^2$$

Element No.	(h_1/h_U)	$(c_1)_1$
1	1.2250	0.9995
2	1.1824	0.9992
3	1.0874	0.9995
4	0.9128	1.0002
5	0.5924	1.0009
6	1.2250	0.9995
7	1.1824	0.9992
8	1.0874	0.9995
9	0.9128	1.0002
10	0.5924	1.0009

Table 4.2. Numerical Results for the 3 x 3 Element Quarter Plate Model shown in Fig. 4.3.

$$(\omega_1)_{\text{OPT}}^2 = 408 D_v / a^4 = 3.40 (\omega_1)_U^2$$

Element No.	(h_1/h_U)	$(c_1)_i$
1	1.7223	0.9996
2	1.5458	0.9996
3	1.0694	0.9997
4	0.10	_____
5	0.10	_____
6	0.10	_____
7	1.7398	1.0145
8	1.5557	0.9961
9	1.0671	1.0000

Table 4.3. Numerical Results for the 3 × 3 Element Quarter Plate Model shown in Fig. 4.4.

$$(\omega_1)_{\text{OPT}}^2 = 212 D_v/a^4 = 2.22 (\omega_1)_U^2$$

Element No.	(h_i/h_U)	$(c_1)_i$
1	2.3968	0.9985
2	2.1484	0.9990
3	1.4877	1.0079
4	0.10	_____
5	0.10	_____
6	0.10	_____
7	0.2405	1.0038
8	0.7470	0.9965
9	1.6798	0.9946

Table 4.4. Numerical Results for the 2×2 Element Quarter Plate Model shown in Fig. 4.5.

$$(\omega_1)_{\text{OPT}}^2 = 1369 D_V / a^4 = 3.56 (\omega_1)_U^2$$

Element No.	(h_1/h_U)	$(c_1)_1$
1	0.9672	0.9983
2	0.1194	1.0172
3	0.1194	1.0172
4	2.7940	0.9991

Table 4.5. Numerical Results for the 3 x 3 Element Quarter Plate Model shown in Fig. 4.5.

$$(\omega_1)_{\text{OPT}}^2 = 2055 D_v / a^4 = 5.35 (\omega_1)_U^2$$

Element No.	(h_i/h_U)	$(c_1)_i$
1	0.5622	0.9999
2	0.3231	1.0000
3	0.0856	0.9999
4	0.3231	1.0000
5	2.7048	1.0000
6	0.0	_____
7	0.0856	0.9999
8	0.0	_____
9	4.9156	1.0000

Table 4.6. Numerical Results for the 4 x 4 Element Quarter Plate Model shown in Fig. 4.5.

$$(\omega_1)_{\text{OPT}}^2 \geq 3645 D_v / a^4$$

Element No.	(h_i/h_U)	$(c_1)_i$
1	0.4107	1.176
2	0.0	_____
3	0.297	1.0878
4	0.0663	1.0978
5	0.0	_____
6	1.8976	1.0095
7	0.661	0.9675
8	0.0	_____
9	0.297	1.0878
10	0.661	0.9675
11	5.96	1.0878
12	0.0899	0.9912
13	0.0663	1.0978
14	0.0	_____
15	0.0899	0.9912
16	6.5022	0.9913

Table 4.7. Numerical Results for the 2×2 Element Quarter Plate Model shown in Fig. 4.6.

$$(\omega_1)_{\text{OPT}}^2 = 252 D_V / a^4 = 3.43 (\omega_1)_U^2$$

Element No.	(h_i/h_U)	$(c_1)_i$
1	1.7407	0.9895
2	0.10	_____
3	0.10	_____
4	2.0592	1.0089

Table 4.8. Numerical Results for the 3 x 3 Element Quarter Plate Model shown in Fig. 4.6.

$$(\omega_1)_{\text{OPT}}^2 = 368.5 D_V / a^4 = 4.625 (\omega_1)_U^2$$

Element No.	(h_i/h_U)	$(c_1)_i$
1	2.8189	1.0047
2	0.10	_____
3	0.10	_____
4	0.10	_____
5	1.9559	0.9956
6	0.10	_____
7	0.10	_____
8	0.10	_____
9	3.6344	0.9987

Table 4.9. Numerical Results for the 4 X 4 Element Quarter Plate Model shown in Fig. 4.6.

$$(\omega_1)_{\text{OPT}}^2 = 377 D_v / a^4 = 5.24 (\omega_1)_U^2$$

Element No.	(h_i/h_U)	$(c_1)_i$
1	2.388	1.0122
2	1.3853	0.9760
3	0.10	_____
4	0.10	_____
5	1.3853	0.9760
6	1.3656	1.0036
7	0.10	_____
8	0.10	_____
9	0.10	_____
10	0.10	_____
11	0.1741	1.0988
12	0.10	_____
13	0.10	_____
14	0.10	_____
15	0.10	_____
16	4.9928	1.0006

Table 4.10. Numerical Results for the 2×2 Element Quarter Plate Model shown in Fig. 4.7.

$$(\omega_1)_{\text{OPT}}^2 = 735 D_v / a^4 = 2.83 (\omega_1)_U^2$$

Element No.	(h_i/h_U)	$(c_1)_i$
1	1.0403	0.9990
2	0.1947	0.9858
3	0.1947	0.9858
4	2.5702	1.0025

Table 4.11. Numerical Results for the 3 x 3 Element Quarter Plate Model shown in Fig. 4.7.

$$(\omega_1)_{\text{OPT}}^2 = 639 D_V / a^4 = 2.455 (\omega_1)_U^2$$

Element No.	(h_i/h_U)	$(c_1)_i$
1	1.1073	0.9990
2	0.8584	0.9991
3	0.0986	1.0001
4	0.8584	0.9991
5	0.001	_____
6	1.7054	1.0050
7	0.0986	1.0001
8	1.7054	1.0050
9	2.5668	0.9944

Table 4.12. Numerical Results for the 3 x 3 Element Quarter Plate Model shown in Fig. 4.8.

$$(\omega_1)_{\text{OPT}}^2 = 262.5 D_v / a^4 = 2.32 (\omega_1)_U^2$$

Element No.	(h_i/h_U)	$(c_1)_i$
1	1.5943	0.9938
2	1.2723	1.0107
3	0.10	_____
4	1.2723	1.0107
5	1.3649	0.9935
6	0.10	_____
7	0.10	_____
8	0.10	_____
9	3.1962	0.9937

Thin Rectangular Plates Under Destabilizing Loads

Assumptions and Objective

The assumptions made for the vibrating plate hold also for the stability analysis. In addition, it is assumed that although the strains are small, the slopes $w_{,x}$ and $w_{,y}$ are moderately large; such that $u_{,x}$, $u_{,y}$, $v_{,x}$ and $v_{,y}$ are of the same order of magnitude as $(w_{,x})^2$, $(w_{,y})^2$ and the corresponding strains.

As regards the objective, it is again required to distribute the material over the extent of the plate with a given aspect ratio, total volume (mass), with various boundary conditions and subjected to a given distribution of in-plane loading, so as to maximize the critical load parameter (see Chapter II for definition of the critical load parameter) subject to the constraint that the minimum thickness is no smaller than a specified value h_0 . Consideration is restricted only to those types of externally applied in-plane loadings for which \bar{N}_x is a constant or at most a function of y , \bar{N}_y is a constant or at most a function of x while \bar{N}_{xy} is a constant (see Fig. 4.9).

Formulation of the Problem

Although the Rayleigh quotient for this problem can be derived in a manner similar to the one used for columns in Chapter II, the details are omitted here for sake of brevity. Instead, the Rayleigh quotient is obtained from Ref. 26, page 168. where it has been derived by the application of the principle of virtual work to an initial stress problem. The expression for this Rayleigh quotient, with the sign convention for positive stress resultants as shown in Fig. 4.9, is given by

$$\lambda = \frac{\int_0^a \int_0^b \frac{Eh^3}{12(1-\nu^2)} \left[(w_{,xx} + w_{,yy})^2 - 2(1-\nu)(w_{,xx} w_{,yy} - w_{,xy}^2) \right] dx dy}{\int_0^a \int_0^b \left[N_{xx}^0 w_{,x}^2 + 2N_{xy}^0 w_{,x} w_{,y} + N_{yy}^0 w_{,y}^2 \right] dx dy} \quad (4.2.1)$$

where λ is stationary with respect to w and N_{xx}^0 , N_{yy}^0 and N_{xy}^0 represent the prebuckled stress distribution.

A simplified form of the Rayleigh quotient can be derived from the virtual work principle based on the assumption of inextensional deformation. This simplified form is

$$\lambda = \frac{\int_0^a \int_0^b D \left[(w_{,xx} + w_{,yy})^2 - 2(1-\nu)(w_{,xx} w_{,yy} - w_{,xy}^2) \right] dx dy}{\int_0^a \int_0^b \left[\bar{N}_x w_{,x}^2 + 2\bar{N}_{xy} w_{,x} w_{,y} + \bar{N}_y w_{,y}^2 \right] dx dy} \quad (4.2.2)$$

where $D = Eh^3/[12(1-\nu^2)]$.

This assumption of inextensionality, although inconsistent, predicts the critical loads surprisingly close to the exact values. This has been verified by a number of uniform plates with non-uniform tractions and non-uniform plates with uniform tractions. Another attractive feature of this assumption is that it simplifies the problem of optimization tremendously. Although no claim is made about obtaining an exact solution to the problem of optimization of a given plate by this simpler form, the conclusions drawn from this analysis lead to useful results associated with the order of magnitude of the critical load.

Hence, for the purposes of the development of the optimality condition, Eq. (4.2.2) will be used as the definition of the critical load parameter λ .

Thus, it is required that λ as defined by Eq. (4.2.2) be stationary with respect to w and h subject to the constant volume constraint

$$\int_0^a \int_0^b h \, dx dy = V. \quad (4.2.3)$$

Hence, the functional that must be extremized is

$$\begin{aligned} \lambda^* = & \frac{\int_0^a \int_0^b D \left[(w_{,xx} + w_{,yy})^2 - 2(1-\nu)(w_{,xx} w_{,yy} - w_{,xy}^2) \right] dx dy}{\int_0^a \int_0^b \left[\bar{N}_x w_{,x}^2 + 2\bar{N}_{xy} w_{,x} w_{,y} + \bar{N}_y w_{,y}^2 \right] dx dy} \\ & - \lambda_1 \left[\int_0^a \int_0^b h \, dx dy - V \right]. \end{aligned} \quad (4.2.4)$$

Setting the variations of λ^* with respect to both w and h , independently equal to zero leads to the governing equation with the associated boundary conditions and the optimality condition respectively. These are

$$\begin{aligned} & \left[D(w_{,xx} + w_{,yy}) \right]_{,xx} + 2(1-\nu) \left[D w_{,xy} \right]_{,xy} + \left[D(w_{,yy} + \nu w_{,xx}) \right]_{,yy} \\ & + \lambda \left[\bar{N}_x w_{,xx} + 2\bar{N}_{xy} w_{,xy} + \bar{N}_y w_{,yy} \right] = 0 \end{aligned} \quad (4.2.5)$$

Eitheror

$$\left. \begin{aligned}
 w = 0 \quad & \left[D(w_{,xx} + \nu w_{,yy}) \right]_{,x} + 2 \left[D(1-\nu)w_{,xy} \right]_{,y} \\
 & + \bar{N}_x w_{,x} + \bar{N}_{xy} w_{,y} = 0 \\
 w_{,x} = 0 \quad & D[w_{,xy} + \nu w_{,yy}] = 0
 \end{aligned} \right\} \begin{array}{l} \text{along } x=0, a \\ \\ \end{array} \quad (4.2.6.1)$$

$$\left. \begin{aligned}
 w = 0 \quad & \left[D(w_{,yy} + \nu w_{,xx}) \right]_{,y} + 2 \left[D(1-\nu)w_{,xy} \right]_{,x} \\
 & + \bar{N}_y w_{,y} + \bar{N}_{xy} w_{,x} = 0 \\
 w_{,y} = 0 \quad & D[w_{,yy} + \nu w_{,xx}] = 0
 \end{aligned} \right\} \begin{array}{l} \text{along } y = 0, b \\ \\ \end{array} \quad (4.2.6.2)$$

and

$$h^2 \left[(w_{,xx} + w_{,yy})^2 - 2(1-\nu)(w_{,xx} w_{,yy} - w_{,xy}^2) \right] = c^2 = \text{constant}. \quad (4.2.7)$$

Equation (4.2.7) is the mathematical expression of the optimality condition. Multiplication of both sides of this equation by $Eh/[12(1-\nu^2)]$ followed by integration with respect to x and y over the extent of the plate yields $U = [Ec^2/12(1-\nu^2)] V$.

That is to say

$$c^2 = \frac{12(1-\nu^2)}{E} \frac{U}{V} .$$

Hence, Eq. (4.2.7) can be written as

$$\frac{W}{h} = \frac{U}{V} = \text{constant} \quad (4.2.8)$$

where

$$W = \frac{Eh^3}{12(1-\nu^2)} \left[(w_{,xx} + w_{,yy})^2 - 2(1-\nu)(w_{,xx} w_{,yy} - w_{,xy}^2) \right] .$$

Optimization Procedure

From the development in Chapter II it follows that the solution of the optimization problem of plates with the underlying assumptions reduces to the solution of the following equations in finite element matrix form

$$\left[[K_s]_p - \lambda [K_G]_p \right] \{q\} = \{0\} , \quad (4.2.9)$$

$$\frac{U_i}{V_i} = \frac{U}{V} = \text{constant} \quad (4.2.10)$$

and

$$\sum_{i=1}^m h_i a_i b_i = \frac{V}{4} \quad (\text{see Fig. C-1}) \quad (4.2.11)$$

where $[K_s]_p$ and $[K_G]_p$ are the assembled nonsingular stiffness and stability matrices for the entire plate. The problem in finite element form is in no way different from the column problem of Chapter II and no further details need be repeated.

Numerical Results and Conclusions

The criterion for convergence on the optimality condition is

$$\left[\left(\frac{U_i}{v_i} \right)_{\max} / \left(\frac{U_j}{v_j} \right)_{\min} - 1.0 \right] \times 100 < 5.0 \quad .$$

A number of cases of plates with various aspect ratios, boundary conditions and in-plane loadings, shown in Figs. 4.10 through 4.17, is discussed next. The numerical results for these cases are tabulated in Tables 4.13 through 4.23. In these tables, the symbol D_g denotes the quantity $(E/[12(1-\nu^2)])(V/ab)^3$; the symbol h_U denotes the quantity $V/(ab)$; the symbols λ_{OPT} and λ_U denote critical loads for the finite element models with the optimum and uniform thickness distributions respectively; and the symbol c_i^2 denotes the quantity $(U_i V / v_i U)$. Normalized thickness is defined to be the ratio h_i/h_U .

Figure 4.10 shows the case of a rectangular plate simply-supported along two opposite edges and forced to bend cylindrically while loaded with a uniform compression acting in a direction normal to the simply-supported edges. This is intended to model a column using plate bending elements. The results agree well (see Table 4.13) with those obtained for a column with $I(x) = \rho A^3(x)$ and $m=10$. Exactly the same results are obtained even when the stability matrix is calculated using the true

prebuckled plane stress distribution at each iteration of the optimization procedure. This implies that the assumption of inextensionality is not in error for buckled surfaces which are cylindrical or very nearly so. This conclusion is also confirmed by the next two cases.

Figure 4.11 shows the case of a rectangular plate with an aspect ratio $a/b = 1/3$, simply-supported along the edges $y = \text{constant}$ and free on the edges $x = \text{constant}$. The plate is loaded with uniform compression in the x -direction. The plate with such an aspect ratio and boundary conditions behaves very much like an Euler column and the assumption of inextensionality is not again very much in error. The numerical results for this case are tabulated in Table 4.14.

Figure 4.12 shows the case of a rectangular plate with an aspect ratio $a/b = 1/3$ and simply-supported along all edges. The plate is loaded with uniform compression in the x -direction. The numerical results for this case are tabulated in Table 4.15. Comparison of these results with those reported in Table 4.14, for Fig. 4.11, shows that the effect of boundary conditions is negligible for this aspect ratio $a/b = 1/3$.

Figure 4.13 shows the thickness distribution for a 4×4 element model of a square plate simply-supported on all sides and loaded with uniform compression in the x -direction. Numerical results for these two models with $h \geq h_o = 0.10 h_U$ are tabulated in Tables 4.16 and 4.17 respectively.

Figure 4.14 shows the thickness distributions for a 4×4 , a 6×6 and an 8×8 element models of a square plate simply-supported on

all sides and subjected to equal biaxial compression. The differences in the final values of the critical loads obtained for these three models (see Tables 4.18 through 4.20) are small enough to perhaps conclude that the corresponding continuous system does possess a finite optimum critical load.

Figure 4.15(i) shows the thickness distribution for a 6×6 element model of a simply-supported square plate under equal biaxial compression and with the inequality constraint of $h \geq h_o = 0.10 h_U$. As a result of this inequality constraint, the critical load of this model (see Table 4.21) is reduced by about seven per cent in comparison with the critical load of the 6×6 element model of Fig. 4.14 (see Table 4.19). Incidentally, the exact critical load for the thickness distribution of Fig. 4.15(i) (the true prebuckled stress distribution is used) shows a reduction of about 17% in comparison with the value shown in Table 4.21.

Figure 4.15(ii), on the other hand, shows the thickness distribution for another 6×6 element model of the same square plate considered in Fig. 4.15(i). This is a model which meets the optimality condition, Eq. (4.2.10), with $h \geq h_o = 0.10 h_U$ although for each iteration of the optimization procedure the true prebuckled stress distribution, as determined by the plane stress analysis, is used for the construction of the stability matrix. This model has therefore been called a quasi-optimum extensional model; and would be much closer to the truly optimum model than the one shown in Fig. 4.15(i). The reason for this is as follows. Had Eq. (4.2.1) been adopted as the definition of the

critical load parameter λ , then the only approximation for this model is that the variation of the denominator of the Rayleigh quotient with respect to h is ignored. This way the same optimality condition, Eq. (4.2.8), is obtained. The numerical results for this quasi-optimum extensional model are tabulated in Table 4.22.

Finally, Fig. 4.6 shows the thickness distribution for a 4×4 element model of a square plate simply-supported on all sides and subjected to a uniform shear. The optimized model which is extremely strong in buckling for the assumed direction of shear seems to be extremely weak in buckling shear acting in the opposite direction. The material is concentrated along the tension diagonal which seems to be the preferential direction for the optimized model. The numerical results for this case with $h \geq h_0 = 0.10 h_U$ are tabulated in Table 4.24.

Next, the 6×6 element model of Fig. 4.13 is compared with a simply-supported stiffened square plate of the same volume and with two equally spaced stiffeners in the direction of the load (see Fig. 4.17). It will be shown that, with a proper choice of stiffener dimensions, such a plate under uniaxial compression is capable of carrying almost three times the critical load of a uniform thickness simply-supported square plate of the same volume.

Consider a simply-supported square plate of uniform thickness h_U and size $a \times a$ under a uniaxial compression $\bar{N}_x = \text{constant}$. The critical value of \bar{N}_x for such a plate is well known to be

$$\left(\bar{N}_{x_{cr}}\right)_U = \frac{4\pi^2}{a^2} \frac{E}{12(1-\nu^2)} (h_U)^3 .$$

Next, consider the stiffened plate shown in Fig. 4.17 with two identical stiffeners which are equally spaced.

Assume $b_s = \frac{a}{120}$, $h_s = 10 h_U$ and $h_1 = \frac{5}{6} h_U$. Total volume of the stiffened plate is given by

$$\frac{5}{6} h_U a^2 + 2 \left(\frac{a}{120} \right) (10 h_U) a = h_U a^2 = v.$$

I_s = Cross-sectional moment of inertia of one stiffener

$$= \frac{1}{12} \left(\frac{a}{120} \right) (10 h_U)^3 = \left(\frac{100}{12} \right) \left(\frac{h_U^3}{12} \right) a.$$

(This seems conservative for stiffeners placed on both sides of the sheet.)

A_s = Cross-sectional area of the stiffener

$$= \left(\frac{a}{120} \right) (10 h_U) = \frac{a}{12} h_U.$$

Hence, in the notation of Ref. 30 (pp. 394-400)

$$\gamma = \frac{EI_s}{aD_1} = \frac{E \left[\left(\frac{100}{12} \right) \left(\frac{h_U^3}{12} \right) a \right]}{\frac{E}{12(1-\nu^2)} \left[\left(\frac{5}{6} h_U \right)^3 a \right]} = 13.10 \quad \text{for } \nu=0.30.$$

$$\delta = \frac{A_s}{ah_1} = \frac{a \left(\frac{h_U}{12} \right)}{a \left(\frac{5}{6} h_U \right)} = 0.10 \quad \text{and } \beta=1.0.$$

Hence, if γ is conservatively assumed to be equal to 10 with $\delta = 0.10$ and $\beta = 1.0$, Table 9-17, page 400, Ref. 30 yields

$$\begin{aligned} (\bar{N}_{x_{cr}})_s &= 25.6 \frac{\pi^2 D_1}{a^2} = 25.6 \frac{\pi^2 \frac{E}{12(1-\nu^2)} \left(\frac{5}{6} h_U\right)^3}{a^2} \\ &\approx 14.248 \frac{\pi^2 D_U}{a^2} \approx 3.56 (\bar{N}_{x_{cr}})_U \end{aligned}$$

where

$$D_U = \frac{E h_U^3}{12(1-\nu^2)}.$$

Thus, the critical load of this stiffener-sheet combination is nearly $3\frac{1}{2}$ times that of the uniform thickness plate of the same volume. It can indeed be argued that this distribution of material $h(x,y)$ does not fall in the same class of functions as was assumed apriori for the derivation of the optimality condition. However, the fact still remains that stiffened plates are indeed very promising candidates in the optimization of thin rectangular plates for buckling more so because they can be manufactured with relatively higher saving in cost and labour in comparison with machined or chem-milled plates. Further, it must be recognized that the stiffener dimensions chosen are by no means unrealistic and for such dimensions, the stiffener crippling will not reduce the design capability of the plate. For instance, consider a 7075-T6 (bare) plate with $a = 30''$ and $h_U = 0.75''$. Then $b_s = 0.25''$ and $h_s = 7.5''$. For such a plate it is found that the crippling allowable for the stiffener is far in excess of the buckling allowable for the

uniform thickness plate. Finally, it must be remarked that there might very well be other stiffener-sheet combinations which might lead to critical loads well in excess of $3.5 \left(\bar{N}_{x_{cr}} \right)_U$. The number of stiffeners, their spacing, orientation and the type of stiffeners cross-section which will maximize the critical load would be a subject of further research -- a research that will most certainly yield very fruitful results.

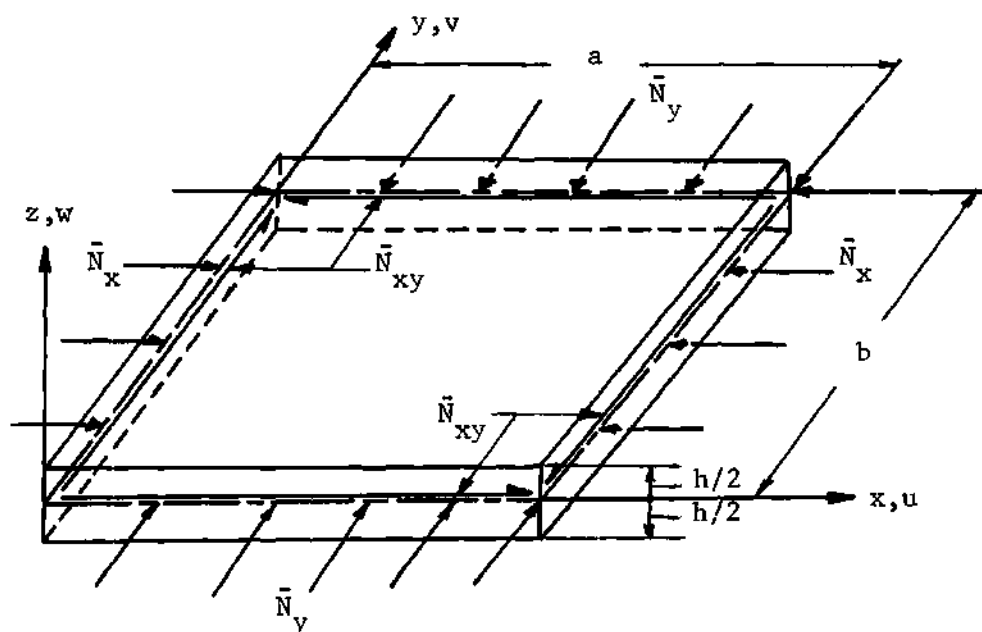


Figure 4.9. A Typical Rectangular Plate Under In-Plane Loading

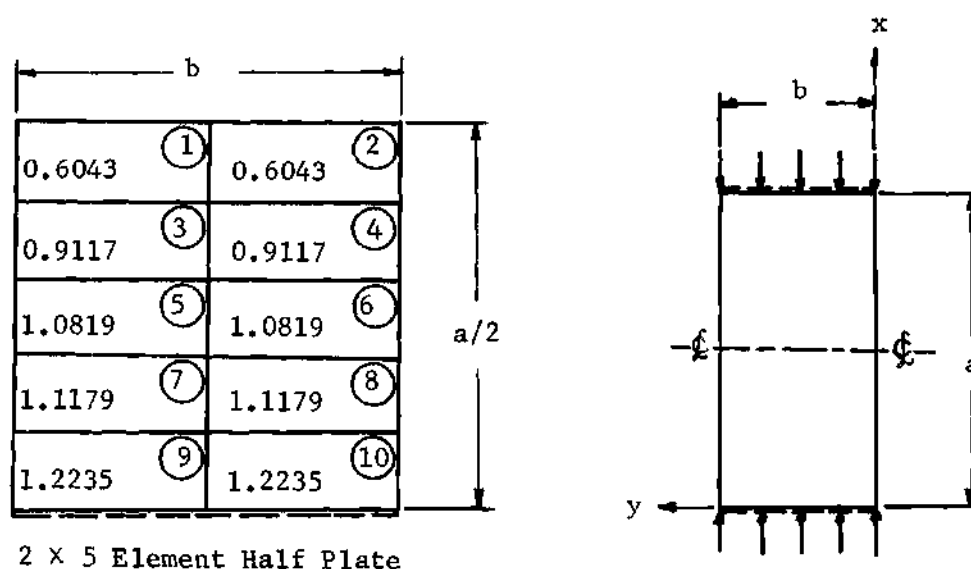
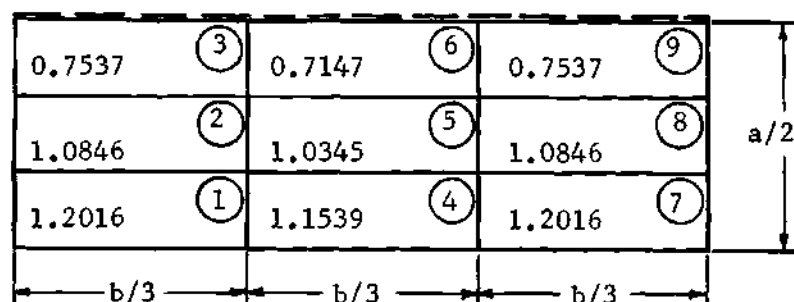


Figure 4.10. Normalized Thickness Distribution for an Optimum Rectangular Plate Simply-Supported on Sides $x = 0, a$ with Imposed Cylindrical Bending Under Uniaxial Compression



3 × 3 Element Half Plate (Not to scale)

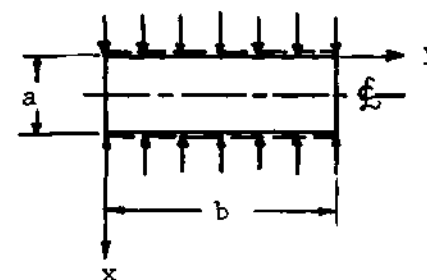
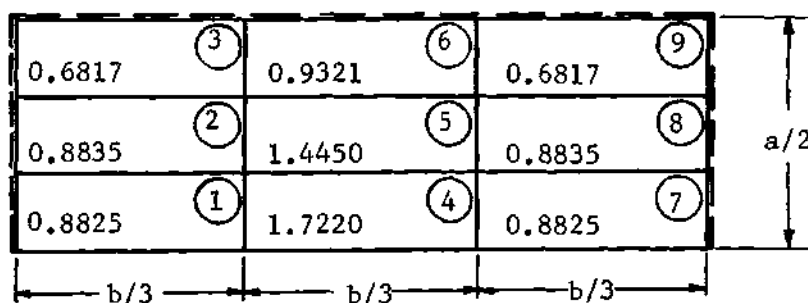


Figure 4.11. Normalized Thickness Distribution for an Optimum Rectangular Plate Simply-Supported on Sides $x = 0, a$ and Free on Sides $y = 0, b$; Under Uniaxial Compression



3 × 3 Element Half Plate (Not to scale)

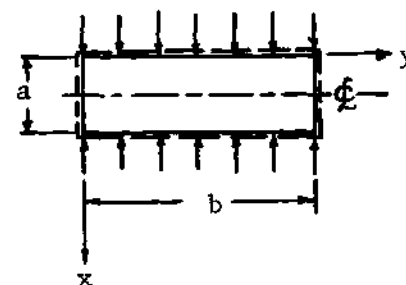
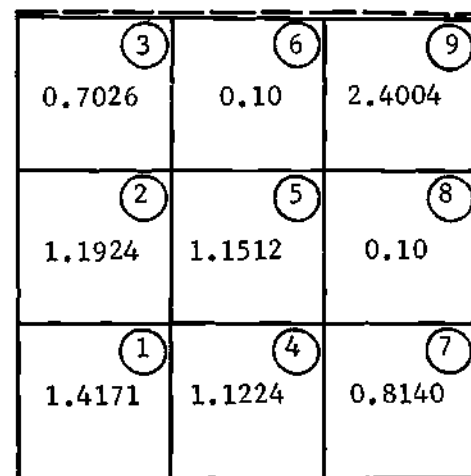
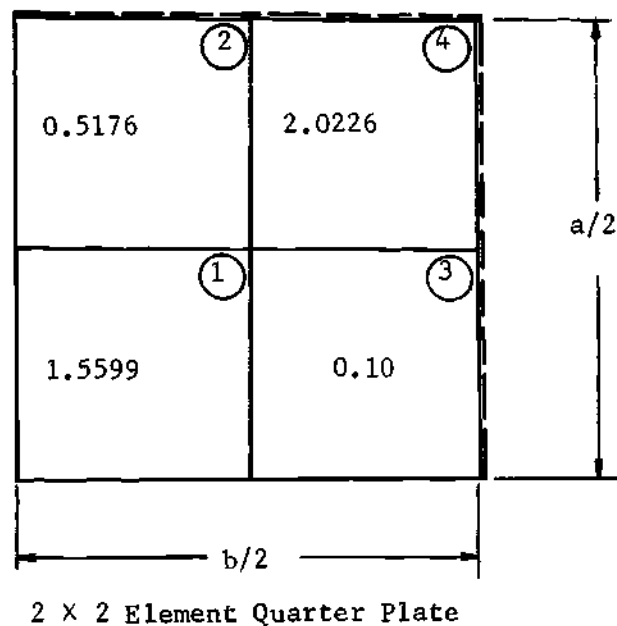


Figure 4.12. Normalized Thickness Distribution for an Optimum Rectangular Plate Simply-Supported on All Sides Under Uniaxial Compression



3 x 3 Element Quarter Plate

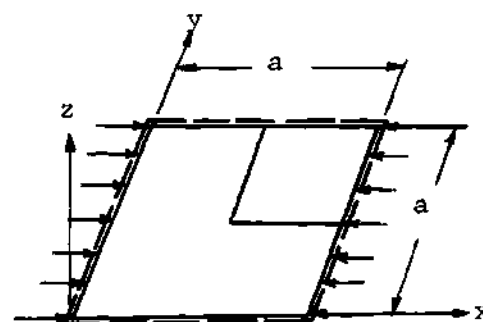


Figure 4.13. Normalized Thickness Distribution for an Optimum Square Plate Simply-Supported on All Sides Under Uniaxial Compression; $h \geq 0.10 h_U$.

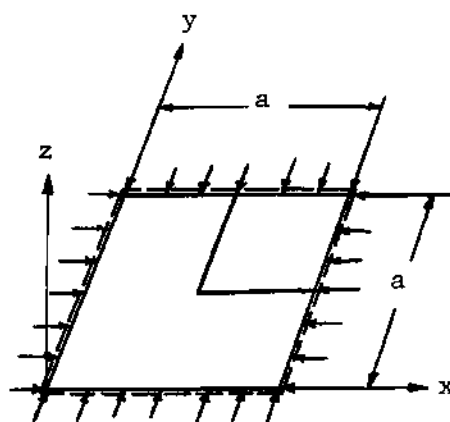
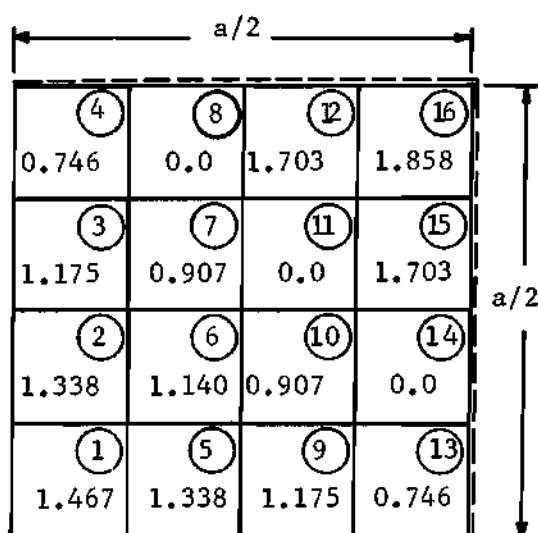
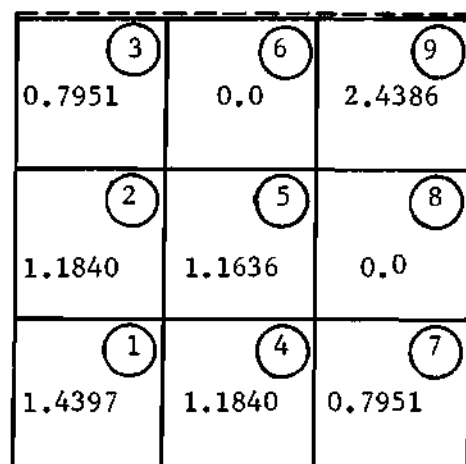
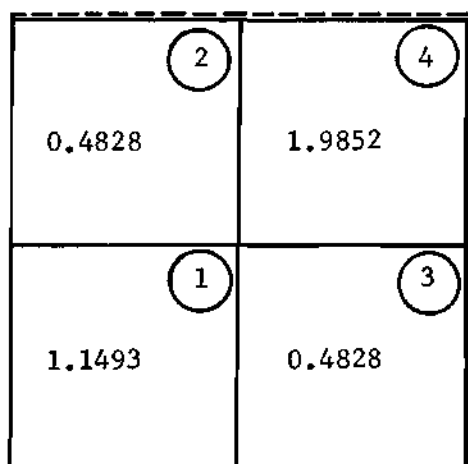
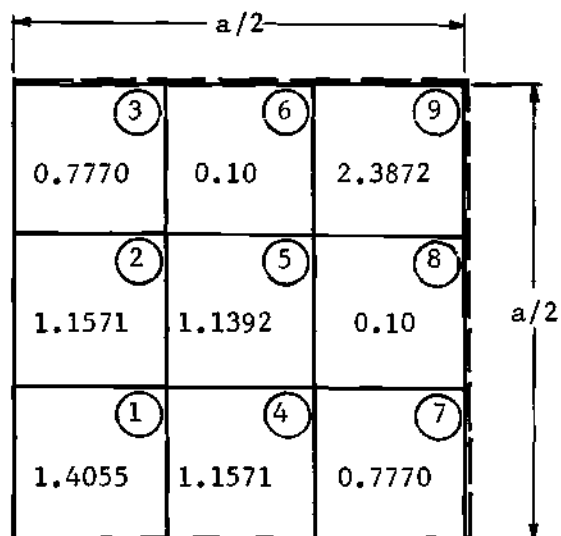
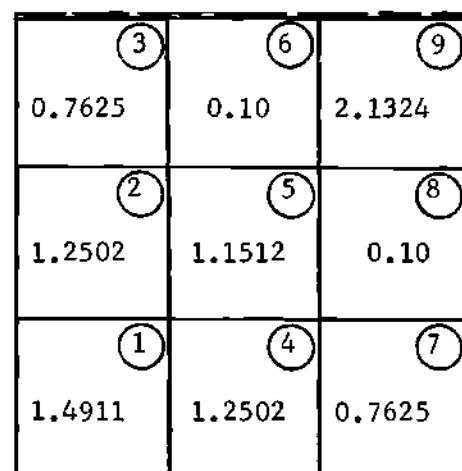


Figure 4.14. Normalized Thickness Distribution for an Optimum Square Plate Simply-Supported on All Sides Under Equal Biaxial Compression.



(i) 3×3 Element Quarter Plate



(ii) 3×3 Element Quarter Plate

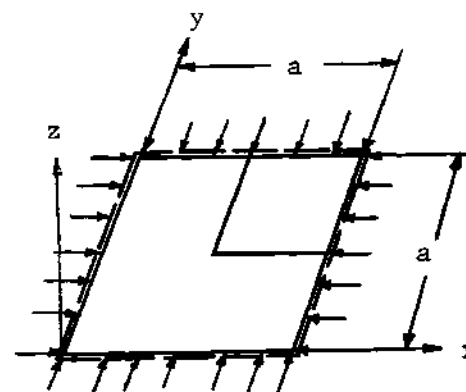
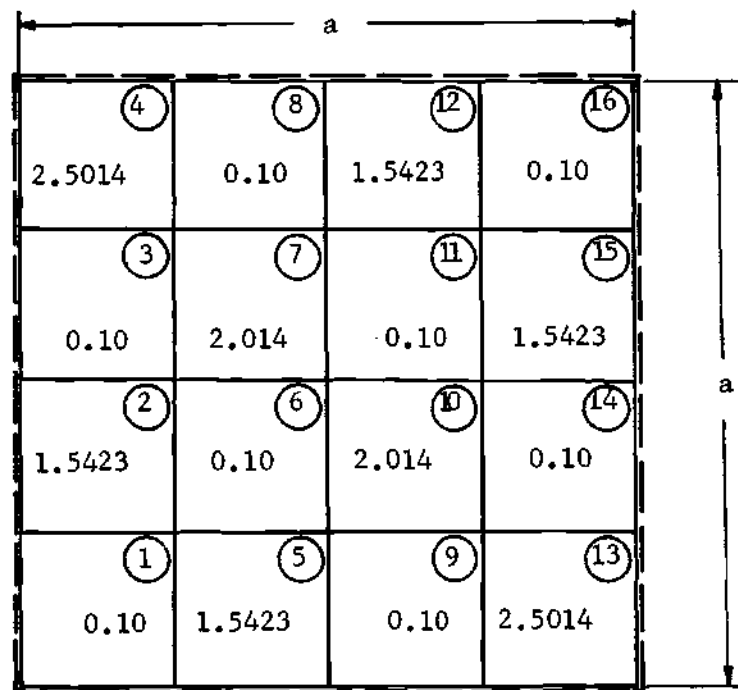


Figure 4.15. Normalized Thickness Distribution for a Square Plate Simply-Supported on All Sides Under Equal Biaxial Compression; (i) Optimum Inextensional Model with $h \geq 0.10 h_U$; (ii) Quasi-Optimum Extensional Model with $h \geq 0.10 h_U$.



4 x 4 Element Quarter Plate

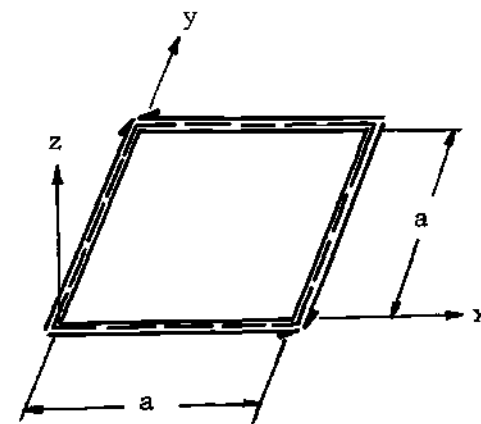
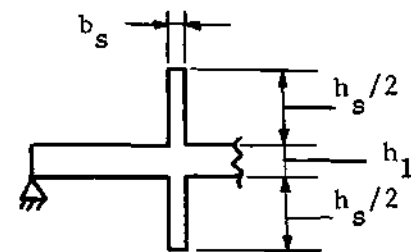
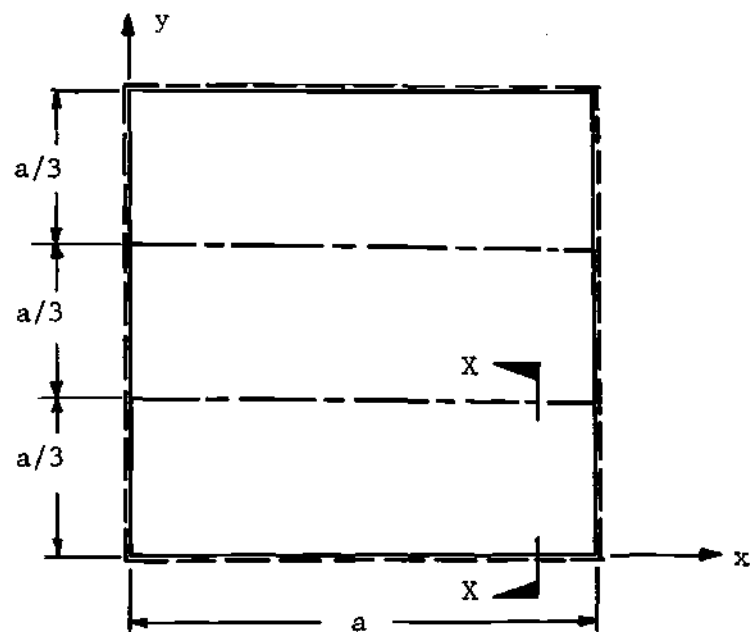


Figure 4.16. Normalized Thickness Distribution for an Optimum Square Plate Simply-Supported on All Sides Under Uniform Shear; $h \geq 0.10 h_U$.



Section XX

Figure 4.17. A Typical Stiffened Square Plate

Table 4.13. Numerical Results for the 2 x 5 Element Half Plate Model shown in Fig. 4.10.

$$\lambda_{\text{OPT}} = 13.05 D_s / a^2 = 1.325 \lambda_U$$

Element No.	(h_i/h_U)	c_i^2
1	0.6043	0.9879
2	0.6043	0.9879
3	0.9117	1.0008
4	0.9117	1.0008
5	1.0819	1.0018
6	1.0819	1.0018
7	1.1179	1.0017
8	1.1179	1.0017
9	1.2235	1.0016
10	1.2235	1.0016

Table 4.14. Numerical Results for the 3 x 3 Element Half Plate Model shown in Fig. 4.11.

$$\lambda_{\text{OPT}} = 12.12 D_s / a^2 = 1.25 \lambda_U$$

Element No.	(h_i/h_U)	c_i^2
1	1.2016	1.0024
2	1.0846	1.0046
3	0.7537	1.0081
4	1.1539	0.9915
5	1.0345	0.9904
6	0.7147	0.9888
7	1.2016	1.0024
8	1.0846	1.0046
9	0.7537	1.0081

Table 4.15. Numerical Results for the 3 x 3 Element Half Plate Model shown in Fig. 4.12.

$$\lambda_{OPT} = 16.82 D_s / a^2 = 1.385 \lambda_U$$

Element No.	(h_i/h_U)	c_i^2
1	0.8825	0.9786
2	0.8835	0.9895
3	0.6817	0.9960
4	1.7220	1.0223
5	1.4450	1.0129
6	0.9321	1.0048
7	0.8825	0.9786
8	0.8835	0.9895
9	0.6817	0.9960

Table 4.16. Numerical Results for the 2×2 Element Quarter Plate Model shown in Fig. 4.13.

$$\lambda_{\text{OPT}} = 41.65 D_s / a^2 = 2.11 \lambda_U$$

Element No.	(h_i/h_U)	c_i^2
1	1.5599	0.9910
2	0.5176	0.9954
3	0.10	_____
4	2.0226	1.0081

Table 4.17. Numerical Results for the 3 × 3 Element Quarter Plate Model shown in Fig. 4.13.

$$\lambda_{\text{OPT}} = 36.7 D_s / a^2 = 1.81 \lambda_U$$

Element No.	(h_i/h_U)	c_i^2
1	1.4171	0.9959
2	1.1924	1.0088
3	0.7026	1.0176
4	1.1224	1.0031
5	1.1512	0.9900
6	0.10	_____
7	0.8140	1.0081
8	0.10	_____
9	2.4004	0.9935

Table 4.18. Numerical Results for the 2×2 Element Quarter Plate Model shown in Fig. 4.14.

$$\lambda_{\text{OPT}} = 31.15 D_s / a^2 = 1.58 \lambda_U$$

Element No.	(h_1/h_U)	c_1^2
1	1.1493	0.9964
2	0.4828	0.9952
3	0.4828	0.9952
4	1.9852	1.0046

Table 4.19. Numerical Results for the 3×3 Element Quarter Plate Model shown in Fig. 4.14.

$$\lambda_{\text{OPT}} = 38.05 D_s / a^2 = 1.90 \lambda_U$$

Element No.	(h_i/h_U)	c_i^2
1	1.4397	1.0000
2	1.1840	1.0000
3	0.7951	1.0000
4	1.1840	1.0000
5	1.1636	1.0000
6	0.0	_____
7	0.7951	1.0000
8	0.0	_____
9	2.4386	1.0000

Table 4.20. Numerical Results for the 4 x 4 Element Quarter Plate Model shown in Fig. 4.14.

$$\lambda_{\text{OPT}} = 36.60 D_s / a^2 = 1.835 \lambda_U$$

Element No.	(h_i/h_U)	c_i^2
1	1.4667	0.9953
2	1.3382	0.9950
3	1.1747	0.9912
4	0.7459	0.9910
5	1.3382	0.9950
6	1.1400	0.9900
7	0.9067	0.9933
8	0.0	_____
9	1.1747	0.9912
10	0.9067	0.9933
11	0.0	_____
12	1.7026	1.0319
13	0.7459	0.9910
14	0.0	_____
15	1.7026	1.0319
16	1.8584	0.9826

Table 4.21. Numerical Results for the 3 x 3 Element Quarter Plate Model shown in Fig. 4.15(i).

$$\lambda_{\text{OPT}} = 35.65 D_s / a^2 = 1.80 \lambda_U$$

Element No.	(h_i/h_U)	c_i^2
1	1.4055	1.0307
2	1.1571	1.0258
3	0.7770	1.0115
4	1.1571	1.0258
5	1.1392	1.0060
6	0.10	_____
7	0.7770	1.0115
8	0.10	_____
9	2.3872	1.0118

Table 4.22. Numerical Results for the 3×3 Element Quarter Plate Model shown in Fig. 4.15(ii).

$$\lambda_{\text{OPT}} = 30.90 D_s / a^2 = 1.565 \lambda_U$$

Element No.	(h_i/h_U)	c_i^2
1	1.4911	1.0369
2	1.2502	1.0410
3	0.7625	1.0353
4	1.2502	1.0410
5	1.1512	1.0432
6	0.10	_____
7	0.7625	1.0353
8	0.10	_____
9	2.1324	1.0234

Table 4.23. Numerical Results for the 4 x 4 Element Full Plate Model shown in Fig. 4.16.

$$\lambda_{\text{OPT}} = 29.45 D_s / a^2 = 3.17 \lambda_U$$

Element No.	(h_i/h_U)	c_i^2
1	0.10	_____
2	1.5423	0.9885
3	0.10	_____
4	2.5014	1.0073
5	1.5423	0.9885
6	0.10	_____
7	2.0140	0.9952
8	0.10	_____
9	0.10	_____
10	2.0140	0.9952
11	0.10	_____
12	1.5423	0.9885
13	2.5014	1.0073
14	0.10	_____
15	1.5423	0.9885
16	0.10	_____

APPENDIX A

FINITE ELEMENT DISPLACEMENT METHOD AS APPLIED TO BUCKLING OF COLUMNS

As a first step it is assumed that the response of the system which has in fact infinite degrees of freedom can be effectively represented by a finite number of degrees of freedom as shown below. To do this, the system is broken into small elements each extending, in this case, between two nodes. The response of each of these elements to externally applied equivalent nodal loads is determined. Finally by assembling all the elements together the response of the complete system is obtained.

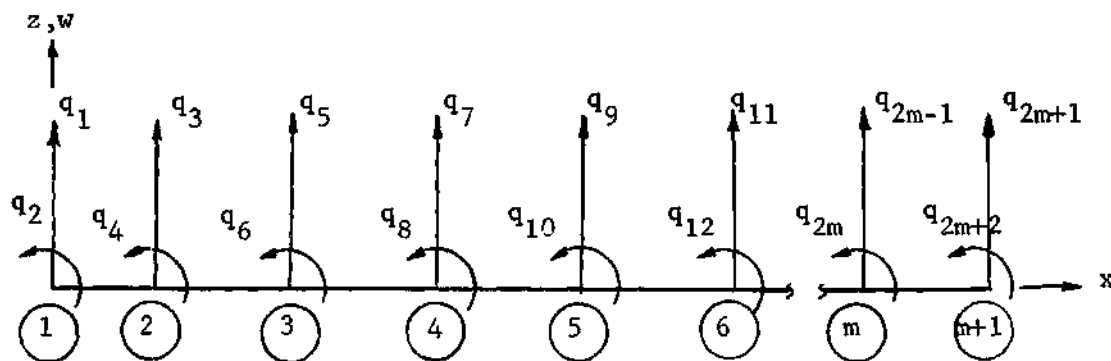


Figure A-1. Finite Element Representation of a Column

In the case of the column, each element has only two generalized forces at each node namely a shear force and a moment and corresponding to these two generalized forces are the two generalized displacements namely the vertical displacement and the slope or the rotation. Let (u_1^i, u_2^i) , (u_3^i, u_4^i) denote these generalized displacements at the two

nodes of the i^{th} element whose length is denoted by ℓ_i .

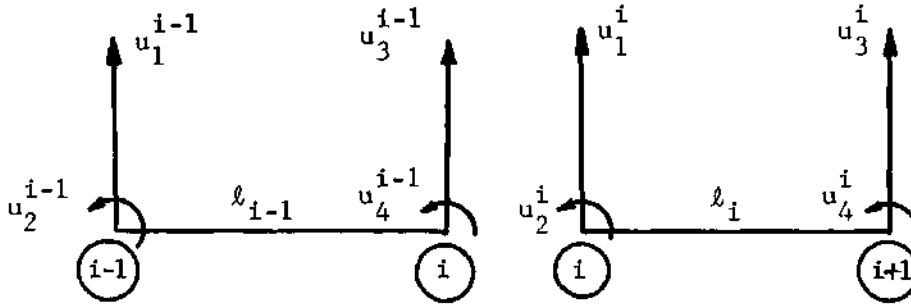


Figure A-2. Two Typical Adjacent Beam Elements

The next step is the choice of a suitable displacement function for each element. Since this method is derived from the principle of the stationary value of total potential, it is necessary that the displacement field be compatible, both within the element and at the interface between the two elements meeting at a node. Necessary compatibility between the two elements will be satisfied if the appropriate generalized displacements are equal at the node common to the two elements. This can be assured by requiring that

$$\left. \begin{aligned} u_3^{i-1} &= u_1^i = q_{2i-1} \\ u_4^{i-1} &= u_2^i = q_{2i} \end{aligned} \right\} \text{ for the } i^{\text{th}} \text{ node (see Fig. A-2).}$$

In addition to these above equations for each of the intermediate nodes, there are similar equations for the two end nodes namely

$$u_1^1 = q_1 \quad u_2^1 = q_2$$

and

$$u_3^m = q_{2m+1} \quad u_4^m = q_{2m+2}$$

All these equations can be written concisely in the matrix form as

$$\underline{u} = \underline{B} \underline{q} \quad (\text{A-1})$$

where \underline{u} and \underline{q} are column vectors with $4m$ and $(2m+2)$ rows respectively and \underline{B} is a rectangular array of size $4m \times (2m+2)$ whose elements are either 0 or 1. An illustration of Eq. (A-1) for a two beam-element idealization of a column would be

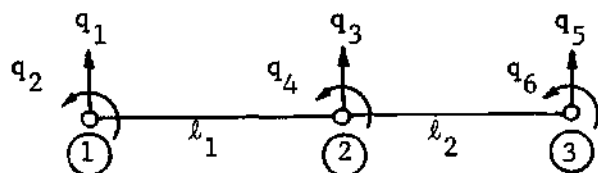


Figure A-3. A Two Beam-Element Model of a Column

$$\begin{Bmatrix} u_1^1 \\ u_1^2 \\ u_2^1 \\ u_2^2 \\ u_3^1 \\ u_3^2 \\ u_4^1 \\ u_4^2 \end{Bmatrix} = \begin{bmatrix} 1 & 0 & 0 & 0 & 0 & 0 \\ 0 & 1 & 0 & 0 & 0 & 0 \\ 0 & 0 & 1 & 0 & 0 & 0 \\ 0 & 0 & 0 & 1 & 0 & 0 \\ 0 & 0 & 1 & 0 & 0 & 0 \\ 0 & 0 & 0 & 1 & 0 & 0 \\ 0 & 0 & 0 & 0 & 1 & 0 \\ 0 & 0 & 0 & 0 & 0 & 1 \end{bmatrix} \begin{Bmatrix} q_1 \\ q_2 \\ q_3 \\ q_4 \\ q_5 \\ q_6 \end{Bmatrix}$$

Compatibility within the element requires that the displacement field be continuous with continuous derivatives within the element. The element has four degrees of freedom and a complete cubic polynomial expansion has also four unknown parameters and is continuous with continuous derivatives. Hence one can write for the i^{th} element

$$w_i(x_i) = a_0 + a_1 x_i + a_2 x_i^2 + a_3 x_i^3 ; \quad 0 \leq x_i \leq \ell_i \quad (\text{A-2})$$

Further this displacement function includes rigid body motion and constant strain (i.e. constant curvature in this case) which are necessary for convergence to the true solution.

Next, it is necessary to relate the unknown parameters a 's to q 's. Equation (A-2) can be written in matrix form as

$$w_i(x_i) = \begin{bmatrix} 1 & x_i & x_i^2 & x_i^3 \end{bmatrix} \begin{Bmatrix} a_0 \\ a_1 \\ a_2 \\ a_3 \end{Bmatrix} ; \quad 0 \leq x_i \leq \ell_i .$$

Next, since

$$w_i(0) = u_1^i$$

$$w_i'(0) = u_2^i$$

$$w_i(\ell_i) = u_3^i$$

$$w'_i(\ell_i) = u_4^i$$

there are four equations which relate a's to q's and these can be expressed in matrix form as

$$[c^i] \{a\} = \{u^i\} \quad (A-3)$$

where

$$[c^i] = \begin{bmatrix} 1 & 0 & 0 & 0 \\ 0 & 1 & 0 & 0 \\ 1 & \ell_i & \ell_i^2 & \ell_i^3 \\ 0 & 1 & 2\ell_i & 3\ell_i^2 \end{bmatrix} \quad (A-4)$$

Hence

$$\{a\} = [c^i]^{-1} \{u^i\}$$

where

$$[c^i]^{-1} = \begin{bmatrix} 1 & 0 & 0 & 0 \\ 0 & 1 & 0 & 0 \\ \frac{-3}{\ell_i^2} & \frac{-2}{\ell_i} & \frac{3}{\ell_i^2} & \frac{-1}{\ell_i} \\ \frac{2}{\ell_i^3} & \frac{1}{\ell_i^2} & \frac{-2}{\ell_i^3} & \frac{1}{\ell_i^2} \end{bmatrix} \quad (A-5)$$

Hence

$$\begin{aligned}
 w_i(x_i) &= \begin{bmatrix} 1 & x_i & x_i^2 & x_i^3 \end{bmatrix} [c^i]^{-1} \{u^i\} \\
 &= (\underline{H}^i)^t \underline{u}^i
 \end{aligned}
 \tag{A-6}$$

Upon letting $\xi_i = x_i/\ell_i$ one has

$$\{\underline{H}^i\}^t = \begin{Bmatrix} (1 - 3\xi_i^2 + 2\xi_i^3) \\ \ell_i(\xi_i - 2\xi_i^2 + \xi_i^3) \\ (3\xi_i^2 - 2\xi_i^3) \\ \ell_i(-\xi_i^2 + \xi_i^3) \end{Bmatrix}^t$$

Hence

$$w'_i(x_i) = \begin{Bmatrix} 1/\ell_i(-6\xi_i + 6\xi_i^2) \\ (1 - 4\xi_i + 3\xi_i^2) \\ 1/\ell_i(6\xi_i - 6\xi_i^2) \\ (-2\xi_i + 3\xi_i^2) \end{Bmatrix}^t \{u^i\} = (\underline{Q}^i)^t \underline{u}^i
 \tag{A-7}$$

and

$$w_i''(x_i) = \left\{ \begin{array}{c} 1/l_i^2(-6 + 12\xi_i) \\ 1/l_i(-4 + 6\xi_i) \\ 1/l_i^2(6 - 12\xi_i) \\ 1/l_i(-2 + 6\xi_i) \end{array} \right\}^t \quad \{u^i\} = (\underline{Y}^i)^t \underline{u}^i \quad (A-8)$$

where primes denote differentiation with respect to x_i . It therefore follows that

$$[w_i(x_i)]^2 = (\underline{u}^i)^t \underline{H}^i (\underline{H}^i)^t \underline{u}^i = \underline{u}^t \underline{G}^i (\underline{G}^i)^t \underline{u} \quad (A-9)$$

$$[w_i'(x_i)]^2 = (\underline{u}^i)^t \underline{Q}^i (\underline{Q}^i)^t \underline{u}^i = \underline{u}^t \underline{L}^i (\underline{L}^i)^t \underline{u} \quad (A-10)$$

$$[w_i''(x_i)]^2 = (\underline{u}^i)^t \underline{Y}^i (\underline{Y}^i)^t \underline{u}^i = \underline{u}^t \underline{R}^i (\underline{R}^i)^t \underline{u} \quad (A-11)$$

In Eqs. (A-9), (A-10) and (A-11) the matrix \underline{u} is a column array having $4m$ entries which represent the $4m$ degrees of freedom of the m elements and matrices \underline{G}^i , \underline{L}^i and \underline{R}^i are nothing but matrices \underline{H}^i , \underline{Q}^i and \underline{Y}^i which are expanded from their original sizes of (4×1) to $(4m \times 1)$ by inserting zeros in all but the elements $(4i, \dots, 4i+4)$ where the four elements of \underline{H}^i , \underline{Q}^i or \underline{Y}^i appear.

Using Eq. (A-1), Eqs. (A-9), (A-10) and (A-11) can be written as

$$[w_i(x_i)]^2 = \underline{q}^t \underline{B}^t \underline{G}^i (\underline{G}^i)^t \underline{B} \underline{q} \quad (\text{A-12})$$

$$[w'_i(x_i)]^2 = \underline{q}^t \underline{B}^t \underline{L}^i (\underline{L}^i)^t \underline{B} \underline{q} \quad (\text{A-13})$$

$$[w''_i(x_i)]^2 = \underline{q}^t \underline{B}^t \underline{R}^i (\underline{R}^i)^t \underline{B} \underline{q} \quad (\text{A-14})$$

Next, the total potential for the column is given by

$$\begin{aligned} \pi &= \frac{1}{2} \int_0^L EI (w'')^2 dx - \frac{\lambda}{2} \int_0^L p(x) w'^2 dx + \frac{\beta}{2} \int_0^L w^2 dx + \frac{1}{2} U_{ss} \\ &= \sum_{i=1}^m \frac{1}{2} \int_0^{\ell_i} EI_i (w''_i)^2 dx_i - \frac{\lambda}{2} \int_0^{\ell_i} p_i(x_i) (w'_i)^2 dx_i + \frac{\beta}{2} \int_0^{\ell_i} w_i^2 dx_i + \frac{1}{2} U_{ss} \end{aligned}$$

where

$$\begin{aligned} U_{ss} &= k_T^0 [w(0)]^2 + k_T^L [w(L)]^2 + k_R^0 [w'(0)]^2 + k_R^L [w'(L)]^2 \\ &= k_T^0 (q_1)^2 + k_T^L (q_{2m+1})^2 + k_R^0 (q_2)^2 + k_R^L (q_{2m+2})^2 \\ &= \underline{q}^t \underline{S} \underline{q} \end{aligned}$$

The matrix \underline{S} is a diagonal matrix of size $(2m+2) \times (2m+2)$ with

$$S_{11} = k_T^0, \quad S_{22} = k_R^0$$

$$S_{2m+1} = k_T^L, \quad S_{2m+2} = K_R^L$$

all the rest of the elements of the matrix \underline{S} being zero.

Using Eqs. (A-12), (A-13) and (A-14) the expression for π becomes

$$\begin{aligned} \pi = & \frac{1}{2} \underline{q}^t \underline{B}^t \left(\sum_{i=1}^m \int_0^{\ell} \left[EI_i \underline{R}^i (\underline{R}^i)^t + \beta \underline{G}^i (\underline{G}^i)^t \right] dx_i \right) \underline{B} \underline{q} \\ & - \frac{\lambda}{2} \underline{q}^t \underline{B}^t \left(\sum_{i=1}^m \int_0^{\ell} p_i(x_i) \underline{L}^i (\underline{L}^i)^t dx_i \right) \underline{B} \underline{q} \\ & + \frac{1}{2} \underline{q}^t \underline{S} \underline{q} \end{aligned}$$

Letting

$$[K] = \underline{B}^t \left(\sum_{i=1}^m \int_0^{\ell} \left[EI_i \underline{R}^i (\underline{R}^i)^t + \beta \underline{G}^i (\underline{G}^i)^t \right] dx_i \right) \underline{B} + \underline{S} \quad (A-15)$$

and

$$[K_G] = \underline{B}^t \left(\sum_{i=1}^m \int_0^{\ell} p_i(x_i) \underline{L}^i (\underline{L}^i)^t dx_i \right) \underline{B} ; \quad (A-16)$$

the expression for π finally becomes

$$\pi = \frac{1}{2} \underline{q}^t \underline{K} \underline{q} - \frac{\lambda}{2} \underline{q}^t \underline{K}_G \underline{q} .$$

The principle of the stationary value of the total potential requires $\delta\pi = 0$ for equilibrium. Hence

$$\delta\pi = \delta\mathbf{q}^t (\mathbf{K} - \lambda\mathbf{K}_G) \mathbf{q} = 0$$

Hence, for arbitrary variations of the generalized displacements \mathbf{q} it follows that

$$[\mathbf{K}] - \lambda[\mathbf{K}_G] \{\mathbf{q}\} = \{0\} \quad (\text{A-17})$$

In the absence of β and $\underline{\mathbf{S}}$, the matrices \mathbf{K} and \mathbf{K}_G will be both singular since rigid body motion has not been eliminated. Hence the boundary conditions must be imposed in order to solve the eigenvalue problem specified by Eq. (A-17). The imposition of the boundary conditions can be made in several ways (see Ref. 22, pp. 233-234), but the best way from the point of view of computation time would be to cross out the rows and columns corresponding to prescribed zero displacements. This, in essence, corresponds to partitioning the matrices \mathbf{K} and \mathbf{K}_G into submatrices retaining the portions of these matrices corresponding to externally applied active loads (which in the case of the homogeneous eigenvalue problem are zero) for eigenvalue analysis and throwing out the rest of the portions of these matrices corresponding to reactive tractions which do not enter into the formulation of the total potential of the system.

Next, returning to Eqs. (A-15) and (A-16) some explicit expressions for the integrated quantities pertaining to the i^{th} element can

be obtained. The matrix represented by

$$\int_0^{l_i} EI_i R^i (R^i)^T dx_i$$

is a symmetric matrix of size $(2m + 2) \times (2m + 2)$ given by

$$\begin{array}{c} \begin{array}{cc} & \begin{array}{cc} 4i & 4i+4 \end{array} \\ \begin{array}{cc} 4i & 4i+4 \end{array} & \left[\begin{array}{cc|cc} 0 & 0 & 0 & 0 \\ 0 & k^i & 0 & 0 \\ 0 & 0 & 0 & 0 \end{array} \right] \end{array}$$

where

$$[k^i] = EI_i \begin{bmatrix} \frac{12}{l_i^3} & \frac{6}{l_i^2} & \frac{-12}{l_i^3} & \frac{6}{l_i^2} \\ & \frac{4}{l_i} & \frac{-6}{l_i^2} & \frac{2}{l_i} \\ & & \frac{12}{l_i^3} & \frac{-6}{l_i^2} \\ \text{SYM} & & & \frac{4}{l_i} \end{bmatrix}$$

$$\int_0^{l_i} \beta G^i (G^i)^T dx_i$$

is also a symmetric matrix of size $(2m + 2) \times (2m + 2)$ given by

$$\begin{array}{c}
 \begin{array}{cc}
 & \begin{array}{cc} 4i & 4i+4 \end{array} \\
 & \begin{array}{cc} \vdots & \vdots \end{array}
 \end{array} \\
 \begin{array}{cc}
 4i \text{ ---} & \begin{bmatrix} 0 & 0 & 0 & 0 \\ 0 & m^i & 0 & 0 \\ 0 & 0 & 0 & 0 \end{bmatrix} \\
 4i+4 \text{ ---} & \begin{array}{cc} \vdots & \vdots \end{array}
 \end{array}
 \end{array}$$

where

$$[m^i] = \frac{\beta \ell_i}{420} \begin{bmatrix} 156 & 22\ell_i & 54 & -13\ell_i \\ & 4\ell_i^2 & 13\ell_i & -3\ell_i^2 \\ & & 156 & -22\ell_i \\ \text{SYM} & & & 4\ell_i^2 \end{bmatrix}$$

$$\int_0^{\ell_i} p_i(x_i) L^i (L^i)^T dx_i$$

is a symmetric matrix of size $(2m+2) \times (2m+2)$. For a linear variation of $p_i(x_i)$ given by $p_i(x_i) = P_1(1-\xi_i) + P_2\xi_i$ the matrix becomes:

$$\begin{array}{c}
 \begin{array}{cc}
 & \begin{array}{cc} 4i & 4i+4 \end{array} \\
 & \begin{array}{cc} \vdots & \vdots \end{array}
 \end{array} \\
 \begin{array}{cc}
 4i \text{ ---} & \begin{bmatrix} 0 & 0 & 0 & 0 \\ 0 & k_G^i & 0 & 0 \\ 0 & 0 & 0 & 0 \end{bmatrix} \\
 4i+4 \text{ ---} & \begin{array}{cc} \vdots & \vdots \end{array}
 \end{array}
 \end{array}$$

where

$$[k_G^i] = \begin{bmatrix} \frac{3}{5\ell_i} (P_1+P_2) & \frac{P_2}{10} & -\frac{3}{5\ell_i} (P_1+P_2) & \frac{P_1}{10} \\ & \frac{\ell_i}{30} (3P_1+P_2) & -\frac{P_2}{10} & -\frac{\ell_i}{60} (P_1+P_2) \\ & & \frac{3}{5\ell_i} (P_1+P_2) & -\frac{P_1}{10} \\ \text{SYM} & & & \frac{\ell_i}{30} (P_1+3P_2) \end{bmatrix}$$

If $P_1 = P_2 = P$ then the matrix $[k_G^i]$ reduces to the one given in Ref. 10 taking the proper signs.

APPENDIX B

EQUATION OF MOTION -- FINITE ELEMENT FORMULATION

For the sake of uniformity of treatment, the equation of motion in terms of finite element formulation will be derived from Rayleigh's principle rather than by the use of Hamilton's principle. From Eq. (3.6), Chapter III, the expression for ω^2 is given by:

$$\omega^2 = \frac{\int_0^L E\rho A^n w''^2 dx + U_s - \int_0^L S_o(x) w'^2 dx}{\int_0^L \frac{\gamma}{g} A w^2 dx + \int_0^L m_d w^2 dx + \sum_{i=1}^k m_{ci} w_i^2} \quad (B-1)$$

where

$$U_s = k_T^0 w^2|_0 + k_T^L w^2|_L = k_R^0 w'^2|_0 + k_R^L w'^2|_L + \beta \int_0^L w^2 dx$$

From Appendix A, Eq. (B-1) can be immediately cast in matrix form as

$$\omega^2 = \frac{\{q\}^t [K_V] \{q\}}{\{q\}^t [M] \{q\}} \quad (B-2)$$

where

$$[K_V] = \underline{B}^t \left(\sum_{i=1}^m \int_0^{\ell_i} \left[EI_i \underline{R}^i (\underline{R}^i)^t + \beta \underline{G}^i (\underline{G}^i)^t - p_i(x_i) \underline{L}^i (\underline{L}^i)^t \right] dx_i \right) \underline{B} + \underline{S} \quad (B-3)$$

$$[M] = \underline{B}^t \left(\sum_{i=1}^m \int_0^{\ell_i} \left\{ \frac{\gamma}{g} A_i + m_{di}(x_i) \right\} \underline{G}^i (\underline{G}^i)^t dx_i \right) \underline{B} + \underline{M}_c \quad (B-4)$$

Assuming as an approximation a linear variation of dead mass distribution between any two consecutive nodes (this assumption is capable of approximating the arbitrarily varying dead mass distribution with increasing number of elements m) the expression for m_{di} can be written as

$$m_{di} = m_{1i}(1 - x_i/\ell_i) + m_{2i}(x_i/\ell_i)$$

and the expression for $[M]$ therefore becomes

$$\begin{aligned} [M] &= \underline{B}^t \left(\sum_{i=1}^m \int_0^{\ell_i} \left\{ \frac{\gamma}{g} A_i + m_{1i} \right\} \underline{G}^i (\underline{G}^i)^t dx_i \right. \\ &\quad \left. + \int_0^{\ell_i} \frac{(m_{2i} - m_{1i})}{\ell_i} x_i \underline{G}^i (\underline{G}^i)^t dx_i \right) \underline{B} + \underline{M}_c \\ &= \underline{B}^t \left[\sum_{i=1}^m \left(\frac{\gamma}{g} A_i + m_{1i} \right) \underline{M}_u^i + \left(\frac{m_{2i} - m_{1i}}{\ell_i} \right) \underline{M}_v^i \right] \underline{B} + \underline{M}_c \end{aligned}$$

where

$$[M_u^i] = \begin{bmatrix} 0 & \overset{4i}{\vdots} & 0 & \overset{4i+4}{\vdots} & 0 \\ - & \vdots & - & \vdots & - \\ 0 & \vdots & m_u^i & \vdots & 0 \\ - & \vdots & - & \vdots & - \\ 0 & \vdots & 0 & \vdots & 0 \end{bmatrix} \begin{matrix} 4i \\ \\ 4i+4 \end{matrix}$$

$$[m_u^i] = \frac{\ell_i}{420} \begin{bmatrix} 156 & 22\ell_i & 54 & -13\ell_i \\ & 4\ell_i^2 & 13\ell_i & -3\ell_i^2 \\ & & 156 & -22\ell_i \\ \text{SYM} & & & 4\ell_i^2 \end{bmatrix}$$

and where

$$[M_v^i] = \begin{bmatrix} 0 & \vdots & 0 & \vdots & 0 \\ & \ddots & & \ddots & \\ 0 & \vdots & m_v^i & \vdots & 0 \\ & \ddots & & \ddots & \\ 0 & \vdots & 0 & \vdots & 0 \end{bmatrix} \begin{matrix} 4i \\ 4i+4 \end{matrix}$$

$$[m_v^i] = \frac{\ell_i^2}{840} \begin{bmatrix} 72 & 14\ell_i & 54 & -12\ell_i \\ & 3\ell_i^2 & 14\ell_i & -3\ell_i^2 \\ & & 240 & -30\ell_i \\ \text{SYM} & & & 5\ell_i^2 \end{bmatrix}$$

both the matrices $[M_u^i]$ and $[M_v^i]$ being of size $(2m+2) \times (2m+2)$ and finally the matrix \underline{M}_c is a diagonal matrix with $[2(i-1) + 1]$ st element being equal to m_{ci} . Returning to Eq. (B-2), by Rayleigh's principle ω^2 is stationary with respect to the generalized displacements $\{q\}$.

Hence, it follows that $\delta(\omega^2) = 0$ i.e.

$$\frac{2\{\delta_q\}^t [K_V] \{q\}}{\{q\}^t [M] \{q\}} - 2\omega^2 \frac{\{\delta_q\}^t [M] \{q\}}{\{q\}^t [M] \{q\}} = \{0\} .$$

Hence, for arbitrary variation of the generalized displacements $\{q\}$ the above finally yields

$$[[K_V] - \omega^2 [M]] \{q\} = \{0\} . \quad (B-5)$$

Equation (B-5) is the equation of motion. If $\beta = 0$ and \underline{S} is the null matrix, suitable boundary conditions are to be imposed before attempting to solve the eigenvalue problem as specified by Eq. (B-5) (see Appendix A). For a free-free beam, however, the two equations of constraint corresponding to the conservation of linear and angular momenta have to be used to transform the stiffness matrix in order to render it nonsingular before solving the eigenvalue problem of Eq. (B-5). This seems very specialized, so hence the problem of the free-free beam is not attempted.

APPENDIX C

FINITE ELEMENT DISPLACEMENT METHOD AS APPLIED TO
VIBRATION AND STABILITY ANALYSIS OF THIN RECTANGULAR PLATES

The details of the assembly of the individual element stiffness and mass matrices to obtain the assembled stiffness and mass or stability matrices for the entire plate are in no way different from those outlined for the column in Appendix A. Hence, this appendix will be devoted solely to the development of individual element stiffness, mass and stability matrices for a plate bending element.

The types of rectangular plate bending elements can be broadly classified into two distinct classes. Firstly, there are the non-conforming elements which do not satisfy compatibility exactly, and depending upon the degree of lack of compatibility an assembly of such elements will converge to the true solution from either side or oscillate (Ref. 27). Secondly, there are the conforming elements which satisfy compatibility exactly, and lead to an assembly which is stiffer than the actual plate because of discretization. For the optimization procedure which has been proposed, it is necessary that the finite elements which are used for the modelling of the plate be fully compatible. If this is not the case, a value of p which will guarantee that $(\lambda_{cr})^{r+1} \geq (\lambda_{cr})^r$ for the stability or that $(\omega_1^2)^{r+1} \geq (\omega_1^2)^r$ for the vibration analysis cannot be shown to exist.

The conforming plate bending element developed in Ref. 28 or 29

will be outlined in detail next and expressions for all the matrices required for the stability and vibration analysis of a plate will be developed. Since the types of plates to be analyzed are rectangular, it would suffice to restrict the following development to a conforming rectangular plate bending element. This element with a total of 16 degrees of freedom i.e. four degrees of freedom namely w_i , $w_{i,x}$, $w_{i,y}$ and $w_{i,xy}$ at each of the four corners of the rectangular plate element can be shown to satisfy compatibility exactly when the displacement function within this element is chosen as

$$w_i(x,y) = \sum_{j=0}^3 \sum_{k=0}^3 a_{jk} x^j y^k \quad (C-1)$$

Note that this representation satisfies the criterion of completeness since it is a complete polynomial of the third degree in x and y . It can also be shown that $w_i(x,y)$ includes constant strain states which are necessary for convergence to the true solution as the mesh is refined (Refs. 22 and 28).

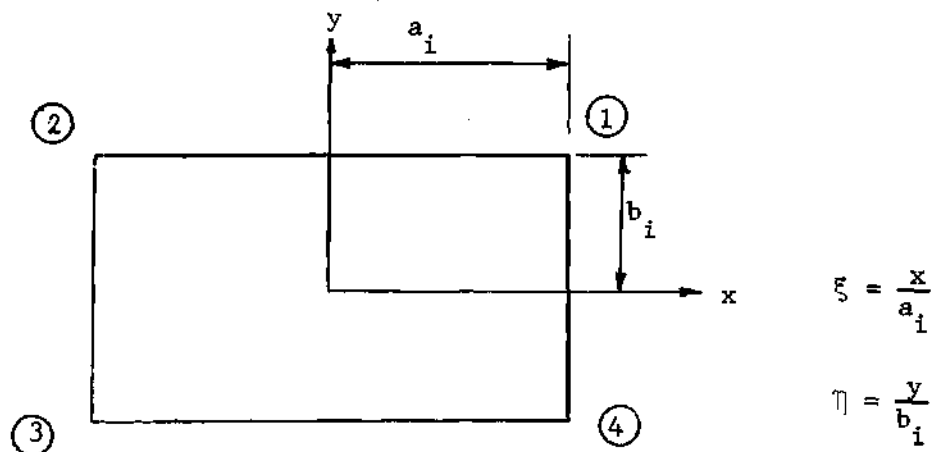


Figure C-1. A Typical Rectangular Plate Bending Element

Consider a rectangular element of size $2a_i \times 2b_i$ with the local coordinates axes located as shown in Fig. C-1. The displacement function given in Eq. (C-1) can be written in the non-dimensionalized form as

$$w_i(\xi, \eta) = \sum_{j=0}^3 \sum_{k=0}^3 \alpha_{jk} \xi^j \eta^k \quad . \quad (C-2)$$

The same can be written in the matrix form as

$$w_i = [1 \ \xi \ \xi^2 \ \xi^3 \ \eta \ \xi\eta \ \xi^2\eta \ \xi^3\eta \ \eta^2 \ \xi\eta^2 \ \xi^2\eta^2 \ \xi^3\eta^2 \ \eta^3 \ \xi\eta^3 \ \xi^2\eta^3 \ \xi^3\eta^3] \{\alpha\} \quad . \quad (C-3)$$

Let $\{u\}_i$ denote the vector of generalized nodal displacements (nondimensionalized for convenience) for the i^{th} element. Then

$$\{u\}_i = \begin{Bmatrix} u^1 \\ u^2 \\ u^3 \\ u^4 \end{Bmatrix}_i \quad \text{where } \{u^n\}_i = \begin{Bmatrix} w_i \\ a_i w_{i,x} \\ b_i w_{i,y} \\ a_i b_i w_{i,xy} \end{Bmatrix}_i^n = \begin{Bmatrix} w_i \\ w_{i,\xi} \\ w_{i,\eta} \\ w_{i,\xi\eta} \end{Bmatrix}_i^n \quad . \quad (C-4)$$

Next, it is necessary to relate the vector $\{u\}_i$ with the vector $\{\alpha\}$. This will enable the displacement function w_i to be expressed in terms of the generalized nodal displacements. This can be done by evaluating the function w_i and its derivatives at all the four corners of the plate and identifying them with the generalized nodal displacements. From

Eq. (C-3), one has upon differentiation

$$w_{,\xi} = [0 \ 1 \ 2\xi \ 3\xi^2 \ 0 \ \eta \ 2\xi\eta \ 3\xi^2\eta \ 0 \ \eta^2 \ 2\xi\eta^2 \ 3\xi^2\eta^2 \ 0 \ \eta^3 \ 2\xi\eta^3 \ 3\xi^2\eta^3] \{\alpha\}$$

$$w_{,\eta} = [0 \ 0 \ 0 \ 0 \ 1 \ \xi \ \xi^2 \ \xi^3 \ 2\eta \ 2\xi\eta \ 2\xi^2\eta \ 2\xi^3\eta \ 3\eta^2 \ 3\xi\eta^2 \ 3\xi^2\eta^2 \ 3\xi^3\eta^2] \{\alpha\}$$

$$w_{,\xi\eta} = [0 \ 0 \ 0 \ 0 \ 0 \ 1 \ 2\xi \ 3\xi^2 \ 0 \ 2\eta \ 4\xi\eta \ 6\xi^2\eta \ 0 \ 3\eta^2 \ 6\xi\eta^2 \ 9\xi^2\eta^2] \{\alpha\}$$

Using these relations the vector $\{u\}_i$ can be related to the vector $\{\alpha\}$ by the relation

$$\{u\}_i = [c] \{\alpha\} \quad (C-5)$$

where the matrix $[c]$ is given by:

(see next page)

$$[c] = \begin{bmatrix} 1 & 1 & 1 & 1 & 1 & 1 & 1 & 1 & 1 & 1 & 1 & 1 & 1 & 1 & 1 & 1 \\ 0 & 1 & 2 & 3 & 0 & 1 & 2 & 3 & 0 & 1 & 2 & 3 & 0 & 1 & 2 & 3 \\ 0 & 0 & 0 & 0 & 1 & 1 & 1 & 1 & 2 & 2 & 2 & 2 & 3 & 3 & 3 & 3 \\ 0 & 0 & 0 & 0 & 0 & 1 & 2 & 3 & 0 & 2 & 4 & 6 & 0 & 3 & 6 & 9 \\ 1 & -1 & 1 & -1 & 1 & -1 & 1 & -1 & 1 & -1 & 1 & -1 & 1 & -1 & 1 & -1 \\ 0 & 1 & -2 & 3 & 0 & 1 & -2 & 3 & 0 & 1 & -2 & 3 & 0 & 1 & -2 & 3 \\ 0 & 0 & 0 & 0 & 1 & -1 & 1 & -1 & 2 & -2 & 2 & -2 & 3 & -3 & 3 & -3 \\ 0 & 0 & 0 & 0 & 0 & 1 & -2 & 3 & 0 & 2 & -4 & 6 & 0 & 3 & -6 & 9 \\ 1 & -1 & 1 & -1 & -1 & 1 & -1 & 1 & 1 & -1 & 1 & -1 & -1 & 1 & -1 & 1 \\ 0 & 1 & -2 & 3 & 0 & -1 & 2 & -3 & 0 & 1 & -2 & 3 & 0 & -1 & 2 & -3 \\ 0 & 0 & 0 & 0 & 1 & -1 & 1 & -1 & -2 & 2 & -2 & 2 & 3 & -3 & 3 & -3 \\ 0 & 0 & 0 & 0 & 0 & 1 & -2 & 3 & 0 & -2 & 4 & -6 & 0 & 3 & -6 & 9 \\ 1 & 1 & 1 & 1 & -1 & -1 & -1 & -1 & 1 & 1 & 1 & 1 & -1 & -1 & -1 & -1 \\ 0 & 1 & 2 & 3 & 0 & -1 & -2 & -3 & 0 & 1 & 2 & 3 & 0 & -1 & -2 & -3 \\ 0 & 0 & 0 & 0 & 1 & 1 & 1 & 1 & -2 & -2 & -2 & -2 & 3 & 3 & 3 & 3 \\ 0 & 0 & 0 & 0 & 0 & 1 & 2 & 3 & 0 & -2 & -4 & -6 & 0 & 3 & 6 & 9 \end{bmatrix}$$

Hence, one can write

$$\begin{aligned} w_i &= [1 \quad \xi \quad \xi^2 \quad \xi^3 \quad \eta \quad \xi\eta \quad \xi^2\eta \quad \xi^3\eta \quad \eta^2 \quad \xi\eta^2 \quad \xi^2\eta^2 \quad \xi^2\eta^3 \quad \eta^3 \quad \xi\eta^3 \quad \xi^2\eta^3 \quad \xi^3\eta^3][c]^{-1}\{u_i\} \\ &= P_{u_i}^t \end{aligned} \quad (C-6)$$

$$\begin{aligned} w_{i,\xi} &= [0 \quad 1 \quad 2\xi \quad 3\xi^2 \quad 0 \quad \eta \quad 2\xi\eta \quad 3\xi^2\eta \quad 0 \quad \eta^2 \quad 2\xi\eta^2 \quad 3\xi^2\eta^2 \quad 0 \quad \eta^3 \quad 2\xi\eta^3 \quad 3\xi^2\eta^3][c]^{-1}\{u_i\} \\ &= Q_{u_i}^t \end{aligned} \quad (C-7)$$

$$\begin{aligned}
 w_{i,\eta} &= [0 \ 0 \ 0 \ 0 \ 1 \ \xi \ \xi^2 \ \xi^3 \ 2\eta \ 2\xi\eta \ 2\xi^2\eta \ 2\xi^3\eta \ 3\eta^2 \ 3\xi\eta^2 \ 3\xi^2\eta^2 \ 3\xi^3\eta^2][c]^{-1}\{u_i\} \\
 &= \underline{R}^t \underline{u}_i
 \end{aligned} \tag{C-8}$$

$$\begin{aligned}
 w_{i,\xi\xi} &= [0 \ 0 \ 2 \ 6\xi \ 0 \ 0 \ 2\eta \ 6\xi\eta \ 0 \ 0 \ 2\eta^2 \ 6\xi\eta^2 \ 0 \ 0 \ 2\xi^3 \ 6\xi\eta^3][c]^{-1}\{u_i\} \\
 &= \underline{s}^t \underline{u}_i
 \end{aligned} \tag{C-9}$$

$$\begin{aligned}
 w_{i,\eta\eta} &= [0 \ 0 \ 0 \ 0 \ 0 \ 0 \ 0 \ 0 \ 2 \ 2\xi \ 2\xi^2 \ 2\xi^3 \ 6\eta \ 6\xi\eta \ 6\xi^2\eta \ 6\xi^3\eta][c]^{-1}\{u_i\} = \underline{G}^t \underline{u}_i \\
 &\tag{C-10}
 \end{aligned}$$

$$\begin{aligned}
 w_{i,\xi\eta} &= [0 \ 0 \ 0 \ 0 \ 0 \ 1 \ 2\xi \ 3\xi^2 \ 0 \ 2\eta \ 4\xi\eta \ 6\xi^2\eta \ 0 \ 3\eta^2 \ 6\xi\eta^2 \ 9\xi^2\eta^2][c]^{-1}\{u_i\} \\
 &= \underline{H}^t \underline{u}_i
 \end{aligned} \tag{C-11}$$

The strain energy of bending of the i^{th} element is given by

$$\begin{aligned}
 U_i &= \left(\frac{Dab}{2}\right)_i \int_{-1}^1 \int_{-1}^1 \left\{ \left(\frac{1}{a_i} w_{i,\xi\xi} + \frac{1}{b_i} w_{i,\eta\eta} \right)^2 - 2(1-\nu) \left(\frac{1}{a_i b_i} w_{i,\xi\xi} w_{i,\eta\eta} \right. \right. \\
 &\quad \left. \left. - \frac{1}{a_i b_i} w_{i,\xi\eta}^2 \right) \right\} d\xi d\eta \\
 &= \left(\frac{Dab}{2}\right)_i \int_{-1}^1 \int_{-1}^1 \left\{ \frac{1}{a_i^2} w_{i,\xi\xi}^2 + \frac{1}{b_i^2} w_{i,\eta\eta}^2 + \frac{2\nu}{a_i b_i} w_{i,\xi\xi} w_{i,\eta\eta} \right. \\
 &\quad \left. + \frac{2(1-\nu)}{a_i b_i} w_{i,\xi\eta}^2 \right\} d\xi d\eta
 \end{aligned}$$

$$\begin{aligned}
= & \left(\frac{Dab}{2} \right)_i \int_{-1}^1 \int_{-1}^1 \left\{ \frac{1}{4} \underline{u}_i^t \underline{s} \underline{s}^t \underline{u}_i + \frac{1}{4} \underline{u}_i^t \underline{G} \underline{G}^t \underline{u}_i + \frac{\nu}{2} \frac{1}{a_i b_i} \underline{u}_i^t \left(\underline{s} \underline{G}^t \right. \right. \\
& \left. \left. + \underline{G} \underline{s}^t \right) \underline{u}_i + \frac{2(1-\nu)}{2} \frac{1}{a_i b_i} \underline{u}_i^t \underline{H} \underline{H}^t \underline{u}_i \right\} d\xi d\eta
\end{aligned}$$

Hence U_i can be expressed as

$$U_i = \frac{1}{2} \underline{u}_i^t \left[\underline{k}_1 + \underline{k}_2 + \underline{k}_3 + \underline{k}_4 \right] \underline{u}_i = \frac{1}{2} \{u_i\}^t [K_{Vi}]_p \{u_i\} \quad (C-12)$$

where $[K_{Vi}]_p$ is the stiffness matrix of the i^{th} element and

$$\underline{k}_1 = \left(\frac{Db}{3} \right)_i \int_{-1}^1 \int_{-1}^1 \underline{s} \underline{s}^t d\xi d\eta \quad (C-13)$$

$$\underline{k}_2 = \left(\frac{Da}{3} \right)_i \int_{-1}^1 \int_{-1}^1 \underline{G} \underline{G}^t d\xi d\eta \quad (C-14)$$

$$\underline{k}_3 = \left(\frac{\nu D}{ab} \right)_i \int_{-1}^1 \int_{-1}^1 (\underline{s} \underline{G}^t + \underline{G} \underline{s}^t) d\xi d\eta \quad (C-15)$$

$$\underline{k}_4 = \left[\frac{2D(1-\nu)}{ab} \right]_i \int_{-1}^1 \int_{-1}^1 \underline{H} \underline{H}^t d\xi d\eta \quad \text{with} \quad D_i = \frac{Eh_i^3}{12(1-\nu^2)} \quad (C-16)$$

It should be noticed that in the case of the stability analysis the strain energy U_i can be interpreted as the incremental bending strain energy from the prebuckled configuration and the displacement function w_i as the incremental deformation from the prebuckled configuration.

Let the stiffness matrix in the case of stability analysis be denoted by $[K_{si}]_p$ instead of $[K_{vi}]_p$ although both are numerically identical.

Next, the kinetic energy for the i^{th} element including the non-structural mass is given by

$$U_{ti} = \frac{\gamma}{2g} a_i b_i h_i \omega^2 \int_{-1}^1 \int_{-1}^1 w_i^2 d\xi d\eta + \frac{a_i b_i \omega^2}{2} \int_{-1}^1 \int_{-1}^1 m_{di} w_i^2 d\xi d\eta$$

Assume $m_{di}(\xi, \eta) = a_0 + a_1 \xi + a_2 \eta + a_3 \xi \eta$ where the coefficients a_0 , a_1 , a_2 and a_3 can be related to the intensities of dead mass distribution namely m_1 , m_2 , m_3 and m_4 at the four corners of the rectangular element. These relations are given by

$$\left. \begin{aligned} a_0 &= (m_1 + m_2 + m_3 + m_4)/4 \\ a_1 &= [(m_1 + m_4) - (m_2 + m_3)]/4a_i \\ a_2 &= [(m_1 + m_2) - (m_3 + m_4)]/4b_i \\ a_3 &= [(m_1 + m_3) - (m_2 + m_4)]/4a_i b_i \end{aligned} \right\} \quad (C-17)$$

Hence, the kinetic energy U_{ti} can be expressed as

$$\begin{aligned} U_{ti} &= \frac{\gamma}{2g} a_i b_i h_i \omega^2 \int_{-1}^1 \int_{-1}^1 \underline{u}_i^t \underline{p} \underline{p}^t \underline{u}_i d\xi d\eta \\ &\quad + \frac{a_i b_i \omega^2}{2} a_0 \int_{-1}^1 \int_{-1}^1 \underline{u}_i^t \underline{p} \underline{p}^t \underline{u}_i d\xi d\eta \end{aligned}$$

$$\begin{aligned}
& + a_i b_i \omega^2 (a_1 + a_2) \int_{-1}^1 \int_{-1}^1 \underline{u}_i^t(\xi \underline{p} \underline{p}^t) \underline{u}_i d\xi d\eta \\
& + \frac{a_i b_i \omega^2}{2} a_3 \int_{-1}^1 \int_{-1}^1 \underline{u}_i^t(\xi \eta \underline{p} \underline{p}^t) \underline{u}_i d\xi d\eta .
\end{aligned}$$

Hence

$$U_{ti} = \frac{\omega^2}{2} \{u_i\}^t [M_i]_p \{u_i\} = \frac{\omega^2}{2} \underline{u}_i^t [\underline{M}^1 + \underline{M}^2 + \underline{M}^3] \underline{u}_i \quad (C-18)$$

where $[M_i]_p$ is the mass matrix for the i^{th} element and

$$\underline{M}^1 = a_i b_i \left(\frac{y}{g} h_i + a_0 \right) \int_{-1}^1 \int_{-1}^1 \underline{p} \underline{p}^t d\xi d\eta , \quad (C-19)$$

$$\underline{M}^2 = a_i b_i (a_1 + a_2) \int_{-1}^1 \int_{-1}^1 \xi \underline{p} \underline{p}^t d\xi d\eta , \quad (C-20)$$

$$\underline{M}^3 = a_i b_i a_3 \int_{-1}^1 \int_{-1}^1 \xi \eta \underline{p} \underline{p}^t d\xi d\eta . \quad (C-21)$$

The effect of concentrated masses can be accounted for by adding to the assembled mass matrix another matrix given by \underline{M}_c which is a diagonal matrix of the same size with the $[4(i-1) + 1]$ th term being equal to m_{ci} (the concentrated dead mass at the i^{th} node) with all the remaining terms being zero.

In the case of the stability analysis it is necessary to construct a stability matrix for each element. This is achieved by expressing the potential $(w_p)_i$ of the internal prebuckled stress field during bending

in the matrix form. Assume the prebuckled stress state can be expressed in the form

$$\begin{aligned}\sigma_{\xi\xi}^0 &= \sigma_{\xi 0}^0 + \xi \sigma_{\xi 1}^0 + \eta \sigma_{\xi 2}^0 \\ \sigma_{\eta\eta}^0 &= \sigma_{\eta 0}^0 + \xi \sigma_{\eta 1}^0 + \eta \sigma_{\eta 2}^0 \\ \tau_{\xi\eta}^0 &= \tau_{\xi\eta 0}^0 + \xi \tau_{\xi\eta 1}^0 + \eta \tau_{\xi\eta 2}^0\end{aligned}\tag{C-22}$$

for any element. (This sort of representation is exactly what one obtains as a result of the plane stress analysis using rectangular elements; see page 182). Then

$$\begin{aligned}(w_p)_i &= \frac{a_i b_i h_i}{2} \int_{-1}^1 \int_{-1}^1 \left[\frac{1}{2} \sigma_{\xi\xi}^0 (w, \xi)^2 + \frac{1}{2} \sigma_{\eta\eta}^0 (w, \eta)^2 \right. \\ &\quad \left. + \frac{2}{a_i b_i} \tau_{\xi\eta}^0 w, \xi w, \eta \right] d\xi d\eta \\ &= \frac{a_i b_i h_i}{2} \int_{-1}^1 \int_{-1}^1 \left[\frac{1}{2} \sigma_{\xi\xi}^0 \underline{u}_i^t \underline{Q} \underline{Q}^t \underline{u}_i + \frac{1}{2} \sigma_{\eta\eta}^0 \underline{u}_i^t \underline{R} \underline{R}^t \underline{u}_i \right. \\ &\quad \left. + \frac{1}{a_i b_i} \tau_{\xi\eta}^0 \underline{u}_i^t (\underline{Q} \underline{R}^t \right. \\ &\quad \left. + \underline{R} \underline{Q}^t) \underline{u}_i \right] d\xi d\eta\end{aligned}$$

or

$$\begin{aligned}
(w_p)_i &= \frac{1}{2} \underline{u}_i^t \left[\underline{K}_{G1} + \underline{K}_{G2} + \underline{K}_{G3} + \underline{K}_{G4} + \underline{K}_{G5} + \underline{K}_{G6} \right. \\
&\quad \left. + \underline{K}_{G7} + \underline{K}_{G8} + \underline{K}_{G9} \right] \underline{u}_i \\
&= \frac{1}{2} \{u_i\}^t [K_{Gi}]_p \{u_i\}
\end{aligned} \tag{C-23}$$

where $[K_{Gi}]$ is the stability matrix for the i^{th} element and

$$\underline{k}_{G1} = \frac{b_i}{a_i} h_i \sigma_{\xi 0}^o \int_{-1}^1 \int_{-1}^1 \underline{Q} \underline{Q}^t d\xi d\eta \tag{C-24}$$

$$\underline{k}_{G2} = \frac{b_i}{a_i} h_i \sigma_{\xi 1}^o \int_{-1}^1 \int_{-1}^1 \xi \underline{Q} \underline{Q}^t d\xi d\eta \tag{C-25}$$

$$\underline{k}_{G3} = \frac{b_i}{a_i} h_i \sigma_{\xi 2}^o \int_{-1}^1 \int_{-1}^1 \eta \underline{Q} \underline{Q}^t d\xi d\eta \tag{C-26}$$

$$\underline{k}_{G4} = \frac{a_i}{b_i} h_i \sigma_{\eta 0}^o \int_{-1}^1 \int_{-1}^1 \underline{R} \underline{R}^t d\xi d\eta \tag{C-27}$$

$$\underline{k}_{G5} = \frac{a_i}{b_i} h_i \sigma_{\eta 1}^o \int_{-1}^1 \int_{-1}^1 \xi \underline{R} \underline{R}^t d\xi d\eta \tag{C-27}$$

$$\underline{k}_{G6} = \frac{a_i}{b_i} h_i \sigma_{\eta 2}^o \int_{-1}^1 \int_{-1}^1 \eta \underline{R} \underline{R}^t d\xi d\eta \tag{C-29}$$

$$\underline{k}_{G7} = h_i \tau_{\xi \eta 0}^o \int_{-1}^1 \int_{-1}^1 (\underline{Q} \underline{R}^t + \underline{R} \underline{Q}^t) d\xi d\eta \tag{C-30}$$

$$\underline{k}_{G8} = h_i \tau_{\xi\eta 1}^o \int_{-1}^1 \int_{-1}^1 \xi (\underline{Q} \underline{R}^t + \underline{R} \underline{Q}^t) d\xi d\eta \quad (C-31)$$

$$\underline{k}_{G9} = h_i \tau_{\xi\eta 2}^o \int_{-1}^1 \int_{-1}^1 \eta (\underline{Q} \underline{R}^t + \underline{R} \underline{Q}^t) d\xi d\eta . \quad (C-32)$$

In the case of inextensional buckling the potential of the externally applied tractions must be expressed in the matrix form. From the known distribution of the externally applied tractions, the values of these tractions along the boundaries of any element i can be determined. These fictitious tractions for the i^{th} element can be approximated by expressions of the form given by Eq. (C-22) and the stability matrix for the i^{th} element can be generated as before. Finally the element stiffness matrices, mass matrices and/or stability matrices can be assembled to yield the corresponding master matrices for the entire plate. Assuming as in Appendix A a relation between the local co-ordinates $\{u_i\}$, $i = 1, \dots, m$ and the global co-ordinates $\{q\}$ in the form

$$\{u\} = [B] \{q\} \quad (C-33)$$

The expressions for the master matrices can be written as

$$[K_v]_p = \sum_{i=1}^m \underline{B}^t [K_{vi}]_p \underline{B} = [K_s]_p \quad (C-34)$$

$$[M]_p = \sum_{i=1}^m \underline{B}^t [M_i]_p \underline{B} \quad (C-35)$$

$$[K_G]_p = \sum_{i=1}^m \underline{B}^t [K_{Gi}]_p \underline{B} \quad (C-36)$$

Finally, at times, due to structural symmetry and/or loading symmetry it may be possible to separate the unrestrained degrees of freedom $\{q\}$ into two distinct sets of variables namely the 'master' variables and the 'slave' variables such that the latter can be related to the former by a relation of the form

$$\{q\} = \begin{bmatrix} \underline{I} \\ \underline{L} \end{bmatrix} \{r\} = [F] \{r\} \quad (C-37)$$

where \underline{I} is the identity matrix while the matrix \underline{L} is a rectangular matrix with elements which are either +1, -1 or 0. Using Eq. (C-37) the master matrices of Eqs. (C-34) through (C-36) can be transformed to a size much smaller than their original size. This leads to a considerable saving of computer time. The transformed matrices can be obtained by the same transformation as in Eqs. (C-34) through (C-36).

All the component matrices which make up the element matrices $[K_{vi}]_p$, or $[K_{si}]_p$, $[M_i]_p$ and $[K_{Gi}]_p$ are generated by numerical integration using Gaussian Quadratures (Ref. 22, pp. 261-267).

As far as the details of the plane stress analysis required for the stability analysis of the plate, the same are developed in full in Ref. 22, pp. 66-69. For the development of the element stiffness matrix the following displacement field is assumed.

$$\left. \begin{aligned} u(x,y) &= \alpha_1 + \alpha_2 x + \alpha_3 y + \alpha_4 xy \\ v(x,y) &= \beta_1 + \beta_2 x + \beta_3 y + \beta_4 xy \end{aligned} \right\} \quad (C-38)$$

The resulting stiffness matrix $[K_i]_8$ for the i^{th} element (see Fig. C-1) is given by

(see next page)

$$[K_i]_s = \frac{Eh_1}{(1-\nu^2)}$$

	$(u_1)_i$	$(v_1)_i$	$(u_2)_i$	$(v_2)_i$	$(u_3)_i$	$(v_3)_i$	$(u_4)_i$	$(v_4)_i$
	$\frac{1}{3}\left(\frac{1}{r} + \varphi_1 r\right)$	$\frac{\varphi_2}{4}$	$\frac{1}{6}\left(\frac{1}{r} - 2\varphi_1 r\right)$	$-\frac{(\nu-\varphi_1)}{4}$	$-\frac{1}{6}\left(\frac{1}{r} + \varphi_1 r\right)$	$-\frac{\varphi_2}{4}$	$-\frac{1}{6}\left(\frac{1}{r} - 2\varphi_1 r\right)$	$\frac{(\nu-\varphi_1)}{4}$
		$\frac{1}{3}\left(r + \frac{\varphi_1}{r}\right)$	$\frac{(\nu-\varphi_1)}{4}$	$-\frac{1}{6}\left(2r - \frac{\varphi_1}{r}\right)$	$-\frac{\varphi_2}{4}$	$-\frac{1}{6}\left(r + \frac{\varphi_1}{r}\right)$	$-\frac{(\nu-\varphi_1)}{4}$	$\frac{1}{6}\left(r - \frac{2\varphi_1}{r}\right)$
			$\frac{1}{3}\left(\frac{1}{r} + \varphi_1 r\right)$	$-\frac{\varphi_2}{4}$	$-\frac{1}{6}\left(\frac{2}{r} - \varphi_1 r\right)$	$-\frac{(\nu-\varphi_1)}{4}$	$-\frac{1}{6}\left(\frac{1}{r} + \varphi_1 r\right)$	$\frac{\varphi_2}{4}$
				$\frac{1}{3}\left(r + \frac{\varphi_1}{r}\right)$	$\frac{(\nu-\varphi_1)}{4}$	$\frac{1}{6}\left(r - \frac{2\varphi_1}{r}\right)$	$\frac{\varphi_2}{4}$	$-\frac{1}{6}\left(r + \frac{2\varphi_1}{r}\right)$
					$\frac{1}{3}\left(\frac{1}{r} + \varphi_1 r\right)$	$\frac{\varphi_2}{4}$	$\frac{1}{6}\left(\frac{1}{r} - 2\varphi_1 r\right)$	$-\frac{(\nu-\varphi_1)}{4}$
						$\frac{1}{3}\left(r + \frac{\varphi_1}{r}\right)$	$\frac{(\nu-\varphi_1)}{4}$	$-\frac{1}{6}\left(2r - \frac{\varphi_1}{r}\right)$
							$\frac{1}{3}\left(\frac{1}{r} + \varphi_1 r\right)$	$-\frac{\varphi_2}{4}$
								$\frac{1}{3}\left(r + \frac{\varphi_1}{r}\right)$
SYM								

(C-39)

where $\varphi_1 = \frac{1-\nu}{2}$, $\varphi_2 = \frac{1+\nu}{2}$ and $r = a_i/b_i$.

The resulting matrix equation after the formation of the master plane stress stiffness matrix with the imposed boundary conditions is given by

$$[K]_s \{q\}_s = \{Q\}_s \quad (C-40)$$

where $\{Q\}_s$ is the vector of work-equivalent nodal forces obtained from the prescribed tractions. It can be seen that for the type of assumed displacement field (see Eq. C-38) the work-equivalent nodal forces are nothing more than the forces that would be obtained by simple beaming of the given tractions to the two nodes of the face on which the tractions are prescribed. From Eq. (C-40) the vector $\{q\}_s$ of the unrestrained degrees of freedom of the plate can be obtained as

$$\{q\}_s = [K]_s^{-1} \{Q\}_s \quad (C-41)$$

Having obtained $\{q\}_s$ the resulting stress resultants distribution in the i^{th} element is given by

(see next page)

$$\begin{Bmatrix} N_{xx}^o \\ N_{yy}^o \\ N_{xy}^o \end{Bmatrix} = \frac{Eh_1}{(1-\nu^2)} \begin{bmatrix} (b+y) & \nu(b+y) & \varphi_1(a+x) \\ \nu(a+x) & (a+x) & \varphi_1(b+y) \\ -(b+y) & -\nu(b+y) & \varphi_1(a-x) \\ \nu(a-x) & (a-x) & -\varphi_1(b+y) \\ -(b-y) & -\nu(b-y) & -\varphi_1(a-x) \\ -\nu(a-x) & -(a-x) & -\varphi_1(b-y) \\ (b-y) & \nu(b-y) & -\varphi_1(a+x) \\ -\nu(a+x) & -(a+x) & \varphi_1(b-y) \end{bmatrix}^t_i \{q\}_{si} \quad (C-42)$$

where $\{q\}_{si}$ is the vector of the eight degrees of freedom for the i^{th} element.

BIBLIOGRAPHY

1. Wasiutynski, Z., and Brandt, A., The Present State of Knowledge in the Field of Optimum Design of Structures, Applied Mechanics Reviews, Vol. 16, No. 5, 1963, pp. 341-350.
2. Sheu, C. Y., and Prager, W., Recent Developments in Optimal Structural Design, Applied Mechanics Reviews, Vol. 21, No. 10, 1968, pp. 985-992.
3. Keller, J. B., The Shape of the Strongest Column, Archive for Rational Mechanics and Analysis, Vol. 5, 1960, pp. 275-285.
4. Tadjbakhsh, I., and Keller, J. B., Strongest Columns and Isoperimetric Inequalities for Eigenvalues, Journal of Applied Mechanics, Vol. 29, 1962, pp. 159-164.
5. Keller, J. B. and Niordson, F. I., The Tallest Column, Journal of Mathematics and Mechanics, Vol. 16, No. 5, 1966, pp. 433-445.
6. Taylor, J. E., The Strongest Column: An Energy Approach, Journal of Applied Mechanics, Vol. 34, No. 2, 1967, pp. 486-487.
7. Salinas, D., On Variational Formulations for Optimal Structural Design, Ph.D. Dissertation, University of California, Los Angeles, 1968.
8. Prager, W., and Taylor, J. E., Problems of Optimal Structural Design, Journal of Applied Mechanics, Vol. 35, 1968, pp. 102-106.
9. Simites, G. J., Kamat, M. P., and Smith, Jr., C. V., The Strongest Column by the Finite Element Displacement Method, AIAA Paper No. 72-141, 1972, pp. 7-9.
10. Hartz, B. J., Matrix Formulation of Structural Stability Problems, Journal of the Structural Division, Proceedings of ASCE, Vol. 91, No. ST6, 1965, pp. 141-157.
11. Widder, D. V., Advanced Calculus, second edition, Prentice-Hall, Inc., Englewood Cliffs, N. J., p. 44.
12. Faddeeva, D. K. and Faddeeva, V. N., Computational Methods of Linear Algebra, W. H. Freeman and Co., 1963.
13. Bessack, P. R., Isoperimetric Inequalities for Non-homogeneous Clamped Rod and Plate, Journal of Mathematics and Mechanics, Vol. 8, 1959, pp. 471-482.

14. Schwarz, B., On the Extrema of Frequencies of Non-homogeneous Strings with Equimeasurable Density, Journal of Mathematics and Mechanics, Vol. 10, 1961, pp. 401-422.
15. Schwarz, B., Some Results on the Frequencies of Non-homogeneous Rods, Journal of Mathematical Analysis and Applications, Vol. 5, 1962, pp. 169-175.
16. Schwarz, B., Bounds for the Principal Frequencies of Nonuniformly Loaded Strings, Israel Journal of Mathematics, Vol. 1, 1963, pp. 11-21.
17. Niordson, F. I., On the Optimal Design of a Vibrating Beam, Quarterly of Applied Mathematics, Vol. 23, No. 1, 1965, pp. 47-53.
18. Turner, M. J., Design of Minimum Mass Structures with Specified Natural Frequencies, AIAA Journal, Vol. 5, No. 3, 1967, pp. 406-412.
19. Taylor, J. E., Minimum Mass Bar for Axial Vibration at Specified Natural Frequency, AIAA Journal,
20. Taylor, J. E., Optimum Design of a Vibrating Bar with Specified Minimum Cross-section, AIAA Journal, Vol. 6, No. 7, 1968, pp. 1379-1381.
21. Brach, R. M., On the Extremal Fundamental Frequencies of Vibrating Beams, International Journal of Solids and Structures, Vol. 4, 1968, pp. 667-674.
22. Zienkiewicz, O. C., and Cheung, Y. K., The Finite Element Method in Structural and Continuum Mechanics, McGraw-Hill Publishing Co., 1967.
23. Archer, J. S., Consistent Mass Matrix for Distributed Mass Systems, Journal of the Structural Division, Proceedings ASCE, Vol. 89, ST4, 1963, pp. 161-178.
24. Olhoff, N., Optimal Design of Vibrating Circular Plates, International Journal of Solids and Structures, Vol. 6, 1970, pp. 139-156.
25. Rubinstein, M. F., Structural Systems - Statics, Dynamics and Stability, Prentice-Hall, Inc., Englewood Cliffs, N. J., 1970.
26. Washizu, K., Variational Methods in Elasticity and Plasticity, Pergamon Press, 1968, pp. 165-168.
27. Kapur, K. K., and Hartz, B. J., Stability of Plates Using the Finite Element Method, Journal of the Engineering Mechanics Division, Proceedings of ASCE, EM2, 1966, pp. 177-195.

28. Bogner, F. K., Fox, R. L., Schmit, L. A., The Generation of Inter Element-Compatibility Stiffness and Mass Matrices by the Use of Interpolation Formulae, Proceedings of the Conference on Matrix Methods in Structural Mechanics, Wright Patterson Air Force Base, Ohio, 1965, pp. 441-443.
29. Carson, W. I., Newton, R. E., Plate Buckling Analysis Using a Fully Compatible Finite Element, AIAA Journal, Vol. 7, No. 3, 1969, pp. 527-529.
30. Timoshenko, S. P., and Gere, J. M., Theory of Elastic Stability, McGraw-Hill Book Co., Second Edition, 1961.
31. Frauenthal, J. C., Constrained Optimal Design of Circular Plates against Buckling, Report SM-50, Harvard University, 1971.

VITA

Manohar Pandurang Kamat was born in Goa, India, on February 20, 1940. He received his Bachelor's degree in Civil Engineering from the University of Poona in June, 1961. After working with several Civil Engineering Consultants in India, he enrolled at the University of Leeds, England, to obtain his post-graduate diploma in concrete technology in July, 1965. Thereafter he worked with Civil Engineering Consultants in England, and was later hired by the Lockheed-Georgia Company in 1967, and since then he has pursued graduate studies at the School of Aerospace Engineering and the School of Engineering Science and Mechanics, on a part-time basis.